Microheating Solution for Molecular Diagnostics Devices

TAMÁS PARDY

TALLINN UNIVERSITY OF TECHNOLOGY
School of Information Technologies
Thomas Johann Seebeck Department of Electronics

This dissertation was accepted for the defense of the degree of Doctor of Philosophy in Electronics and Telecommunication on November 15th 2017

Supervisor: **Professor Toomas Rang**
Thomas Johann Seebeck Department of Electronics,
Tallinn University of Technology, Tallinn, Estonia

Co-supervisors: **Indrek Tulp, Ph.D.**
Selfdiagnostics Deutschland GmbH, Leipzig, Germany

Ants Koel, Ph.D.
Thomas Johann Seebeck Department of Electronics,
Tallinn University of Technology, Tallinn, Estonia

Opponents: **Professor Márta Rencz – Istvánné Kerecsen**
Department of Electron Devices, Budapest University
of Technology and Economics, Budapest, Hungary

Professor Ørjan Grøttem Martinsen
Department of Physics, The Faculty of Mathematics
and Natural Sciences, University of Oslo, Oslo, Norway

Defense of the thesis: January 15th, 2018, Tallinn

Declaration:
Hereby I declare that this doctoral thesis, my original investigation and achievement, submitted for the doctoral degree at Tallinn University of Technology has not been submitted for any academic degree.

Tamas Pardy

Mikrosoojendamine molekulaardiagnostika seadistes

TAMÁS PARDY

Table of Contents

ABSTRACT

Novel molecular diagnostics devices, primarily nucleic acid amplification tests (NAAT) mandate the use of precise temperature control. Lab-on-a-Chip (LoC) devices are self-contained molecular diagnostics devices, meaning they rely on no additional external instrumentation, thus the term non-instrumented NAAT (NINAAT). Integrating microheating into a non-instrumented molecular diagnostics device is challenging due mainly to the restrictions on cost, space and power. This limits commercialization efforts and therefore widespread use of rapid tests that would otherwise help decentralize clinical diagnostics, reduce waiting times for patients and healthcare costs in general.

This PhD thesis proposes a workflow and methodology for the development of temperature control for non-instrumented molecular diagnostics devices and demonstrates its application to a LoC NINAAT device, called the InTime NINAAT. In its first part the thesis details the evaluation process for temperature control options as well as describes the evaluation of four microheating options, namely chemical heating, self-regulating electrical heating, thermostat-regulated electrical heating and thermoelectric heating. For the evaluation, physical and simulated thermal models are constructed. These thermal models are simplified representations of the molecular diagnostics device in development and are used solely for thermal analysis. The thesis proposes self-regulating heating and thermostat-regulated heating for use as integrated microheating candidates and demonstrates that both are capable of temperature regulation in the specified target range with 0.5 °C steady-state error (SSE) in the LoC NINAAT system being developed.

The second part of the work describes the process by which the proposed microheating candidates are developed further and prepared for integration with the molecular diagnostics device. This part describes how to evaluate the candidates for multiple assay targets (demonstrated in the thesis through isothermal NAAT protocols) as well as in-detailed thermal analysis for a single assay target (the LAMP protocol in this work). Both microheating candidates developed for the NINAAT platform were demonstrated compliant with assay requirements and could maintain target temperatures for the LAMP protocol in 95% of the reaction volume in steady state as calculated from simulated thermal models. The self-regulating heating candidate was chosen as the final solution due to its simplicity and lower cost compared to the alternative. A microheating solution was proposed based on a polymer resin PTCR self-regulating heater for use with the functional prototype of the NINAAT microfluidic chip. The heating solution was demonstrated to be capable of maintaining reaction temperatures in the required 60-63 °C range for 20 minutes powered by 2xAAA alkaline batteries

and to reach the target range in 10 minutes. From the simulated thermal model, it was calculated that about 85% of the reaction volume was in range in steady state. In a final experiment the functional prototype NAAT chip along with the microheating solution were demonstrated capable of executing the LAMP protocol and successfully detected the target DNA.

The final part details the integration of the microheating solution into the functional prototype of the developed molecular diagnostics device. In this part the proposed microheating solution is integrated into the InTime NINAAT functional prototype device, complete with all fluidic and user interface functions. The InTime NINAAT device is a self-contained non-instrumented NAAT platform that carries a DNA amplification workflow from sample input to result output. After integrating the heater and a final compliance check, the device is demonstrated to work, as it would be used by the end-user.

ACKNOWLEDGEMENTS

LIST OF PUBLICATIONS

The work of this thesis is based on the following publications, copies of which can be found in the Appendices (A-E):

A   **Tamas Pardy**, Toomas Rang, Indrek Tulp

"Finite element modelling of the resistive heating of disposable molecular diagnostics devices", WIT Transactions on Modelling and Simulation, 2015, pp. 381–391. (ETIS 3.1)

B   **Tamas Pardy**, Toomas Rang, Indrek Tulp

"Finite Element Modelling for the Optimization of Microheating in Disposable Molecular Diagnostics", International Journal of Computational Methods and Experimental Measurements, vol. 5, no. 1, pp. 13–22, Jan. 2017. (ETIS 3.1)

C   **Tamas Pardy**, Toomas Rang, Indrek Tulp

"Modelling and experimental characterisation of thermoelectric heating for molecular diagnostics devices", The 16th Biennial Baltic Electronics Conference, 2016, pp. 27–30. (ETIS 3.1)

D   **Tamas Pardy**, Toomas Rang, Indrek Tulp

"Development of Temperature Control Solutions for Non-Instrumented Nucleic Acid Amplification Tests (NINAAT)", Micromachines, vol. 8, no. 7, p. 180, Jun. 2017. (ETIS 1.1)

E   **Tamas Pardy**, Indrek Tulp, Clemens Kremer

"Microfluidic test device", PA 2017 70310 (patent application)

OTHER RELATED PUBLICATIONS

F **Tamas Pardy**, Toomas Rang, Indrek Tulp

"Finite element modelling of the resistive heating of disposable molecular diagnostics devices", WIT Transactions on Modelling and Simulation, 2015, pp. 381–391. (ETIS 3.1)

G **Tamas Pardy**, Toomas Rang, Indrek Tulp

 "Chemical heating for non-instrumented nucleic acid amplification on Lab-on-a-Chip devices", VIII. Annual Conference of the Estonian National Doctoral School in Information and Communication Technologies, Tallinn, 2014, vol. VIII., pp. 95–98.

AUTHOR'S CONTRIBUTION TO THE PUBLICATIONS

Contribution to the papers in this thesis are:

A   The author proposed the use of self-regulating electrical heating elements in conjunction with the developed molecular diagnostics device, designed the experimental setup (thermal model) based on device specifications and core chip schematics from the supervisors. The author performed the experiments, processed measurement data, built the finite element model and did the comparison of results. The author wrote the paper and supervisors helped with revision.

B   The author proposed thermostat-regulated electrical heating for use with the developed molecular diagnostics device as well as designed and built the prototype thermostats and experimental setup (thermal model) in compliance with device specifications and core chip schematics provided by the supervisors. The author performed the experiments, processed results and constructed the finite element model as well as compared simulation and measurement results. The author wrote the paper and supervisors helped with revision.

C   The author proposed thermoelectric heating as a microheating option for use with the developed molecular diagnostics device. The author built the thermal model for use with the core chip prototype provided by supervisors, in compliance with device specifications. The author performed experiments, constructed the finite element model and evaluated data as well as compared simulated and experimental results. The author wrote the paper and supervisors helped with revision.

D   The author proposed the experimental methodology described in the paper as well as designed experimental setups and built finite element thermal models. The author performed the experiments and evaluated data as well as reached the conclusions detailed in the article. The author wrote the paper and supervisors helped with revision.

E   The author contributed to this patent as inventor, and with specific technical information regarding the microheating component and certain other technical details regarding the structure of the test device relevant to his field. During the device development project that led to filing this patent, the author was responsible for the development of the heating element and temperature regulation as a whole for the molecular diagnostics device developed. The author contributed with several thermal models (design and manufacturing), thermal and electrical characterization, simulations as well as evaluation and interpretation of results.

Abbreviations

Explanations of the abbreviations used in the thesis:

ABS	Acrylonitrile Butadiene Styrene
CAD	Computer Aided Design
CMOS	Complementary Metal-Oxide-Semiconductor
CNC	Computer Numerical Control
COTS	Commercial Off-The-Shelf
DLP	Digital Light Processing
DNA	Deoxyribonucleic Acid
GUI	Graphical User Interface
HIV	Human Immunodeficiency Virus
LAMP	Loop-Mediated Isothermal Amplification
LED	Light-Emitting Diode
LF	Lateral Flow
LoC	Lab-On-A-Chip
LOD	Limit Of Detection
MAE	Mean Absolute Error
NAAT	Nucleic Acid Amplification Test
NINAAT	Non-Instrumented Nucleic Acid Amplification Test
PCM	Phase-Change Materials
PCR	Polymerase Chain Reaction
PID	Proportional-Integral-Derivative
PMMA	Polymethyl Methacrylate

PTC   Positive Temperature Coefficient

PTCR   Positive Temperature Coefficient Of Resistance

qLAMP   Quantitative LAMP

RDT   Rapid Diagnostic Test

SSE   Steady-State Error

STD   Sexually Transmitted Disease

WHO   World Health Organization

List of Figures

List of Tables

INTRODUCTION AND MOTIVATION

Novel approaches to medical diagnostics and in particular, molecular diagnostics, such as Lab-on-a-Chip (LoC) devices, promise to bring diagnostic tools to a much wider audience than traditional clinical diagnostics practices [1], [2]. Some of these devices are designed for use at decentralized clinics, brining testing to the point of care [3]–[6], reducing waiting lines and healthcare costs through early diagnosis, while others are targeted for use in homecare.

According to data collected by the WHO (World Health Organization), the number of deaths worldwide associated with infectious diseases has decreased significantly since 1990 in comparison with other causes, such as injuries [7]. On the other hand, in low-income regions, infectious diseases were still among the leading causes of death in 2010 and large-scale outbreaks, such as the 2014 Ebola outbreak in West Africa, continue to occur [8]. According to a WHO report, between 2001 and 2013, 84% of all health hazards worldwide were due to infectious disease outbreaks [9]. Pathogens with long incubation times and potentially severe complications are of great concern, even in highly developed regions of the world. Sexually transmitted diseases (STD) have a high prevalence in high-income regions such as the USA, are passed on easily from host to host before symptoms occur, and may cause infertility [10]. Early detection and treatment to prevent or contain outbreaks is paramount. Rapid diagnostic tests (RDTs) are molecular diagnostic tests that meet the ASSURED (affordable, sensitive, specific, user-friendly, rapid, equipment-free and delivered) guidelines of the WHO [11]. First generation RDTs are typically cheap (<50 EUR per test), disposable tests that rely on immunoassays [12], such as the well-known pregnancy tests. They are readily available in pharmacies for various pathogen targets (HIV-1, Chlamydia Trachomatis etc.), but they cannot detect pathogens without an immune response from the host, which takes several days to build up, during which time the host is already infectious. Thus, they are inefficient at preventing outbreaks. Second-generation RDTs on the other hand rely on novel molecular diagnostics methods that are on par with clinical diagnostics. RDTs as bases of treatment have a low acceptance rate among medical doctors at present, but the market demand for a reliable second-generation RDT is strong. Their predicted share in the RDT market is in the range of 10 billion USD by 2021 [13].

In pathogen detection, nucleic acid amplification testing (NAAT) has been the long-standing gold standard with the PCR (polymerase chain reaction) protocol the most widespread [14]–[17]. PCR requires thermal cycling with high temperatures (up to 96 °C) maintained for well-defined durations in each cycle, and the cycles repeated 20-40 times until the desired DNA concentration is achieved. This practice requires sophisticated equipment that is hard to build into handheld, portable devices. Isothermal NAAT protocols on the other hand require only a single temperature or temperature range to be maintained for a specified amplification time [18]–[21], making them more suitable for use in Lab-on-a-Chip applications. These protocols mostly require reaction temperatures in the

30-70 °C range and incubation times are typically less than an hour. In the ideal case, a LoC NAAT device should be fully disposable, self-contained and non-instrumented [22]–[25]. Self-contained and non-instrumented devices require no external instrumentation and are capable of performing a complete diagnostic workflow from sample input to result output. However, implementing temperature control in a non-instrumented nucleic acid amplification test (NINAAT) is technically challenging, given the constraints on space, power and cost. These constraints make commercialization efforts difficult and thus slow down the distribution of these devices to the public.

Most existing LoC devices in the literature are instrumented and rely on external means for temperature control, such as Peltier cells [26]–[29] or pre-heated liquids [30] introduced via channels surrounding the reaction volume. However, a fully portable system requires an integrated solution. Electrical heating is well known and widely used in consumer electronics, however, integration into Lab-on-a-Chip systems is challenging for the reasons mentioned before. The heating element may be integrated into the device frame, or the Lab-on-a-Chip itself. For the former approach, most reported works use Peltier cells [31]–[34], for the latter, primarily thin film resistive heating elements [35]–[37] but also micro-Peltier cells [33], [34], [38]. In the case of microfabricated LoC systems, the thin film heater can be integrated on the same substrate as the fluidic channels, resulting in a more compact and power-efficient layout. On the other hand, the previously mentioned heating elements all required external thermostats, which may limit integration. Self-regulating resistive heating elements [39]–[41] rely on the PTCR (positive temperature coefficient of resistance effect) for regulation: the resistance of the element increases rapidly beyond a threshold temperature, thereby regulating input currents. These elements offer an attractive solution for integrated heating [42], but their power efficiency may be lower than that of thermostat-regulated elements. An interesting alternative is offered by chemical heating, which is a heating element based on a highly exothermic chemical reaction of two or more components [43], [44], typically an oxidative process regulated by the addition of a phase-change material (PCM). Advantages are their low cost and simplicity; disadvantages are their large size and the difficult regulation of their temperature output.

Despite the earlier mentioned challenge of realizing portable thermal cycling, many LoC systems with integrated heating reported in the literature execute the PCR protocol [36], [45]. There are examples of devices performing isothermal amplification protocols as well [46]–[48]. The Alere Influenza A&B [49], [50] is a benchtop instrument that relies on isothermal NAAT for a rapid influenza test on par with clinical diagnostics procedures in accuracy. However, it is not a handheld instrument. Some LoC NAAT chips exist that are more portable but require external heating [51]–[53]. Chemical heating was demonstrated in literature [54]–[56] and patented [57] as an integrated heater for LoC NAAT devices. Recently a highly integrated compact CMOS NAAT chip was

demonstrated by Gurrala et al. for HIV-1 detection with a very high sensitivity [58], but the demonstrated chip lacked integrated temperature regulation (but included a heating element) and a power source.

Using microfabricated LoC devices with on-dye heating solutions is attractive in research but less cost-effective in mass-production due to the need of highly specialized microfabrication techniques as well as a clean room. Injection molded plastics are better suited for mass-production, primarily due to the low per-device cost and the high aspect ratio achievable in mass-production [59]–[61]. Furthermore, they do not require a clean room. However, mold fabrication is expensive and so design errors should be avoided. Finite element thermal analysis can greatly reduce development time and design errors by providing a tool to analyze heat transfer and thermally optimize device geometry and insulation. Most research efforts have targeted the thermal analysis of integrated heating elements developed in-house, primarily within the same clean room process as the fluidic chip itself [62]–[64]. However, injection-molded plastics require a separately manufactured heating element - preferably a commercially available heating element – that requires optimization of the thermal system.

PROBLEM STATEMENT AND RESEARCH QUESTIONS

As detailed in the introduction, there are no off-the-shelf solutions suitable for temperature control in a non-instrumented molecular diagnostics platform. There are many temperature regulation options available on the market and in research, but none of them particularly suited for our proposed application as is. The implementation of a microheating solution is challenging due to the factors detailed in the introduction.

This PhD work will focus on the development of temperature regulation for non-instrumented molecular diagnostics devices and a disposable LoC NINAAT device in particular. It will 1) evaluate available temperature control options, 2) detail the process by which these options are characterized and evaluated for use in the proposed diagnostics device as well as the optimization process by which the best candidate(s) are integrated into the device, and 3) demonstrate the functional prototype of a NINAAT device. This PhD work, while it aims to provide guidelines for the development of a microheating solution for molecular diagnostics devices, will also demonstrate a complete microheating development process for a specific device, from start to finish.

Summarily, this PhD work focuses on the following research questions:

1. What temperature control options are available for use in non-instrumented molecular diagnostics devices?
2. What are the performance characteristics of these options related to the NINAAT concept device in this work?
3. What are the most suitable temperature control options for the NINAAT concept device?
4. How to evaluate the performance characteristics of a microheating candidate for multiple assay protocols?
5. What are the performance characteristics of the microheating candidates in this work related to isothermal NAAT protocols and the LAMP protocol in particular?
6. How is a microheating option developed into a microheating solution optimized for use in a particular molecular diagnostics device?
7. How is a microheating solution integrated into a molecular diagnostics device?
8. What is the development workflow of temperature regulation for a non-instrumented molecular diagnostics device?
9. How can thermal analysis via the finite element method aid in this development process?

CONTRIBUTION OF THE THESIS

As mentioned before, this thesis aims to demonstrate the process by which temperature regulation is developed for use in non-instrumented molecular diagnostics devices. Furthermore, it demonstrates the development process of a particular non-instrumented molecular diagnostics device built for the execution of isothermal NAAT protocols and the LAMP protocol in particular. The main contributions (i.e. theses/claims) of this PhD thesis are:

I. The methodology to characterize and evaluate microheating options for their use in molecular diagnostics devices: experimental characterization and finite element modelling of heat transfer. In particular, the proposal of whole-device thermal modelling via the finite element method rather than solely focusing on the heater-chip thermal interface.

II. Application of the methodology in Contribution I. to evaluate four microheating options for a portable NAAT device. All options were characterized experimentally as well as modelled via the finite element method: chemical heating, self-regulating resistive heating, thermostat-regulated resistive heating and thermoelectric heating. Physical, as well as simulated thermal models of the diagnostics device were created for the evaluation. Chemical and thermoelectric heating were proven unsuitable for the targeted application, whereas self-regulated and thermostat-regulated heating were established as microheating candidates.

III. The methodology and the development process by which microheating candidates are developed into microheating solutions for application in the functional prototype of a molecular diagnostics device. Testing for additional temperature targets, geometry optimization and heat transfer analysis via finite element modelling are described.

IV. Application of the methodology in Contribution II. to develop two microheating candidates into microheating solutions for use in the functional prototype of the developed molecular diagnostics device. Both self-regulating and thermostat-regulated heating were demonstrated to comply with requirements for the loop-mediated isothermal amplification (LAMP) protocol. Both temperature control methods had less than 0.6 °C SSE for the prescribed 20 minutes incubation time and 62 ± 2 °C incubation temperature. Finally, self-regulating resistive heating was chosen as the microheating solution for the proof-of-concept prototype due to its lower complexity and cost. A PTCR polymer resin self-regulating heating element is demonstrated and evaluated for use in the functional prototype. In

the proof-of-concept demonstration detailed in this work, the Lab-on-a-Chip functional prototype in conjunction with the aforementioned polymer heating element was capable of executing a LAMP reaction that successfully detected a pathogen.

V.   The microheating solution developed for the InTime NINAAT (Non-Instrumented Nucleic Acid Amplification Test) functional prototype and its proof-of-concept demonstration. The demonstration involved executing the test, as it would be at the end-user side, starting with sample input and finishing with visualizing results for a successfully executed amplification of the target pathogen's DNA.

The above-mentioned contributions are related to research papers (listed previously and available in full in appendices A-E) as described in Table 1. The thesis contains unpublished work that extends beyond the listed research papers.

Table 1: Contributions partially or fully covered in published works

Contributions	Paper A	Paper B	Paper C	Paper D	Paper E
I.	✓	✓	✓		
II.	✓	✓	✓		
III.				✓	
IV.	✓	✓		✓	
V.					✓

ORGANIZATION OF THE THESIS

This PhD thesis is divided into 5 chapters. The introductory chapter introduced the background and motivation of the research work including research trends to date related to microheating in molecular diagnostics devices.

Chapters 1-3 detail the development process of microheating solutions in general and in relation to the NINAAT device prototype demonstrated in Chapter 3.

Chapter 1 describes the characterization and evaluation of microheating options chosen based on literature and patent search. The options most suitable for use in the targeted device concept are developed further as microheating candidates

Chapter 2 details how microheating candidates compliant with device requirements are evaluated further for their use in the functional prototype of the molecular diagnostics device under development, and steps are taken to integrate them with the Lab-on-a-Chip component of the device. Please note that a microheating candidate is not necessarily a single specific heating element but rather a heating principle. At the end of the chapter, a microheating solution optimized for the molecular diagnostics device is presented.

Chapter 3 demonstrates integration and final validation of the microheating solution in the context of the functional prototype of the molecular diagnostics device under development. A proof-of-concept demonstration of the diagnostic test as would be executed by the end-user is presented at the conclusion of this chapter.

The final chapter is the conclusion of this PhD thesis.

Figure 1 below shows how chapters cover the complete development process of a temperature control solution for non-instrumented molecular diagnostics devices:
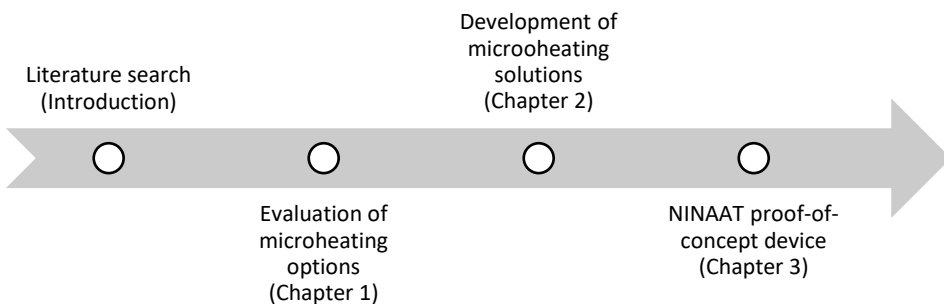
Figure 1: Chapters in this work and how they relate to the heater development workflow

1 CHARACTERIZATION AND EVALUATION OF MICROHEATING OPTIONS

This chapter covers the following topics:

- Methodology by which to analyze and evaluate integrated microheating options for their viability in molecular diagnostics devices,
- Literature results to date,
- Outcome of the evaluation of microheating candidates conducted during this PhD work.

This PhD work primarily focuses on disposable, non-instrumented isothermal nucleic acid amplification tests (NAAT) that require reaction temperatures in the 20-65 °C range [18], but the methodology described in Chapter 1-2 is applicable to other molecular diagnostics assays as well, provided that they are performed in aqueous solutions. Being non-instrumented means that no additional instrumentation is required to perform the test, the device arrives in a single package as self-contained unit [56], [65], [66]. Being disposable means that as a minimum, the part of the device exposed to the biological sample must be disposable in household waste. Ideally, the whole device should be disposable.

1.1 Characterization and evaluation methodology

The core of the thermal system in a non-instrumented molecular diagnostics device is composed of the heating element, the reaction chamber and the thermal interface in between them. This core must be thermally insulated from the rest of the device as well as from the ambient environment. The goal of the evaluation is to determine whether the heated reaction volume is in the correct temperature range for the incubation time specified by the assay. In this section we cover the experimental characterization and evaluation process, as well as describe the instrumentation, prototypes and methodology used in this PhD work and in this chapter of the work in particular.

1.1.1 Experimental characterization and evaluation

Before development begins, requirement specifications for the device are drafted, followed by literature and patent search as well as analyzing user requirements. Once a microheating candidate is selected, the process for experimental characterization and evaluation is the following (Figure 2):

1. **Basic characterization**: Dimensions are characterized first. In the case of electrical heating elements, the heating element is characterized electrically (base resistance and steady-state resistance if applies, input voltage range). If compliance with basic operational parameters (power supply, dimensions) is established, step 2 follows.
2. **Functional characterization**: The heating element is characterized in context of the molecular diagnostics device. This is achieved by building a thermal model and equipping it with temperature sensors in key

positions (see details below), then measuring transient thermal response. This means applying a certain input (voltage/current/amount of chemical fuel) and measuring temperature in the reaction chamber. This defines a specific steady-state temperature and thermal time constant for a given input. Again, a compliance check follows for the following parameters: reaction temperature (steady-state temperature), incubation time and total assay time (derived from the time constant).

3. **Evaluation**: If compliance is established in both steps, the microheating candidate is considered for further development. If not, the candidate is discarded and the process starts again from step 1 with a new candidate. Following successful evaluation, the candidate is modelled via the finite element method (see Section 1.1.2) to aid in future development, and the simulated model is validated using experimental data.

For the experimental thermal characterization we use simplified or defeatured thermal models of a particular molecular diagnostics device. In this work, physical prototypes represent different design iterations of the same device. There are several key device components in a thermal model:

- **Core chip**: A Lab-on-a-Chip (LoC) module that houses the reaction chamber and performs liquid handling functions via microfluidic channels. The model is heavily defeatured to simplify prototyping and save cost.
- **Reaction chamber** (reactor): The heated reaction chamber where the reaction takes place.
- **Heater** (heating element): The heating element or device that is directly interfaced with the core chip, and provides the correct reaction temperature for the prescribed incubation time.
- **Temperature regulation**: A method or instrument by which the heat output of the heater is regulated.
- **Thermal interface**: The core chip-heater thermal interface is a particularly important component. No thermal interface material was used, as the modelled device was planned to have a disposable chip.
- **Housing**: The device frame that houses the core chip and the heater
- **Temperature sensor**(s): Digital thermometer probes: temperature sensors are placed in key positions inside the thermal model.
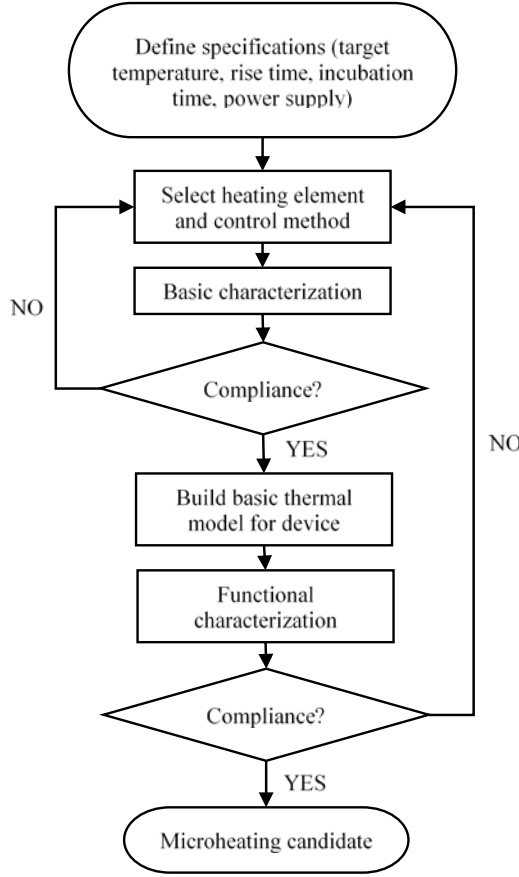
Figure 2: Experimental characterization and evaluation process of microheating candidates

1.1.2 Finite element model for thermal analysis

Thermal analysis via finite element modelling provides a tool to analyze spatial or spatiotemporal heat distribution in a simulated thermal model. It is best to build a simulated thermal model for a particular microheating solution and device concept after the experimental evaluation process established compliance with specifications (Figure 2). Once the microheating model is in place and experimentally validated, device geometry can be modified as needed according to future developments.

Modelling efforts in the literature to date have primarily focused on modelling in-house heater developments, primarily thin film heaters built in the same clean room process as the core chip itself [67]–[69], with a focus on the chip-heater thermal interface. In this chapter, we focus on whole-device models with commercially available heaters. Modelling commercially available heaters is

challenging due to the scarcity of material data the manufacturers disclose. However, for a molecular diagnostics device targeted at the commercial market, in-house heater development comes with a higher risk and higher cost than adapting commercial heaters. Whole-device modelling is a novel approach that is an improvement above thermal interface models of the past. As compared to solely modelling the chip-heater thermal interface, whole-device modelling reveals far more data and provides better insight into the thermal system of the device under study, such as (Figure 3):

- The heat distribution in the reaction chamber. For instance, the LAMP protocol requires 60-65 °C reaction temperature, which can be verified by modelling.
- Surface temperature modelling (user safety evaluation): standard IEC60601-1 mandates a maximum of 45 °C surface temperature for a skin exposure of less than 1 minute. Compliance can be checked by modelling.
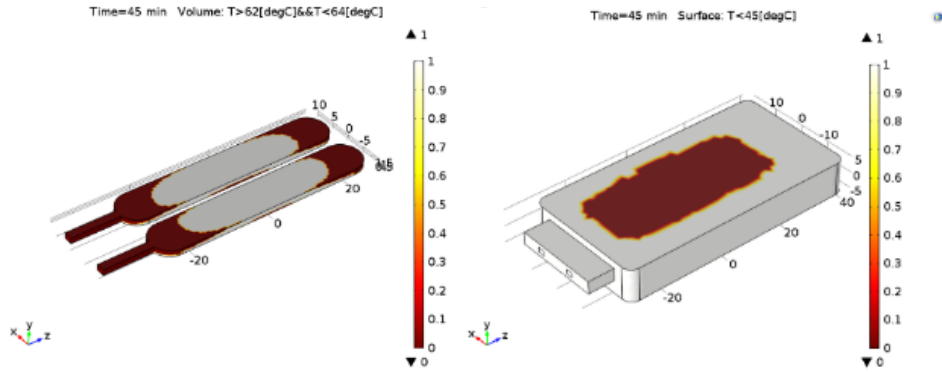
Figure 3: Examples for reaction temperature compliance check (left) and device surface temperature compliance check (right) using a simulated thermal model

On the other hand, the added complexity of whole-device modelling involves a higher computational space requirement as well as more potential sources of simulation errors than interface modelling, thus great care must be taken to match boundary conditions and initial parameters to experimental data.

The thermal model used in this PhD work consists of two main components: a heat generation and a heat distribution model. In the molecular diagnostics devices modelled in this work, the reaction liquid is stationary for the incubation time, thus we need not factor flow into our equations. Thermal models used in this work are built and solved in COMSOL® Multiphysics (version 5.2).

Heat distribution model

We primarily model spatial heat/temperature distribution in three-dimensional models. Heat distribution is modelled with the well-known heat transfer equation in the following form [70]:

$$\rho C_p \frac{\partial T}{\partial t} - \nabla q = Q$$
$$q = -k\nabla T$$

(1)

where ρ [kg/m³] is the density of the medium, C_p [J/kg K] the specific heat capacity at constant pressure, T [K] the absolute temperature in the system, k [W/(mK)] the thermal conductivity, t [s] is the time, and Q [W/m³] is the heat source (sink). The heat generation model is coupled with the heat distribution model through Q. Convective, conductive and radiative heat losses are calculated on the external boundaries as boundary conditions. This model is valid if the modelled physical prototype is in a temperature-controlled, sealed environment with restricted ventilation. Ideally the physical thermal model is sealed in a climate chamber, but a closed, air conditioned laboratory is also sufficient. Through these conditions, we avoid having to perform conjugate heat transfer analysis, saving on computational space. The heat distribution model is solved via the Heat Transfer interface of COMSOL. Temperature sensors in the physical thermal model were modelled as Domain Point Probes.

Heat generation model

We will use two heat generation models in this work, one for chemical heating and one for electrical heating. In this section, we will describe the base model. For each specific microheating option, their respective section will describe additional model components.

Chemical heating model: The chemical heating model consists of two sets of equations: reaction heat generation is modelled by a reaction model and reaction species concentrations are calculated from a convection-diffusion model. A two-component exothermic reaction is considered for modelling, namely an A + B → C reaction where A is the chemical fuel, B is water and C is the product species. Reaction rate R_i [mol/(m³s)] for chemical species i is calculated as the product of the species concentration c_i [mol/m³] of all other species and rate constant k (calculated from the well-known Arrhenius equation). Species transport is calculated from the convection-diffusion equation in the following form:

$$\nabla \cdot (-D_i \nabla c_i) + \underline{u} \cdot \nabla c_i = R_i$$

(2)

Where D_i [m²/s] is the diffusion coefficient, $\underline{u}$ [m/s] the flow velocity of the flow field. Walls have a no-diffusion boundary condition. Reaction heat Q [W/m³] is

calculated as the product of the reaction rate and the enthalpy of formation H [J/mol] of the product species.

Electrical heating model: The electrical heating model is a Joule heating model with additional input terms for each specific heating element. The model consists of two sets of equations. Heat generation is expressed by the formula of power $\frac{dP}{dV_{heater}} = J \cdot E$ [71] where P [W] is the power, V_{heater} [m^3] the volume of the heating element, J [A/m^2] the current density, and E [V/m] the electric field. Fields J and E are derived from the following set of equations [72]:

$$\nabla J = Q_j$$

$$J = \left(\sigma + \varepsilon_0 \varepsilon_r \frac{\partial}{\partial t}\right) E + J_e \qquad (3)$$

$$E = -\nabla V$$

where Q_j [A/m^3] are current sources (sinks), J_e [A/m^2] the external current density (if there is one), V [V] the potential drop in all directions, σ [S/m] the conductivity, ε_0 the relative permittivity of vacuum, and ε_r the relative permittivity of the material at the point of the geometry where the equations are evaluated. The materials in the simulated geometry are characterized electrically through their conductivity and relative permittivity, whereas heat transfer properties are characterized by their density (ρ [kg/m^3]), heat conductivity (k [W/(m · K)]), and specific heat capacity (C_p [J/kg · K]) for each spatial point of the geometry. The electrical heating model is solved via the Electrical Currents interface in COMSOL and is coupled with the heat distribution model through the Joule Heating interface.

Domains, boundaries, meshing and performance

As mentioned before, whole-device models were built in this work. Device geometry was imported from Auotdesk Inventor in the form of three-dimensional CAD (computer-aided design) models. Boundary conditions and initial parameters were derived from the physical prototypes used for experimental characterization. Wires and screws were removed from the simulated model to decrease mesh complexity, and where applicable, axes of symmetry were used to cut the geometry. All physical domains are to be taken into account in the simulated model, but please note that in the case of prototypes described in later chapters, simulated prototypes were heavily defeatured and simplified to reduce computation space requirements. For all models, COMSOL generated tetrahedral meshes. For the model of each specific microheating option in this chapter we will display the average mesh element quality as calculated by the widely used radius ratio method [73]. Models were solved on a desktop computer with an Intel Core i5-4570 CPU and 16 GB RAM plus a 256 GB SSD storage. Solution times ranged from 2 minutes to 1 hour depending on model complexity.

1.1.3 Specifications for this PhD work

The specifications will be the same for all microheating options evaluated in this PhD work, and at the end of this chapter, they will be compared with respect to their compliance with these specifications. As mentioned in the introduction, the developed device will execute the LAMP protocol, which is a highly sensitive and specific DNA amplification method developed by Eiken Chemical Co. that requires incubation for 15–60 min at 60–65 °C temperature [74]. Despite LAMP being the chosen protocol, in this chapter we will evaluate heater options for the 25-65 °C temperature range, which covers most isothermal NAAT protocols [18], should the need arise to switch the protocol.

Table 2: Specifications for the evaluation of microheating options in this chapter

	Property	Value
Basic requirements	Total dimensions	60 mm (W) x 120 mm (L) x 60 mm (H)
	Cost in mass-production	Max. 5 - 6 EUR
	Ambient temperature	22 – 24 °C
	Disposability	No hazardous/toxic parts allowed
Assay requirements	Reaction chamber temperature limits (lower; upper)	25 °C; 65 °C
	Temperature regulation SSE	1 °C
	Reaction target temperature	62.5 ± 2.5 °C
	Heat up time	10 minutes
	Incubation time	20 minutes

1.1.4 Test setups and instrumentation

For measuring dimensions, a digital caliper was used. For the basic electrical characterization (see Section 1.1.1), an Agilent 34410A Digital Multimeter was used.

The test setups used for functional characterization (see Section 1.1.1) consisted of:

1. A thermal model according to principles detailed in Section 1.1.1.
2. Digital thermometer:
    a. 10 kΩ NTC thermistors connected to the aforementioned digital multimeter.
    b. K-type thermocouples connected to a TENMA 72-7715 digital thermometer
3. Agilent E3631A Triple Output DC Power Supply (for electrical heating only)

Injection molded plastics are becoming vastly popular [75], [76] for molecular diagnostics devices designed for commercial applications due to the low per-device cost and high aspect ratio achievable in mass-production. Rapid prototyping methods help in upscaling designs. In this PhD work, two rapid prototyping methods were used for fabricating prototypes: 3D printing and milling. The substrate of choice were ABS (acrylonitrile butadiene styrene) for the former and PMMA (polymethyl methacrylate) for the latter. For 3D printing, a DLP (digital light processing) printer (Envisiontec Perfactory XL), for milling, a CNC (computer numerical control) milling machine (Datron M7 HP) was used.

The thermal model consisted of the following components:

- **Core chip** (Figure 4): In this chapter, we used 2 core chips: (1) a plastic chip (75 mm x 25 mm x 3.5 mm) with 2 reaction chambers and (2) a glass chip (30 mm x 20 mm x 3.5 mm) with 1 reaction chamber.
- **Reaction chamber** (Figure 4): The reaction chamber in core chip (1) was designed to hold 0.7 ml liquid, whereas in (2) was designed to hold 0.05 ml.
- **Heater** (Figure 5): The heating element or device that is directly interfaced with the core chip, and provides the correct reaction temperature for the prescribed incubation time.
- **Temperature regulation**: Temperature regulation methodologies will be detailed along with the microheating options in this chapter.
- **Thermal interface**: In the devices demonstrated in this PhD work, the thermal interface is a flat contact with no thermal interface material between two plastic, or plastic and metal surfaces.
- **Housing** (Figure 6): Dimensions for each housing concept will be detailed with the respective microheating options.

The thermal model designs for each microheating option/device concept tested in this Chapter are shown in Figure 6 and listed below:

- Chemical heating (Figure 6/A)
- Self-regulating resistive heating (Figure 6/B)
- Thermostat-regulated resistive heating (Figure 6/C)
- Thermoelectric heating (Figure 6/D)
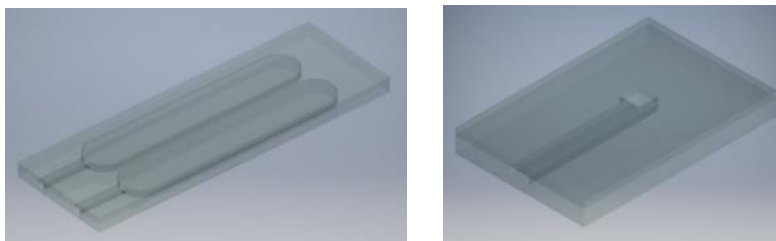
Figure 4: Core chip prototypes used in this section with the reaction chambers in view
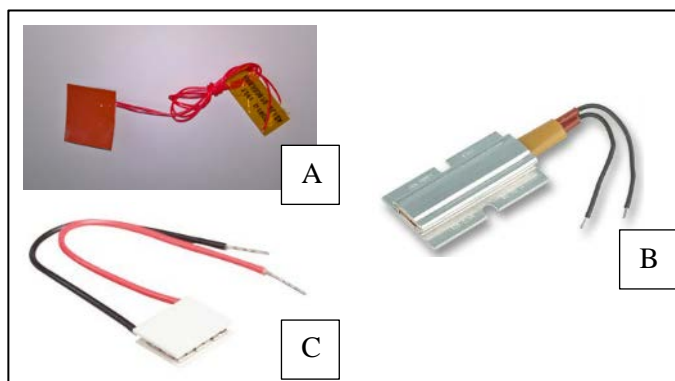
Figure 5: Electrical heating elements tested in this chapter[1]

[1] B: http://uk.farnell.com/dbk/hp04-1-04-24/heater-ptc-f-plate-10w/dp/4408329, C: http://uk.farnell.com/european-thermodynamics/aphc-03107-s/peltier-cooler-module-3-6vdc-17w/dp/2484938
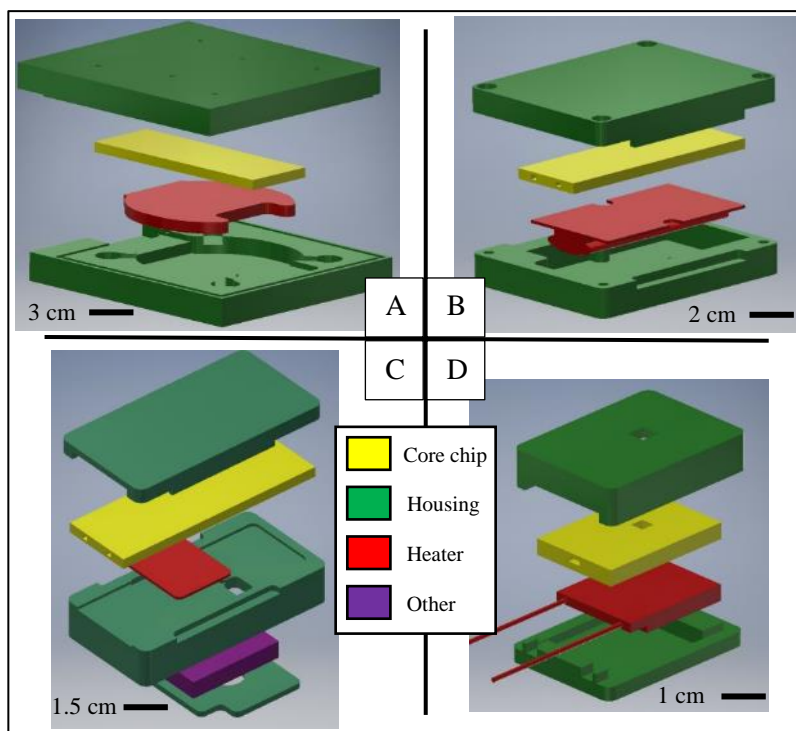
Figure 6: Thermal models for each microheating option and housing concept

Given the fact that we target to develop a Point-of-Care molecular diagnostics device, test conditions were selected to simulate the target environment on the end-user side. Tests were conducted in free air, in an air conditioned lab at room temperature (22-24 °C ambient), with minimal ventilation.

1.2 Chemical heating

Chemical heating relies on heat release from highly exothermic chemical reactions, which are typically regulated by the additional of engineered phase-change materials (PCM) that melt in a specific temperature range and carry away the excess heat [55], [65], [77], [78]. In the context of molecular diagnostics tests, chemical heating would be a cheap and simple heating method, but the development risk is higher than for electrical heating methods due to the highly nonlinear heat release profile and difficult temperature regulation [52], [56]. In this PhD work, we will deal with two types of reactions in particular: salt hydration reactions and corrosive reactions. The most prominent literature example for salt hydration is the device of LaBarre et al. [54], [56], [79] that relied on a calcium oxide hydration reaction ($CaO(s) + H_2O(l) \rightleftharpoons Ca(OH)_2(aq) + heat$). While CaO is easy to acquire, its quality and heat output may vary heavily. For salt hydration reactions, the volume change of the salt must be taken into account in the design. The most widely used implementation of a corrosive reaction is the flameless ration heater of the US Army [80], [81]. The

34

ration heater relies on a controlled oxidation reaction of a magnesium-iron alloy, initiated by adding water to the mixture (Mg + 2H$_2$O → Mg(OH)$_2$ + H$_2$ + heat), supplemented by salt and carbon to catalyze the galvanic corrosion of iron. The MgFe alloy is a commercially available engineered material that has a consistent heat output and reliable quality. For this reaction, outgassing of hydrogen must be taken into account (0.8 l/g of MgFe). The PATH group successfully demonstrated a nucleic acid amplification test (NAAT) device that relied on the MgFe alloy for heat generation and an engineered PCM for heat regulation [57], [65], which was developed further into a patented test device [57], [66].

We go through the evaluation process as detailed in Section 1.1.1. The specifications are defined in Section 1.1.3. Two specific reactions were evaluated:

1. Lithium bromide salt hydration reaction (LiBr(s) + H$_2$O(l) ⇌ BrH$_2$LiO(aq) + heat)
2. Magnesium-iron alloy corrosive reaction (previously mentioned)

Heat output was regulated by adding Palmitic acid (melting point: 62.9 °C) to the mixture. In the case of lithium bromide, a filter paper layer divided the PCM and the chemical fuel to assure proper hydration. Lithium bromide is toxic if ingested in large amounts, therefore precautions must be taken with its applications. The magnesium-iron alloy has no toxic components.

The volume of the heater cavity was determined experimentally to maximize reaction heat output given that no stirring or other external manipulation was allowed in this microheating option. The cavity was sized for the lithium bromide hydration reaction, intended as the primary candidate. Maximum heat output was achieved with 11 g of material (Table 3), which took 7.5 ml volume. Adding additional space for the PCM, the final heater cavity volume was 11 ml.

Table 3: Experiment to determine chemical heater volume

Water [g]	LiBr [g]	Maximum temperature [°C]
3	5	72
6	5	84
9	5	67

Dimensions of the thermal model were 90 mm (W) x 80 mm (L) x 20 mm (H), which complied with the specifications. The thermal model (see Section 1.1.4) was milled from PMMA plastic to house the plastic core chip with 2 reaction chambers, a cavity for the chemical reaction, four inlets for hydration and two for degassing (Figure 6/A). The plastic housing was encased in a polyurethane mold for thermal insulation.

We did two series of tests, one with each reaction type. In both cases, water and reagent volume were fixed and the PCM volume varied (volumes were calculated to fit the heater cavity). The reagents were filled into the heater cavity of the

thermal model and water was added to start the reaction. In each case, temperature was measured for 10 minutes (past 10 minutes all reactions dropped heat output) and the average temperatures for this duration were compared. Table 4 shows the reagent mixtures and the 10-minute temperature averages for the conducted experiments.

Table 4: Reagent mixtures and average temperature outputs for the first 10 minutes of each conducted chemical heating experiment

H_2O [g]	LiBr [g]	MgFe [g]	PCM [g]	10-minute average [°C]
4	3.5	0	0	36.96
4	3.5	0	1	43.71
4	3.5	0	2	47.61
4	3.5	0	3	39.81
10	0	2	0	48.64
10	0	2	1	41.58
10	0	2	1.5	48.58
10	0	2	2	48.78
10	0	2	2.5	46.81
10	0	2	3	43.89
10	0	2	4	21.57

For the sake of demonstrating a simulated thermal model, LiBr-water reaction was modelled in COMSOL based on the principles detailed in Section 1.1.2. Average mesh element quality was 0.65 (element size: 0.91 mm^3). The finite element model estimated measured temperatures with a MAE of 1.67 ($\pm$ 0.5) °C.
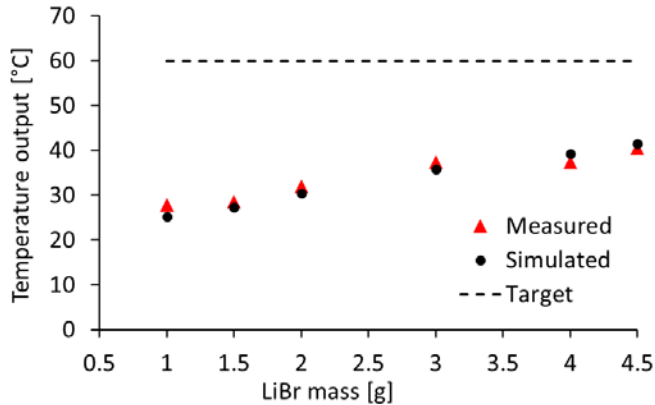
Figure 7: Chemical heating simulated thermal model demonstration

Results from the simulated thermal model are shown in Figure 7.

In conclusion, none of the conducted experiments was capable of producing the required target temperature, therefore compliance with assay specifications was

not established with this microheating option, and the development of chemical heating was halted due to a lack of time and resources. Lithium bromide hydration has the inherent issue that hydrate crystals will start forming very early on in the reaction and enclose lithium bromide inside them, inhibiting the reaction and limiting maximum output without stirring. We attempted to counter this by adding layers of filter paper between lithium bromide layers, but lithium bromide is highly hygroscopic and will immediately gather moisture from the environment, thus making experimentation challenging. As a result, finite element modelling of LiBr hydration is also very challenging as this imperfect hydration is hard to model. Furthermore, LiBr is toxic if ingested, and therefore does not comply with disposability requirements.

1.3 Thermostat-regulated resistive heating elements

Resistive heating is the most well-known and widespread electrical heating method. In the literature, primarily custom-made heater developments are reported, mostly thin film resistive heating elements [82]–[85] in conjunction with external thermostats for temperature regulation. Some of these heaters are integrated with the core chip for improved power efficiency [85], [86]. Using COTS (commercial off-the-shelf) heating elements, such as etched foil heating elements, can reduce development risks and costs (particularly advantageous for research projects), therefore in this section we will focus on integrating COTS heaters. This section reports and extends published work (see also Appendix B).

We proceed by going through the evaluation process as detailed in Section 1.1.1. The specifications are defined in Section 1.1.3. The selected heating element, the Minco HR5303R70.2LI2A (from Minco Products Inc., Fridley, MN, USA), was a heating element made of a resistive film (chrome-nickel) etched to form heating tracks, encased in polyimide and silicone rubber sheets. According to manufacturer data, the (base and steady-state) resistance of the unit was 70.2 Ω [87], which we measured to be $76.38 \pm 0.37 \Omega$. Heater dimensions were measured to be 21.6 mm (L) x 25.4 mm (W). For temperature regulation, we designed and implemented two open-source smart thermostat units based on an Arduino-compatible hardware:

1. **Mini-thermostat**: Thermostat box based on an Arduino Uno. This box has a USB interface and a graphical user interface (GUI). Further details on the mini-thermostat are available in Appendix B, schematics and program code are available online under the GPL 3+ license[2]. Therefore, this thermostat will not be detailed in this section. Dimensions: 62 mm (W) x 112 mm (L) x 35 mm (H)
2. **Micro-thermostat**: Miniaturized version of the thermostat box designed for integration. This prototype was based on an Arduino-compatible

---

[2]URL: https://www.hackster.io/salhar1/mini-thermostat-e732ed

microcontroller board (Adafruit Trinket 3V). Schematics and program code for a basic implementation are available online under the GPL 3+ license[3]. The interface board of the prototype reported in this section was designed in an open-source design software (Fritzing) and implemented on a printed circuit board (Figure 8). Dimensions: 20 mm (W) x 30 mm (L) x 6 mm (H).
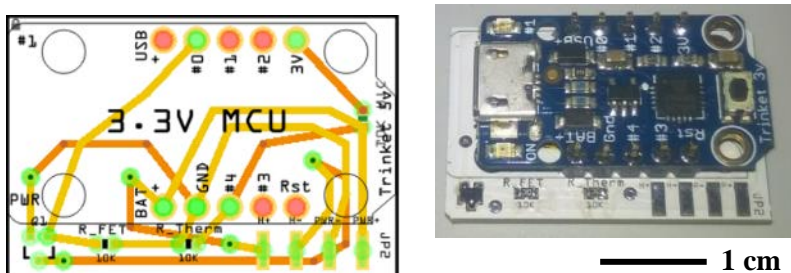
Figure 8: Micro-thermostat interface board PCB design from Fritzing (left), and prototype implementation (right)

The thermostat relied on proportional control to regulate power inputs to the heater. This method was chosen over PID (proportional-integral-derivative) control for its minimal computational space requirement, in order to ensure easy downscaling to smaller microcontrollers while retaining timer and user feedback functionality. The thermostat software had a built-in timer that monitored incubation time and automatically stopped heating once it was over. Furthermore, it had built-in software-based overheat protection that would turn off the heater above the specified threshold.

A heavily defeatured thermal model was designed (Figure 6/C) to include basic device components according to principles detailed in Section 1.1.1. For this model, a 25 mm x 75 mm plastic core chip was used, fitted with two thermistors in each of its channels. The thermostat and its enclosure were not included in the thermal model along with user and fluidic interfaces present in the final device implementation described in Chapter 3. Given the identical design of the two thermostats, results will not be reported separately for each. Dimensions of the thermal model were 37.5 mm (W) x 72 mm (L) x 10 mm (H). The footprint of the complete concept device design (Figure 6/C) excluding power supply was 37.5 mm (W) x 72 mm (L) x 20 mm (H). The experimental setup consisted of the thermal model, including a core chip fitted with a thermistor as well as the heater, wired to one of the thermostats. The thermostat and the heater were connected to the DC power supply (15 V input voltage, 1 A limit), one thermistor was connected to the multimeter and the other to the thermostat (components are

---

[3]URL: https://www.hackster.io/salhar1/micro-thermostat-deed1b

described in Section 1.1.4). Proportional gain was set to 20 [1/K] for fast convergence.
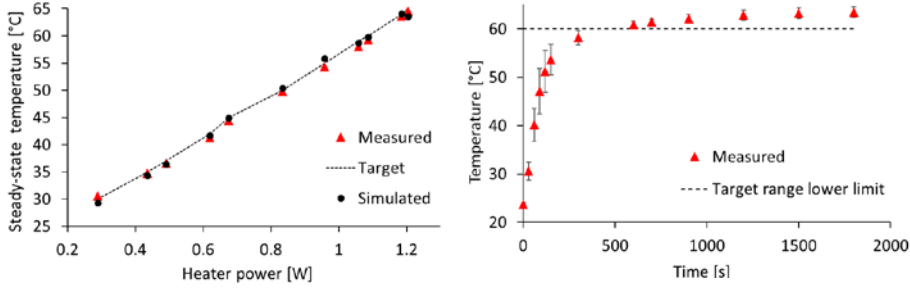
Figure 9: Results of functional characterization for the thermostat-regulated resistive heating option. The microheating option complied with all assay-related requirements.

A finite element model was built based on the principles detailed in Section 1.1.2. Proportional control was factored into the model through the following equation [71]:

$$V_{in}(t) = K_p \cdot e(t) \tag{4}$$

where V_{in} [V] is the potential drop on the heating element (which contributes to the potential drop V in equation (3)), K_p [1/K] the proportional controller gain, and $e(t) = T_{set} - T_{current}$ the process error at time instant t [s]. T_{set} [K] is the temperature set point of the control algorithm, and $T_{current}$ [K] is the measured temperature at time instant t. Average mesh element quality for this model was 0.673 (element size: 0.18 mm^3).

The functional characterization consisted of two steps:

1. Evaluation of steady-state temperatures and SSE considering target temperatures in the 25-65 °C range
2. Evaluation of 62.5 °C target temperature, 20 minutes incubation time

Results are shown in Figure 9. This microheating option was able to maintain temperatures within the 62.5 ± 2.5 °C target temperature range for 20 minutes, the SSE was 0.53 °C (± 0.19 °C). The thermal time constant for this setup was 9 minutes. Therefore, this microheating option complies with all requirements listed in Section 1.1.3 and qualifies as a microheating candidate. The finite element model estimated experimentally recorded steady-state temperatures with a MAE of 0.64 °C. The proposed micro-thermostat unit is novel in the sense that it is an integrated smart device controller for molecular diagnostics, which has a built-in timer that automatically stops the reaction and can notify the user when the assay is done. Furthermore, the controller has built-in overheat protection and in the future could be upgraded by additional user interfaces, such as wireless data communication.

1.4 Self-regulating resistive heating elements

As mentioned in Section 1.3, most resistive heating element developments reported in the literature in the context of molecular diagnostics devices rely on external temperature regulation. However, self-regulating resistive heating elements are capable of regulating their current input through the positive temperature coefficient of resistance (PTCR) effect, which means a rapid increase in resistance above a threshold temperature. Therefore, out of the 3 electrical heating solutions tested in this chapter, this is the simplest as well as the cheapest, as will be indicated at the end of the chapter. Existing commercially available self-regulating heating solutions to date are primarily based on ceramic semiconductors [39], [88]–[92]. Some more recent developments rely on polymer composites [40], [93], [94]. Despite their potential, not many Lab-on-a-Chip devices using self-regulating resistive heaters have been demonstrated thus far. The group of Wyzkiewicz et al. [95] demonstrated a self-regulating heater for microfluidics that relies on interdigitated carbon-copper-silver tracks to produce 30-70 °C reaction temperatures. This heater could support a wide variety of assays in disposable tests. However, in this paper we focus on adapting commercially available heaters.

According to the design process in Section 1.1.1 and specifications in 1.1.3, a ceramic PTC heating element was chosen for the evaluation in this section. The DBK HP04-1/04-24 was a PTC ceramic heating element with an aluminum profile that had a flat face (35 mm (W) x 40 mm (L) x 8.5 mm (H)). Although not stated explicitly by the manufacturer, related patents [90], [91] indicated that the heater relied on doped (3-or 5-valent dopants) polycrystalline barium titanate (BaTiO$_3$) ceramic pellets [96]. The threshold temperature for the PTCR effect is called Curie temperature, at which a transition from ferroelectric to paraelectric phase occurs inside the ceramic. This temperature is adjusted by doping [92], [97] to determine the temperature set point of the heating element. The PTCR effect of the heater can be modelled in three ways:

1. Using an experimentally recorded temperature-dependent resistivity profile when one is available
2. Estimating with the linear approximation [98]: $R(T) = R_0 \cdot [1 + \alpha \cdot (T - T_0)]$. $\alpha \, [1/K]$ is the temperature coefficient of resistivity. This method requires the least amount of data.
3. Estimating with the Steinhart-Hart equation for thermistors [99] if the coefficients are given

A heavily defeatured thermal model was designed (Figure 6/B) to include basic device components according to principles detailed in Section 1.1.1. For this model, a 25 mm x 75 mm plastic core chip was used with a single thermistor. Dimensions of the thermal model were 60 mm (W) x 78 mm (L) x 20 mm (H). The heating element was connected to the DC power supply and the thermistor to the multimeter. The maximum input voltage for the heater stated by the

manufacturer was 30 V_{DC} [100]. To model the PTCR effect, the linear approximation was used. The base resistance of the heating element was measured to be 10 ± 0.4 Ω at room temperature. To determine the temperature coefficient, the heating element was encased in a polyurethane mold for thermal insulation, then connected to the power supply, and the input current was recorded at 1–24 V input voltage with 1 V steps while recording surface temperatures. At each step, the heater was allowed to reach a steady state and then to cool down to room temperature. The reference temperature was defined as 24 °C (room temperature), and monitored with a digital thermometer. The temperature coefficient of resistivity was calculated as 0.16 ± 0.09 [1/K] from recorded data. The heating element complied with basic requirements.

For the functional characterization, input voltages were selected in the 5-24 V range (1 A current limit) and reaction temperatures were recorded. A finite element model was built based on the principles detailed in Section 1.1.2, using the linear approximation to model the PCTR effect.
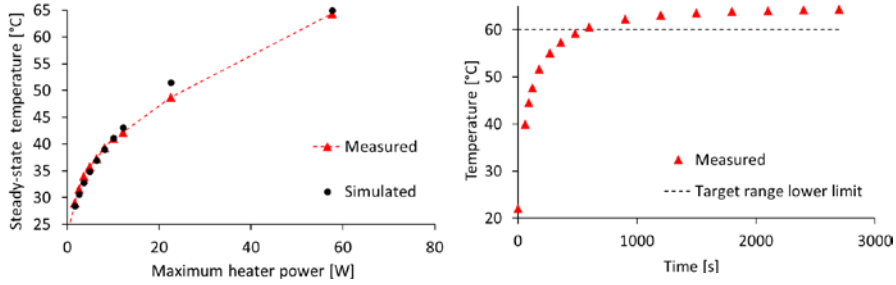
Figure 10: Results of functional characterization for the self-regulating resistive heating option. The microheating option complied with all assay-related requirements

Results are shown in Figure 10. This microheating option was able to maintain temperatures within the 62 ± 2 °C target temperature range for 20 minutes, the SSE was 0.59 °C (± 0.39 °C). The thermal time constant for this setup was 7.5 minutes. Therefore, this microheating option complies with all assay requirements listed in Section 1.1.3 and qualifies as a microheating candidate. The finite element model estimated experimentally recorded steady-state temperatures with a MAE of 0.96 °C. The proposed self-regulated heating concept was developed further (see Chapter 2) into a novel, patented microheating solution.

1.5   Thermoelectric heating elements

Peltier (thermoelectric) elements have been extensively covered in the literature as potential candidates for Lab-on-a-Chip temperature control, both as external and integrated solutions. Integrated thin-film Peltier elements (micro-Peltier cells) have been demonstrated in the context of NAAT chips, namely for PCR (polymerase chain reaction) [85], [86]. Although Peltier elements can work both in cooling and heating regimes [101], their power efficiency is largely determined

by the quality of the heat sink installed, as well as thermal design factors (effective heat transfer and heat losses). Finite element modelling is a great tool to optimize the thermal structure of the device, and thereby improve the efficiency of the Peltier element. Literature work in this regard has primarily focused on modelling the element itself [102], and primarily in the cooling regime [67]. A wide variety of COTS Peltier elements are available but they are far more expensive than the other 3 options evaluated in this chapter, making them unattractive for disposable tests. The true potential of Peltier elements lies in benchtop applications where cooling is also utilized and cost is not so much a determining factor. This section reports on work published in Appendix C.

We proceed by going through the evaluation process as detailed in Section 1.1.1. The specifications are defined in Section 1.1.3. The selected heating element was the APHC-03107-S from European Thermodynamics Ltd. Manufacturer data [103] stated the maximum temperature difference as 65 °C, maximum input voltage as 3.6 V and maximum input current as 7.4 A (maximum power output 17 W) for this element. Thermoelectric elements are composed of series of junctions made up of n-doped and p-doped semiconductors, sandwiched between two metal plates (hot and cold sides). Most thermoelectric elements are composed of Bi_2Te_3 junctions [67], [104], and although not stated by the manufacturer explicitly, we will assume the same material composition for the tested element. The dimensions of the thermoelectric element were 20 mm x 24.5 mm x 3.5 mm.

A heavily defeatured thermal model was designed to include basic device components according to principles detailed in Section 1.1.1. This model was built around the glass core chip. Dimensions of the thermal model were 37 mm (L) x 27 mm (W) x 11 mm (H). During testing, the core chip was fitted with a thermistor, and the Peltier element was connected to the DC power supply. See Section 1.1.4 for further details on the test setup. Input voltages were tested in the 1-3.5 V range, with 0.25 V steps, and steady-state temperatures were recorded in each step.
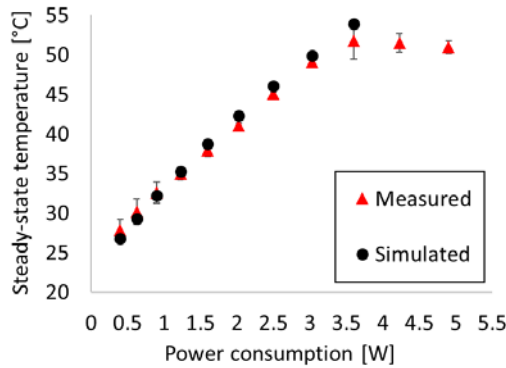
Figure 11: Results of functional characterization for the thermoelectric heating option. The microheating option did not comply with requirements.

A finite element model was built for this concept device based on the principles detailed in Section 1.1.2. A thermoelectric element is essentially an electrical heat pump. When a current (I) flows through a junction of dissimilar conductors A and B,

42

heat (Q) is generated or removed at the junction, resulting in a heat flux between A and B sides of the thermoelectric element: $Q = (P_A - P_B) \cdot I$. This is called the Peltier effect, P_A and P_B are Peltier coefficients. The second Thomson relation (P=ST) relates Peltier coefficients to the Seebeck coefficients. The following relation determines the contribution of thermoelectric elements to local current densities in our finite element model [105]:

$$J_e = -\sigma S \nabla T \qquad (5)$$

Where J_e [A/m^2] marks the current density that contributes to J_e in equation (3), σ [S/m] the electrical conductivity, S[V/K] the Seebeck coefficient and T [K] the temperature. The conductive term of the heat transfer equation (equation (1)) is modified as $q = -k\nabla T + PJ$ to factor in contributions from the thermoelectric effect.

Results are shown in Figure 11. The thermoelectric element in the tested setup was capable of regulating reaction temperatures in the 25-52 °C range. An increase beyond 3.5 W power consumption did not lead to an increase in steady-state temperature. Therefore, this microheating option did not comply with requirements set out in Section 1.1.3, and did not qualify as a microheating candidate. The finite element model estimated experimentally recorded steady-state temperatures with a MAE of 0.97 °C in the compared range (0.5-3.5 W).

1.6   Chapter summary

In this chapter, we covered the methodology by which to analyze and evaluate integrated microheating options for use in molecular diagnostics devices. We described the evaluation workflow, and evaluated four microheating options (chemical heating and three electrical heating options). We demonstrated two microheating candidates that were proven suitable for use in our molecular diagnostics device prototype. The above claims correspond to Contribution I. and II., as well as Papers A-C of this PhD thesis.

Along with the evaluation of each option, we described related results demonstrated in the literature. This evaluation was part of a device development process that culminated in the prototype in Chapter 3, and each thermal model described in this chapter represented one early device concept. Each thermal model was designed for use with a particular microheating option. Each microheating option was experimentally characterized by itself as well as in the context of the diagnostics device. The outcome of the experimental evaluation is summarized in Table 5. Furthermore, finite element models were created for all four options to simulate heat transfer, and were demonstrated to estimate experimental results accurately. At the end of the evaluation, two out of four options complied with specifications and were designated as microheating candidates fit for further development. Resistive heating, both self-regulated and thermostat-regulated, proved to be the best candidates for our molecular diagnostics test device. Although the other two microheating options had certain attractive properties, their development was discontinued due to a lack of time and resources.

Table 5: Evaluation summary of all microheating options tested in this chapter

Property	Chemical heating	Self-regulating resistive heating	Thermostat-regulated resistive heating	Thermoelectric heating
Complexity (by number of components)	Low	Low	High	Medium
Disposable?	Only MgFe alloy	Yes	Yes	Yes
25 °C & 65 °C limits met?	No	Yes	Yes	No
SSE [°C]	Not measured	0.59 ± 0.39	0.53 ± 0.19	Not measured
Incubation time compliance?	No	Yes	Yes	No
Heat up time compliance?	No	Yes	Yes	No
Incubation temperature compliance?	No	Yes	Yes	No
Thermal model dimensions [cm]	W: 90 L: 80 H: 20	W: 60 L: 78 H: 20	W: 37.5 L: 72 H: 20	W: 27 L: 37 H: 11
Battery-operated? (IEC 60601-1 applies)	No	Yes	Yes	Yes
Unit cost in mass-production [EUR]	~1	~2	~6	~30
Microheating candidate? (reason)	**NO (unreliable)**	**YES**	**YES**	**NO (too expensive)**

2 DEVELOPMENT PROCESS FOR MICROHEATING SOLUTION

This chapter covers the following topics:

- Testing microheating candidates for additional temperature targets (an optional step in the development process)
- Developing microheating candidates into microheating solutions for a specific molecular diagnostics device and diagnostics protocol
- Optimizing the microheating solution and testing the targeted molecular diagnostics protocol in the core chip functional prototype

This chapter will demonstrate the process by which microheating candidates are developed further into microheating solutions fit for use in a proof-of-concept molecular diagnostics device prototype. Please note that a microheating candidate does not necessarily mean a single microheater, but a microheating solution does. Furthermore, we demonstrate the evaluation of microheating candidates for additional temperature targets, should the need arise during development to alter the assay targets. The chapter is concluded by a proof-of-concept demonstration of a prototype device performing the targeted molecular diagnostics assay.

2.1 Process overview

In the previous chapter, we described the process by which several microheating options were evaluated and two compliant options were declared microheating candidates for the molecular diagnostics device under development. In this section we will describe the process by which these candidates are developed further into microheating solutions applicable in a functional prototype device implementation (Figure 12). This development process starts with microheating candidates and the requirements specification from the previous chapter and ends with a proof-of-concept demonstration of the assay using the developed microheating solution. Until this point, the assay parameters may have changed for any previously unforeseen reason. If they did, it could be necessary to test alternative assay targets (covered in Section 2.2). Once the assay targets (incubation time and temperature) are fixed, development can continue with the selected microheating candidate. First, physical and simulated thermal models are created for the functional prototype of the diagnostics device, including liquid handling functions to perform the assay without instrumentation. User interfaces are not included in the thermal model. The thermal model is tested to ensure assay target temperature and incubation time are met. If compliance is established, the heater is combined with the functional prototype device and a proof-of-concept diagnostics assay is executed in the device. In this step, a sample concentration above the limit of detection (LOD) is used to avoid false negatives. If the assay is successful, development concludes with a working microheating solution.
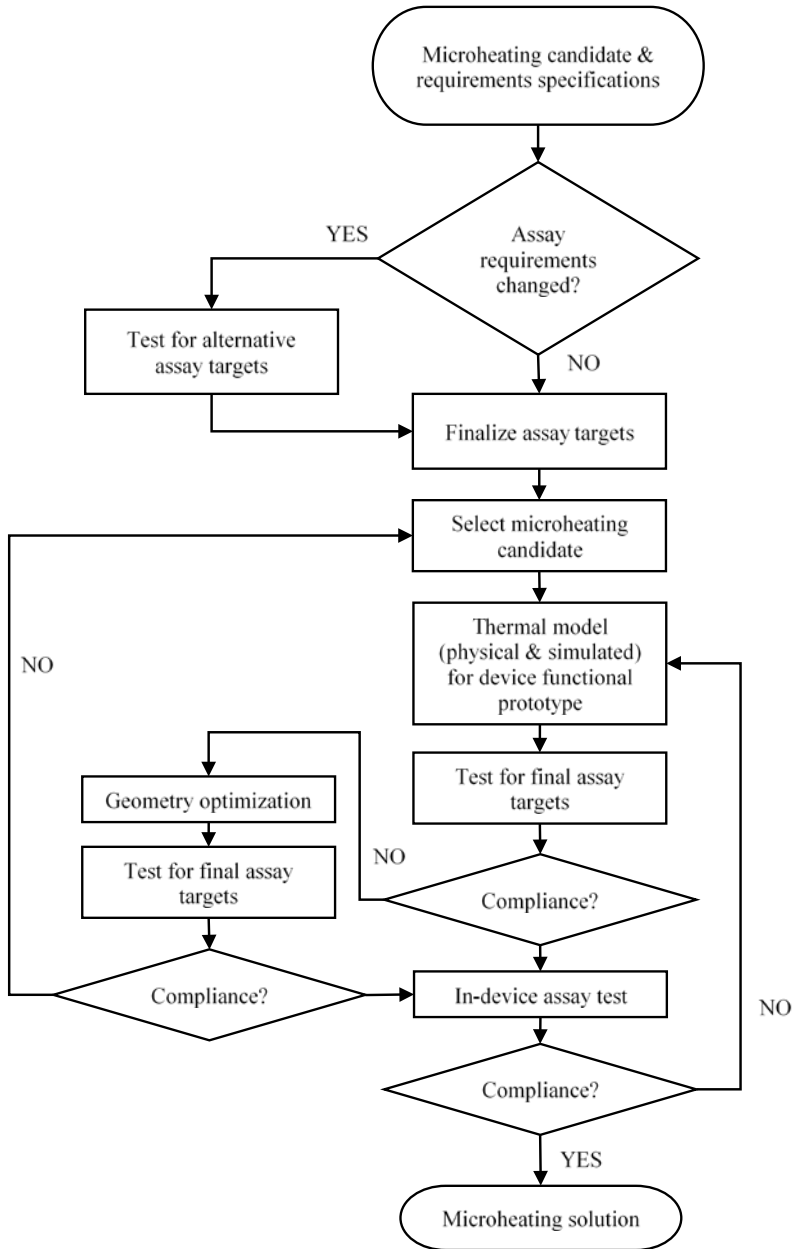
Figure 12: Developing microheating candidates into microheating solutions for use in the functional prototype molecular diagnostics device

If parameter compliance is not established with the thermal model, a geometry optimization is performed. Deficiencies in heat transfer and insulation are eliminated and compliance with assay targets is checked again. If this check fails,

the microheating candidate does not meet requirements and a new candidate is selected.

2.2 Testing for multiple temperature targets

In this section, we evaluate a scenario where the originally chosen assay did not work and a variety of alternatives had to be tested. In this PhD work, we focus on the development of a molecular diagnostics device that performs the LAMP protocol to amplify target DNA, but a multitude of other isothermal DNA amplification protocols exist, as summarized in Table 6. All of these protocols have incubation temperature targets in the 25-65 °C range, thus the previously established microheating candidates can be used for this test. For this evaluation, we use the setups described in Section 1.1.4. The thermostat-regulated setup was run with 15 V input, 1 A current limit, with a 20 [1/K] proportional gain, whereas the self-regulated setup was run with a range of inputs between 5-24 V (1 A current limit). Target temperatures were defined according to the evaluated NAAT protocols. Table 6 summarizes test results. Both microheating candidates were capable of regulating temperatures with SSEs less than 2 °C for all selected target temperatures.

Table 6: Target temperatures for isothermal NAAT protocols [18]

Method	Full Name	Target range	SSE (Self-Reg.)	SSE (Thermostat)
NASBA	Nucleic Acid Sequence Based Amplification	41 °C	0.1 °C	0.6 °C
HDA	Helicase dependent amplification	64 °C	Not tested	0.3 °C
LAMP	Loop mediated isothermal amplification	60–65 °C	0.6 °C	0.3 °C
NEAR	Nicking Enzyme Amplification Reaction	55–59 °C	Not tested	0.7 °C
RCA	Rolling Circle Amplification	30–65 °C	0.9 °C	0.6 °C
RPA	Recombinase Polymerase Amplification	37–42 °C	0.2 °C	0.2 °C
SPIA	Single primer isothermal amplification	45–50 °C	1.2 °C	0.2 °C
RAM	Ramification amplification method	35 °C	0.75 °C	0.2 °C

2.3 Performance analysis for a single temperature target

Using the requirements detailed in Section 1.1.3 and the test structures in Section 1.1.4, we evaluated our two microheating candidates for the LAMP protocol, comparing their performance. Figure 13 shows a comparison of reaction temperatures between the two solutions, indicating a minor difference (1.5 ± 0.9 °C) between the two.
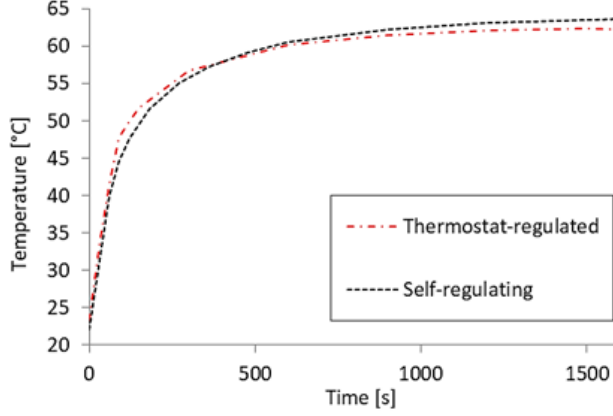
Figure 13: Performance comparison of self-regulating and thermostat-regulated heating related to the LAMP NAAT protocol

Using the finite element models from Sections 1.3 and 1.4, heating efficiency η_h of the two solutions was compared. The evaluation was performed based on the following expression:

$$\eta_h = \frac{1}{\text{coord}} \cdot \sum\nolimits_{\text{coord}} (T > 59.99[°C] \cap T < 65.01[°C]) \qquad (6)$$

where coord denotes the spatial coordinates (x, y, z), and $\eta_h \in [0; 1]$. This expression was evaluated in steady state to determine the maximum heating efficiency for both setups for a direct comparison (Figure 14). In the self-regulated setup, 95% of the reaction volume was in range (0.66 mL out of 0.7 mL). In the thermostat-regulated setup, 8% of the reaction volume was in range (0.06 mL). However, adding a heat spreader —a 1 mm thick aluminum sheet— to the heater–chip interface in the thermostat-regulated setup increases the reaction volume in range to 95% (0.66 mL).
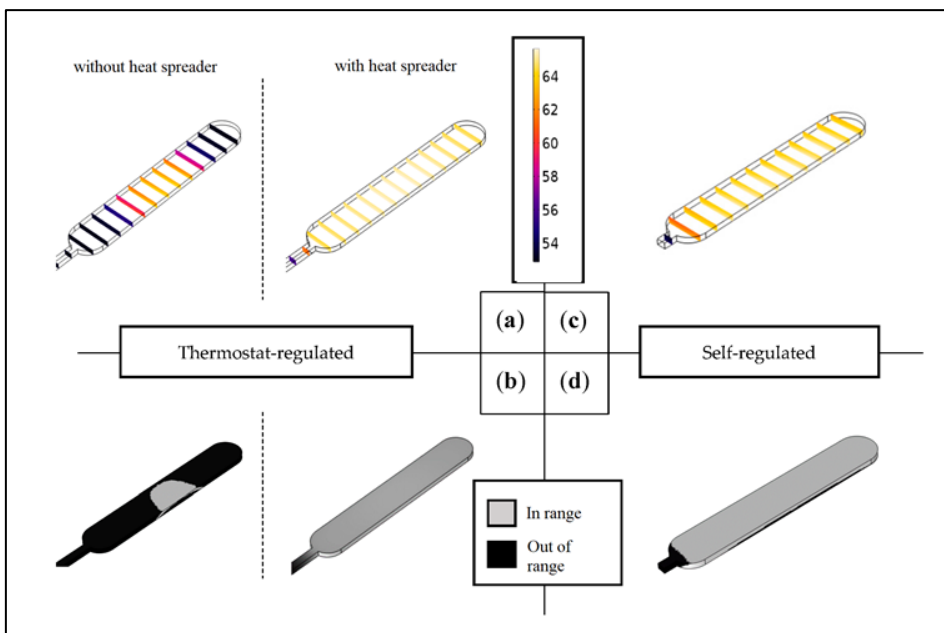
Figure 14: Finite element thermal analysis to check heating efficiency for the self-regulating and thermostat-regulated microheating candidates

The experimental evaluation indicated that the self-regulated setup reached the control target 1.5 min earlier than the thermostat-regulated setup, whereas steady state was reached 25 min earlier in the thermostat-regulated system. The controller gain was set high to ensure rapid heating, but the algorithm cut down the output near the set point to prevent overheating, which resulted in a longer heat up. In a portable application, the thermostat-regulated setup would be powered by 2 pieces of 9 V alkaline batteries, whereas the self-regulated setup would be powered by 3 pieces. Considering the dimensions of the thermal models, both microheating candidates require sizeable power supplies, which would constitute the largest part of the microheating solution. If the size of the reaction chamber and the heating element are reduced, the size of the power supply can also be reduced, and with that the size of the whole device. Self-regulating heating is more favorable for a disposable application given its lower cost and lower complexity resulting in a smaller footprint and therefore less waste generated. Therefore, at this stage in the development process, the decision was made to significantly reduce device size by reducing the size of the reaction chamber and fitting it with a new self-regulating microheater operated by AAA alkaline batteries.

2.4 Optimized microheating solution for the LAMP NAAT protocol

The LAMP NAAT protocol used in the functional prototype device was demonstrated by Jevtuševskaja et al. [106] for the bacterial pathogen chlamydia trachomatis. Assay parameters were refined according to qLAMP (quantitative

49

LAMP) test results: the target temperature range was changed to 61.5 ± 1.5 °C as tests indicated a maximum amplicon yield in this range. The expected heat up time was restricted to 5 minutes to make sure a longer incubation time of 25 minutes.

As mentioned in Table 2, the heater was expected to bring the reaction volume to target in maximum 5 minutes and hold it at least for another 20 minutes. The input voltage was defined as $3V_{DC}$. 2xAAA alkaline batteries were chosen as the power supply for their low price, small size and comparatively good energy density. In addition, alkaline batteries do not generate hazardous waste and some recycling options are available for them. BM117 batch PTCR polymer self-regulating heaters were provided by Heatron Inc. [107] in two different sample lots with different electrical characteristics and target temperatures (Table 7). The heater had a sandwich structure consisting of the resin sandwiched between 2 conductive films.

Table 7: Design parameters of BM117 sample lot heaters

Batch and lot nr.	Input voltage [V]	Base resistance at room temperature [Ω]	Set temperature range by design [°C]
BM117-83-A	3	1.15	58-62
BM117-83-B	3	0.5	60-64

Each heater was electrically characterized using an Agilent 34410A digital multimeter. Base resistance values were measured at room temperature (Table 8).

Table 8: Experimental electrical and thermal characterization of BM117 sample lot heaters

Heater (BM117-83-)	Base resistance at RT [Ω]	Steady-state power output [W]	Time constant [mm:ss]	Steady-state reaction temperature in chip [°C]	SSE[4] [°C]
A18	1.5	0.77	06:28	61.98	0
A20	1.15	0.71	05:56	62.7	0
A24	1.12	0.72	07:20	59.8	-0.2
A34	1.12	0.72	08:52	61.79	0
A36	1.11	0.62	06:48	59.33	-0.67
B1	0.5	0.79	04:45	62.79	0
B4	0.63	0.63	05:47	60.79	0
B7	0.64	0.76	04:23	63.68	+0.68
B8	0.56	0.62	04:14	63.62	+0.62
B12	0.52	0.75	04:39	63.95	+0.95
B13	0.55	0.64	04:17	64.21	+1.21

A thermal model was created for the core chip functional prototype including a frame for the chip and the heater, as well as a carrier platform for the heater (Figure 17). A temperature probe was attached to one of the reaction chambers while the other was sealed airtight with thermoplastic adhesive. The chip was sealed with a Greiner multiwell plate sealer film (P/N A5596 from Sigma-Aldrich). The core chip had reaction chambers with 0.5 ml reaction volume, 2 inlets, 2 outlets, microchannels and a liquid splitting junction that would split

---

[4] Considering 60°C as the control target

the initial volume into the two microreactors. The heater was contacted by adhesive copper tape (3M-1245) and connected to a DC power supply. Under the heated area, a block of polyurethane foam (ESD P/N 961.1000.10) was placed for insulation. Reaction chambers were filled with distilled water using a 3 mm syringe. The other inlet was sealed off. In the functional prototype, the heater would be directly interfaced with the reaction chambers of the core chip with no thermal interface material involved. Test results (Table 8) indicated that out of the 11 tested heaters only 5 were compliant with the temperature criterion and out of these, only sample B1 was compliant with the time criterion (Figure 15).
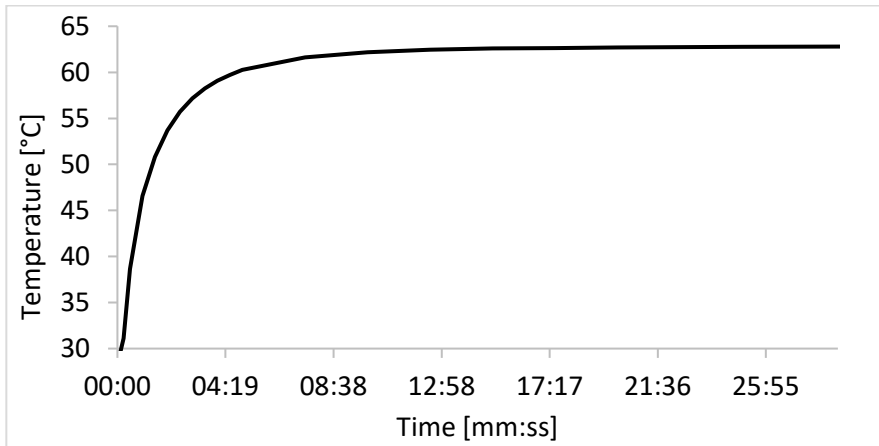
Figure 15: Reaction temperature in the functional prototype core chip over 30 minutes using heater sample BM117-83-B1

A simulated thermal model was set up according to the principles in Section 1.1.2. The model was set up for heater sample BM117-83-B1. Material properties were defined by library values from COMSOL or manually inputted based on data sheets from the supplier. Boundary conditions and initial parameters were derived from the physical prototype. Convective, conductive and radiative heat losses were taken into account. A quadratic mesh was generated for the model with average element quality 0.68 and element size 0.07 mm^3. A steady-state thermal simulation (solved by the Stationary Solver of COMSOL) had an average solution time of 40 s on a PC with a Core i5-4570 CPU and 16 GB RAM. The model was validated through comparing simulated and experimentally recorded temperature data. A thermistor was embedded in the reaction chamber and the exterior of the device was recorded by an infrared camera (Jenoptik VarioCAM 384 HiRes IR) in steady state (Figure 16/a, b). Furthermore, a domain point probe was defined in COMSOL at the location of the physical temperature probe in the experimental setup and comparison between experimentally recorded and simulated temperatures indicated an absolute error of 0.16 °C. The volumetric temperature condition from Equation (4) was applied to the model with the

revised temperature target boundaries. The reaction volume in range was calculated to be 84.6 % of the whole volume (≈42 µl per chamber), which was sufficient to run the LAMP protocol and produce a positive result (Figure 16/c, d). Temperature maps indicated a deficiency in heat transfer on the outer side of the reaction chamber. This will be solved in future device iterations by adding more insulation to the outer reactor wall.
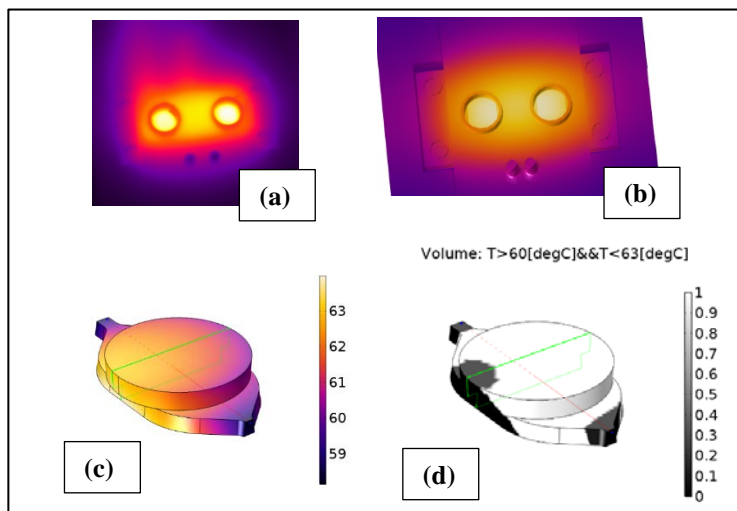
Figure 16: Thermal modelling for the core chip functional prototype indicated about 85% of the reaction volume was in the defined target temperature range

For our proof-of-concept demonstration of in-device LAMP, template DNA (Serotype E; DSMZ; DSM 19131 at a concentration of 1000 copies per reaction) was used instead of DNA extracted from patient samples. Two equal volumes of liquid master mix and buffer were prepared in Eppendorf tubes, and mixed with the DNA samples, resulting in a 250 µl total volume. The core chip was attached to a large base plate with two 10 ml syringes, the heater carrier and the heater. A polyurethane block was placed under the heater carrier for insulation. The 10 ml syringes were connected to the outlet features to serve as gas springs for liquid splitting. The sample volume was sucked into a 3ml syringe connected to one inlet, while a 3ml syringe filled with air was connected to the other. After sealing the chip and inputting the reaction mix, batteries were connected to the heater. To prevent cross-contamination, the prototype setup was sealed in a plastic bag and incubation was performed under a lateral flow hood (Figure 18). For the duration of the experiment, the reaction chambers were covered from above by a paper towel for added thermal insulation (discarded after each use). Incubation time was 30 minutes in total, including the 5 minutes allowed for the heating element to reach steady state. The test protocol was repeated twice, for both reaction chambers of the Lab-on-a-Chip prototype device. After incubation, reaction volumes were extracted and pipetted into Eppendorf tubes, into which lateral flow

strips were placed to detect amplicons. Results indicated a successful amplification in all 4 reaction chambers tested.
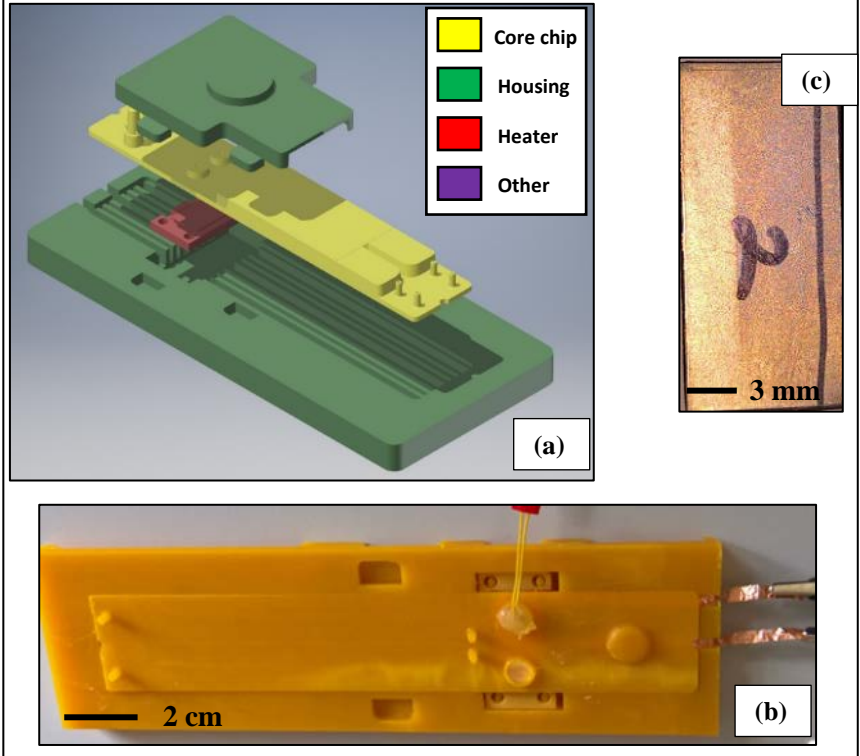
Figure 17: Thermal model for the core chip functional prototype (a) including a frame, electrical connections (b) and a heater (c)
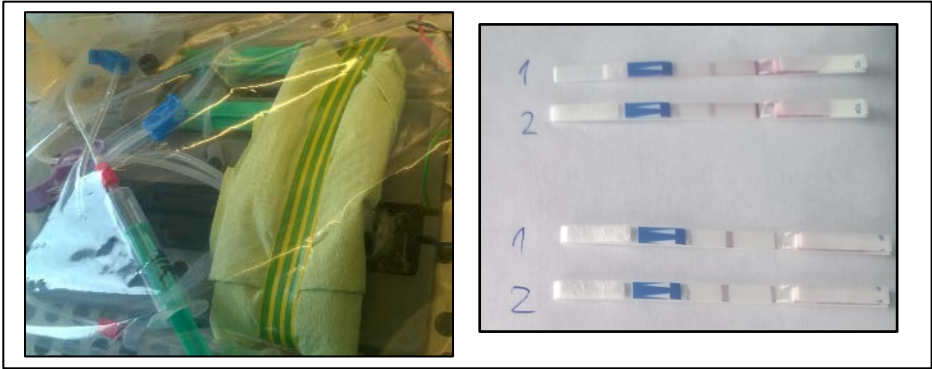
Figure 18: LAMP testing in core chip functional prototype (left) resulted in successful DNA amplification (right)

2.5   Chapter summary

In this chapter, we covered the process and methodology by which microheating candidates are developed into a single microheating solution optimal for the molecular diagnostics device and chosen diagnostic assay protocol. We evaluated the two microheating candidates established in the previous chapter as potential microheating solutions and established a novel microheating solution based on a self-regulating PTCR polymer resin heater. This novelty formed part of the patent published as Paper E. The above claims correspond to Contribution III. and IV., as well as Papers A, B and D of this PhD thesis.

During development, it may occur that the assay protocol is changed or temperature targets are revised. Therefore, this chapter detailed an evaluation for the two microheating candidates from the previous chapter for a wide array of isothermal amplification protocols with target temperatures in the 30-65 °C range. Both candidates regulated temperatures with less than 2 °C SSE. The two microheating candidates were further analyzed for their performance with the LAMP protocol. Both candidates were capable of sustaining the reaction within the specifications, with only 1.5 °C difference in steady-state reaction temperatures between the two. Both candidates met the time targets as well. From the simulated thermal model, it was calculated that 95% of the reaction volume was in range in the self-regulated heating setup and with some thermal optimization also in the thermostat-regulated setup. However, at the end of this evaluation process, self-regulated heating was chosen as the final candidate due to its lower cost and complexity compared to the alternative. Our early device concept would have required a sizeable power supply, so the device geometry was overhauled and a new self-regulating heater was selected for a far smaller heated area and thus, lower power consumption. BM117 PTCR polymer heater samples from Heatron Inc. were powered by 2xAAA batteries. By this point the functional prototype for the core chip of the device was ready and a thermal model was constructed. Out of the 11 heater samples only 1 complied with all specifications and was evaluated further in the simulated thermal model. It was concluded that about 85% of the reaction chamber would be in range, and so a LAMP assay was performed with the functional prototype device and yielded positive amplification results.

3 MICROHEATING IMPLEMENTATION FOR INTIME NINAAT

This chapter covers the following topics:

- Integrating the microheating solution into the functional prototype of the molecular diagnostics device
- Final assay compliance check (temperature, heat up time)
- Demonstrating the InTime NINAAT device prototype for LAMP assays

This chapter will demonstrate the process by which the microheating solution is integrated into the functional prototype of the molecular diagnostics device (Figure 19). By this point in the development process, the housing design, including user interface functions, is assumed to be ready. The heater is adapted to the housing design (including the user interface) and a final test to check compliance with assay targets (time, temperature) follows. Once compliance is established, the device is tested as a molecular diagnostics test. In the case of this work, the InTime NINAAT device prototype performs the LAMP protocol for the detection of chlamydia trachomatis in the demonstration.
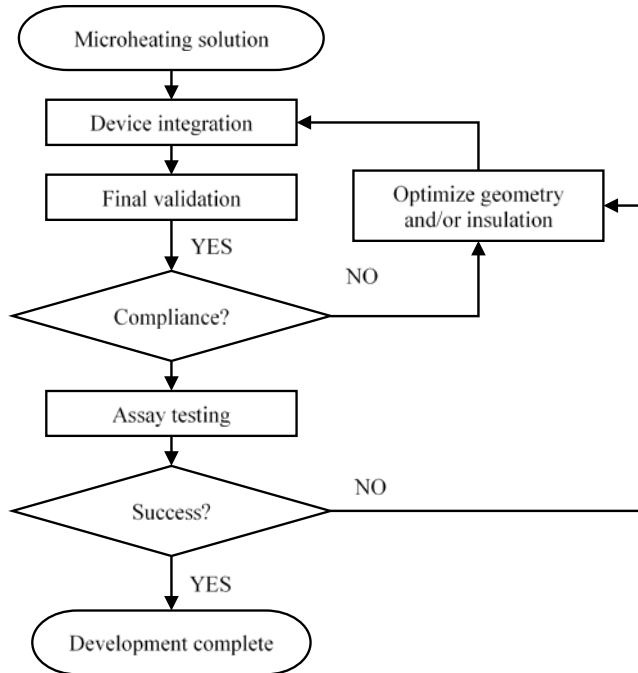
Figure 19: The final steps in the development process: integrating and testing a microheating solution in the functional prototype of the molecular diagnostics device

3.1 Process overview

In the previous chapter, we detailed the development of a microheating solution optimized for the functional prototype of the core chip. In this section, we describe the final steps of the development process. This process (Figure 19) starts with the microheating solution from the previous chapter. The requirements specifications stay the same (Section 1.1.3). Any user requirements concerning the heater are also taken into account at this step. At this point in the development process, the device housing and user interface designs must be ready. Heater integration with the device concept means adapting device geometry to house the heater, factoring in insulation needs, electrical connections and integration with the user interface. For instance, in the demonstrated device, heating must be initiated by the user by pulling a paper/plastic tab and thereby closing the electrical circuit. Following integration, a final validation is performed to check compliance with assay targets, that is, reaction target temperature and heat up time. If the test is successful, the molecular diagnostics assay is tested in the functional prototype. If not, then device geometry and insulation optimization follows. If the assay test is successful, the development is concluded and the device is cleared for production as far as heating is concerned.

3.2 Device integration of the microheating solution

The functional prototype of the InTime NINAAT device (Figure 22) was designed as a closed, self-contained unit with user interfaces in place. It consisted of the following components:

- Core chip functional prototype (described in the previous chapter) with lateral flow (LF) strips for amplicon detection
- Supporting fluidic components (buffer reservoirs, tubing) for the core chip
- Heater with insulation and electrical connections
- Battery compartment for 2xAAA alkaline batteries
- LED backlight module to increase contrast during readout of the LF strips
- User interfaces and I/O functions

During operation, the device was designed to be sealed airtight. The final device would be fully disposable, but in the functional prototype, the core chip and fluidic components are discarded after each test but the rest is reused. The heater used in this prototype demonstration was a pre-production sample based on BM117-83-B1 detailed in the previous chapter. The heater was contacted by two copper clips (RS Pro P/N 680-959) cut to shape, and wires soldered to the clips. A polyurethane foam block was used to support the heater and insulate the system from the bottom. The heater was contacted directly with the core chip, no thermal interface material was used. Above the reaction chamber, another polyurethane foam block was placed for additional insulation. In this device, an LED was included to improve the contrast of the lateral flow strips used to detect and

visualize amplicons (Figure 20). This LED was a 3V (forward voltage range: 2.8-3.2 V) white backlight module from Dayear Electric Co. Ltd (size: 23 mm x 60 mm x 2 mm). The LED was connected in parallel to the heater. The LED was designed to be on during the whole 30 minutes of operation and would in turn indicate to the user that the device was working correctly. The battery compartment was designed for 2xAAA alkaline batteries and relied on commercially available metal battery contacts (Keystone P/N 324-7319 and 324-7331). Connections to the LED and heater were established with wires. The circuit was closed by removing a plastic tab that was between the battery and the contact on the negative end. Dimensions of the complete device prototype were 10 cm (W) x 20 cm (L) x 10 cm (H).
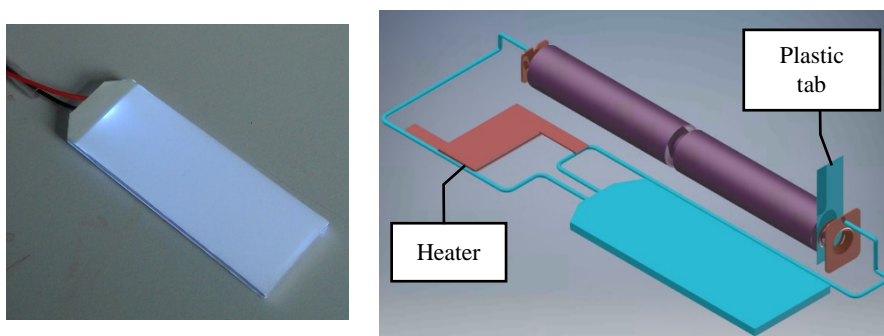
Figure 20: LED backlight module (left) and a rendering of the complete electrical circuit of the molecular diagnostics device (right)
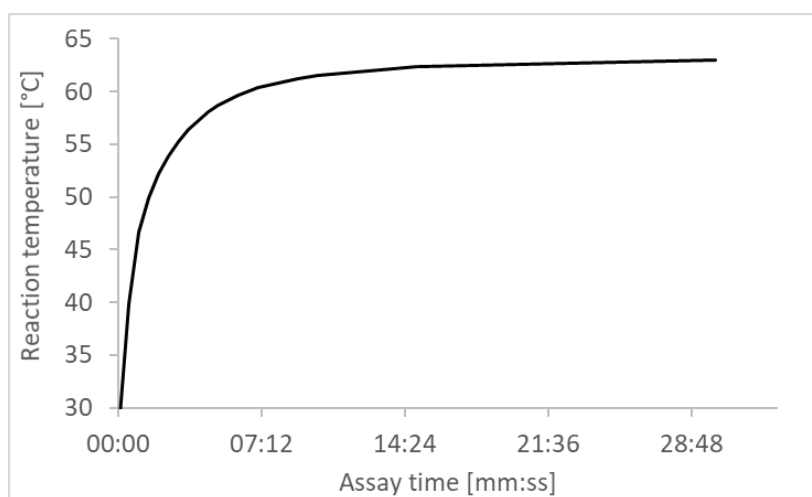
Figure 21: Reaction temperature during the assay duration in the functional prototype device

58

3.3 Final assay compliance check

For the final compliance check, an injection molded core chip and its fluidic components were taken from the stock at Selfdiagnostics Deutschland GmbH, whereas the housing and additional plastic components were 3D printed (see Section 1.1.4 for details about the printer). The core chip was fitted with a temperature sensor in one of the reaction chambers, and filled with distilled water from a syringe. Two 3 ml syringes were used as gas springs for liquid splitting. The device was assembled and prepared for testing with all device components, and the measurement started with the removal of the plastic tab and closing the electrical circuit inside. The test was run for 30 minutes at 22-24 °C ambient, and temperatures inside the reaction chamber were recorded. The recording indicated that compliance with assay targets was maintained (Figure 21).
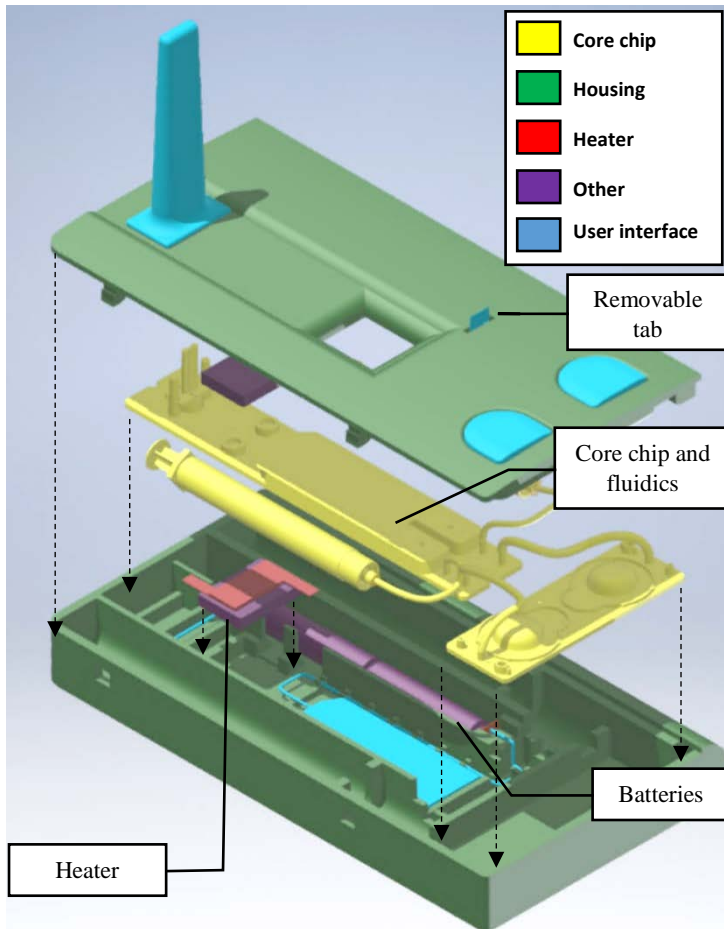
Figure 22: Functional prototype of the InTime NINAAT device in exploded view

3.4 InTime NINAAT device demonstration

LAMP reaction parameters were identical to those in Section 2.4, but the buffer and master mix were separately contained within the core chip and/or its connecting fluidic components, whereas the sample was introduced via the sample stick. The sample stick had a separate disposable tip that would permanently fix into the core chip. After testing, the core chip and its connecting fluidic components were discarded along with the batteries, but the rest of the prototype was reused.
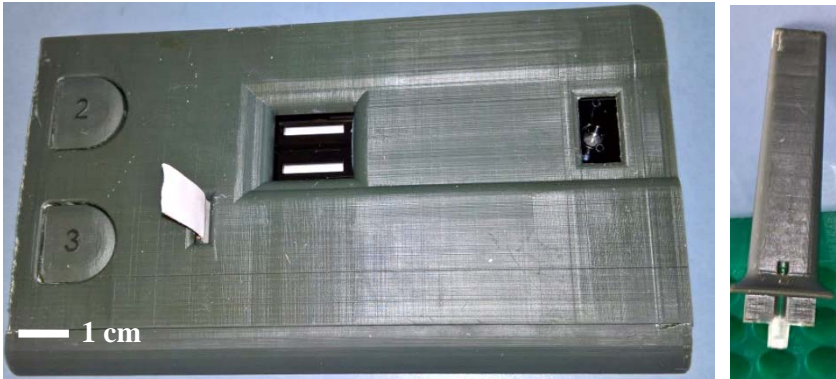
Figure 23: InTime NINAAT device functional prototype test (I.): the device is fully assembled (left) except for the sample stick, which is laid on the workbench (right)
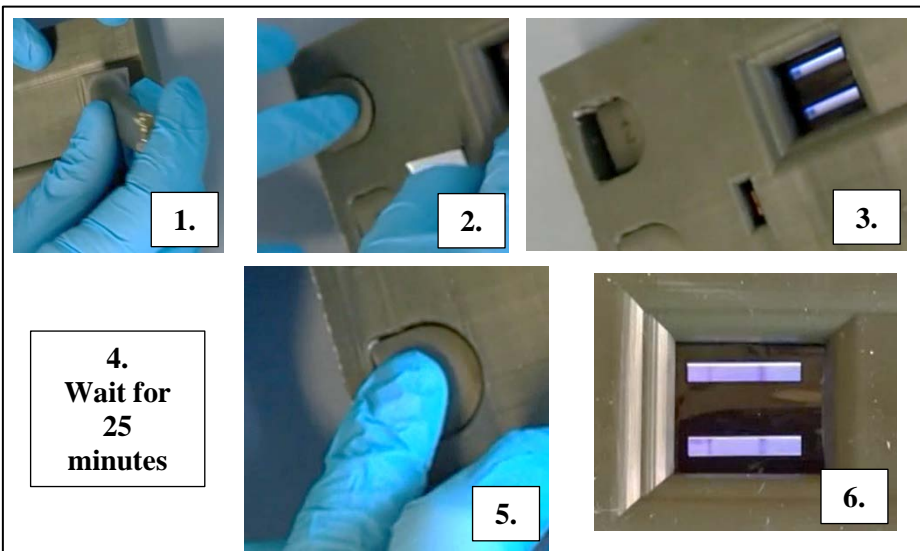
Figure 24: InTime NINAAT device functional prototype test (II.): First, the sample is inserted (1.), then the plastic tab is removed and button 2 pushed (2.). After 25 minutes wait time button 3 is pushed (5.) and the results become visible in 2 minutes (6.)

As the first step in the process, the device prototype was prepared with all its components attached, except for the sample stick (Figure 23). Then the sample stick was dipped into the sample (not shown) and inserted into the device (Figure 24/1.). Then the plastic tab was removed and button nr. 2 was pushed all the way in (Figure 24/2.). This initiated heating, turned on the LED and inputted the buffer solution into the core chip (Figure 24/3.). Next, the user had to wait for 25 minutes for the amplification reaction to take place. Finally, button nr. 3 was pushed to forward the amplicons to the lateral flow strip for detection and visualization (Figure 24/5.). After about 2 minutes, the control and test lines were visible on the lateral flow strips indicating successful amplification and a positive result (Figure 24/6.). In the case of a real-life test, this would mean the pathogen was present in the sample.

3.5   Chapter summary

In this chapter, we detailed the method by which the microheating solution optimized for the developed molecular diagnostics device is integrated into its functional prototype. We demonstrated the integration of the previously claimed microheating solution into the functional prototype of the developed molecular diagnostics device. Finally, we demonstrated that the functional prototype of the NINAAT device could function as a molecular diagnostics test, and could successfully amplify and detect the DNA of the target pathogen. We therefore claim a novel molecular diagnostics device, which is a second-generation RDT that is, to the knowledge of the authors, the first of its kind. This device formulates the basis of the patent application published in Paper E. The above claims correspond to Contribution V. and Paper E of this PhD thesis.

A functional prototype design was made, adapted to using the microheating solution from chapter 2. This prototype was designed as a self-contained unit, including user interfaces and input/output functions as well as all internal components. The functional prototype was fitted with the functional prototype of the core chip including supporting fluidic components (buffer reservoirs, tubes) as well as integrated lateral flow strips for visualizing results. An LED was added to increase contrast for the readout and connected in parallel with the heater. A battery compartment for two AAA alkaline batteries was included in the design. Sampling was done by a sampling stick with a disposable tip, which would get fixed into the core chip, allowing for the separate disposal of the core chip assembly after each test. The device was assembled from a 3D printed housing and injection molded fluidic components. A final assay compliance check was performed: a core chip was fitted with a temperature sensor and filled with distilled water. Reaction temperature was recorded for 30 minutes while heating was turned on. Results indicated that both the 5 minutes heat up time condition and 60-63 °C target temperature range were met. Finally, the device was assembled with all components for a LAMP test. This test was performed as it would be at the end user's side. The amplification reaction took place and positive results were visualized correctly. Therefore, the development of temperature regulation for this particular device is concluded and may be released for production.

CONCLUSIONS

This PhD thesis focused on the development of integrated microheating for the temperature regulation of non-instrumented molecular diagnostics devices. Temperature regulation is essential for a wide variety of diagnostic protocols, primarily nucleic acid amplification testing. In this work, the methodology by which to develop temperature regulation for such tests was discussed and as an example, the development process of microheating for the InTime NINAAT device was detailed. This PhD thesis explored the experimental methodology involved in this process and described the workflow with which similar applications can be developed.

As mentioned in the introduction, the thesis was divided into 5 chapters, the first being an introduction that reviewed literature results and the background of this application. Chapter 1-3 covered the development process, introducing the methodology along with its application to a real-world development, which concluded with a functional prototype demonstration using the integrated heating solution developed during this process.

In the introductory chapter of this PhD thesis, the following research questions were proposed:

1. What temperature control options are available for use in non-instrumented molecular diagnostics devices?
2. What are the performance characteristics of these options related to the NINAAT concept device in this work?
3. What are the most suitable temperature control options for the NINAAT concept device?
4. How to evaluate the performance characteristics of a microheating candidate for multiple assay protocols?
5. What are the performance characteristics of the microheating candidates in this work related to isothermal NAAT protocols and the LAMP protocol in particular?
6. How is a microheating option developed into a microheating solution optimized for use in a particular molecular diagnostics device?
7. How is a microheating solution integrated into a molecular diagnostics device?
8. What is the development workflow of temperature regulation for a non-instrumented molecular diagnostics device?
9. How can thermal analysis via the finite element method aid in this development process?

This section of the thesis discussed the contributions of the thesis and how they help in answering the above questions.

Paper A

This paper proposed self-regulating electrical heating as a novel integrated microheating option for disposable non-instrumented molecular diagnostics. The paper demonstrated the application of this heater in an early concept of our molecular diagnostics device built for a plastic microfluidic chip. The paper reported on the electrical and thermal characterization of this heating option as well as evaluated its performance related to the LAMP NAAT protocol. The paper demonstrated that the heating element could control with 0.13 °C SSE for the 60-65 °C set temperature range required by LAMP. Furthermore, the paper demonstrated accurate heat transfer simulation via thermal modelling (0.31 °C estimation error of experimental results) for the proposed prototype. The paper corresponds to research questions 1., 2., 5., 9.

Paper B

This paper focused primarily on modelling heat transfer in a disposable molecular diagnostics device with thermostat-regulated electrical heating. A thermostat was demonstrated that relied on open-source hardware. A thermal model was built for the early concept device (relying on the same microfluidic chip as paper A with a different housing) and experimentally evaluated for temperature targets required by various isothermal NAAT protocols. A simulated thermal model was constructed and its performance compared to experiments. The thermostat regulated temperatures with and SSE of 0.53 °C for 12 distinct temperature set points in the 30-70 °C typical for isothermal NAAT protocols. The model estimated experimental results with a MAE of 0.5-0.7 °C for all three experimental setups. In this paper, battery operation is discussed as well. The paper corresponds to research questions 1., 2., 4., 5., 9.

Paper C

For the sake of completeness, thermoelectric heating was evaluated as a microheating option for use in our molecular diagnostics device. This paper reported results on the experimental and simulated thermal characterization of a second iteration of our device concept using a glass microfluidic chip and a plastic housing. Experimental and simulated results were compared to indicate a MAE of 0.5-1 °C for the described experimental setups. The paper corresponds to research questions 1., 2., 9.

Paper D

This journal article was a summary of the development process that was detailed in this thesis. It built on the results of Paper A and B in the sense that it used the microheating candidates proposed by those papers and evaluated them as potential microheating solutions. The paper described the process by which these candidates were characterized for their performance with several isothermal NAAT protocols and LAMP in particular. Furthermore, it detailed the use of finite element modelling for thermal analysis to reveal design deficiencies and

evaluate heating performance in a molecular diagnostics device. According to the simulated thermal analysis, both the self-regulating and thermostat-regulated microheating candidates could keep the about 95% of the reaction volume in range in steady state, although the thermostat-regulated setup would need some thermal optimization to achieve this performance (installing a heat spreader). The paper concluded by proposing self-regulating microheating as the final solution due to its lower complexity and smaller size. The paper corresponds to research questions 3.-9.

Paper E

The patent application described temperature regulation for the InTime NINAAT device concept. Based on results disclosed in Paper A and D, self-regulating electrical heating was chosen as the microheating solution for use in our NINAAT device due to its low cost and simplicity. The microfluidic chip was redesigned to have a smaller heated area than in early device concepts and a PTCR polymer resin heater was acquired to regulate reaction temperatures. The heating element was designed to fit tightly under the reaction chambers of the fluidic chip. This paper covers research questions 3., 6., 7.

Summary of claims

Below is a summary of the theses/claims of novelty that this PhD thesis made. The claims correspond the Contributions I.-V. as well as papers A-E as detailed.

Claim 1: The evaluation methodology for microheating options, including experimental characterization and whole-device finite element modelling. The methodology is described in detail as well as applied in practice. To the knowledge of the authors, such an extensive summary has not been published previously. Furthermore, whole-device modelling is a novel approach that can yield more information than heater-chip thermal interface models could. This corresponds to Contributions I.-II. and Papers A-C.

Claim 2: Four distinct integrated microheating options (chemical heating, self-regulated electrical heating, thermostat-regulated electrical heating and thermoelectric heating) evaluated and two successfully demonstrated as microheating candidates for application in non-instrumented molecular diagnostics devices. Integrated thermostat-regulated heating based on a microcontroller carries novelty due to the fact that additional user-related functions can be integrated into the controller, such as the demonstrated built-in timer and overheat protection. Self-regulated heating was developed further into a novel microheating solution that formed part of the patent application published in Paper E. This corresponds to Contributions I.-II. and Papers A-C.

Claim 3: The methodology and process by which microheating candidates are developed into integrated microheating solutions. The methodology is detailed and demonstrated through practical applications. The process includes evaluating for additional assay targets, geometry optimization and heat transfer analysis via

finite element modelling. To the knowledge of the authors, this process has not been published in such detail previously. This corresponds to Contribution III. And Paper D.

Claim 4: Two microheating candidates evaluated for use with the functional prototype of the NAAT chip of the NINAAT platform. Self-regulating heating was developed further into a novel microheating solution based on a PTCR polymer resin heater that could be operated from two alkaline AAA batteries. The heating solution was demonstrated to work with the functional prototype of the NINAAT chip through the successfully amplification and detection of a pathogen target. This novel heating solution formed part of the patent in Paper E. This corresponds to Contribution IV. and Papers A,B and D.

Claim 5: The final microheating solution demonstrated in the NINAAT device functional prototype. The NINAAT device is a self-contained second-generation RDT test that can perform NAAT assay workflows form sample input to result output. To the knowledge of the authors, this device, and the heating solution within, are the first of their kind. This novelty formed the basis for the patent in Paper E as well as Contribution V.

Perspectives

As mentioned previously, the author hopes that other teams presented with the problem of developing integrated temperature control for their non-instrumented molecular diagnostics devices may benefit from the workflow described in this work and will reach results faster. The work described in this thesis took part under a research and development project targeted at implementing the first fully self-contained and disposable nucleic acid amplification test in a Lab-on-a-Chip format, which was designed to have the same accuracy and sensitivity metrics as centralized clinical diagnostics. The InTime NINAAT platform was designed to facilitate NAAT assays with various targets and make rapid testing more robust and reliable, preferably to allow treatment based on decentralized rapid testing to strengthen preventive medicine and save healthcare costs. LAMP and RT-LAMP (reverse transcription LAMP) protocols cover a wide variety of DNA and RNA targets, therefore applications are not limited to the pathogen used as an example in this work.

REFERENCES

[1]   S. Haeberle and R. Zengerle, "Microfluidic platforms for lab-on-a-chip applications," *Lab. Chip*, vol. 7, no. 9, p. 1094, 2007.

[2]   J. P. Lafleur, A. Jönsson, S. Senkbeil, and J. P. Kutter, "Recent advances in lab-on-a-chip for biosensing applications," *Biosens. Bioelectron.*, Aug. 2015.

[3]   C. D. Chin, V. Linder, and S. K. Sia, "Commercialization of microfluidic point-of-care diagnostic devices," *Lab. Chip*, vol. 12, no. 12, p. 2118, 2012.

[4]   J. H. Nichols, "Point of Care Testing," *Clin. Lab. Med.*, vol. 27, no. 4, pp. 893–908, Dec. 2007.

[5]   D. A. Anderson, S. M. Crowe, and M. Garcia, "Point-of-Care Testing," *Curr. HIV/AIDS Rep.*, vol. 8, no. 1, pp. 31–37, Mar. 2011.

[6]   J. Hirsch, T. Wendt, P. Kuhly, and W. Schaffartzik, "Point-of-care testing. apparatus. Measurement of coagulation," *Anaesthesia*, vol. 56, no. 8, pp. 760–763, Aug. 2001.

[7]   R. Lozano *et al.*, "Global and regional mortality from 235 causes of death for 20 age groups in 1990 and 2010: a systematic analysis for the Global Burden of Disease Study 2010," *The Lancet*, vol. 380, no. 9859, pp. 2095–2128, Dec. 2012.

[8]   I. Abubakar, T. Cohen, H. R. Stagg, and L. C. Rodrigues, Eds., *Oxford specialist handbook of infectious disease epidemiology*, First edition. Oxford: Oxford University Press, 2016.

[9]   C. Dye, "After 2015: infectious diseases in a new era of health and development," *Philos. Trans. R. Soc. B Biol. Sci.*, vol. 369, no. 1645, pp. 20130426–20130426, May 2014.

[10]   C. L. Satterwhite *et al.*, "Sexually Transmitted Infections Among US Women and Men: Prevalence and Incidence Estimates, 2008," *Sex. Transm. Dis.*, vol. 40, no. 3, pp. 187–193, Mar. 2013.

[11]   P. K. Drain *et al.*, "Diagnostic point-of-care tests in resource-limited settings," *Lancet Infect. Dis.*, vol. 14, no. 3, pp. 239–249, Mar. 2014.

[12]   N. P. Pai, C. Vadnais, C. Denkinger, N. Engel, and M. Pai, "Point-of-Care Testing for Infectious Diseases: Diversity, Complexity, and Barriers in Low- And Middle-Income Countries," *PLoS Med.*, vol. 9, no. 9, p. e1001306, Sep. 2012.

[13]   D. Yole, "2015 Microfluidic Applications in the Pharmaceutical, Life Sciences, In-Vitro Diagnostic, and Medical Device Markets," Yole Développement, 2015.

[14] G. Schochetman, C.-Y. Ou, and W. K. Jones, "Polymerase Chain Reaction," *J. Infect. Dis.*, vol. 158, no. 6, pp. 1154–1157, 1988.

[15] H. A. Erlich, "Polymerase chain reaction," *J. Clin. Immunol.*, vol. 9, no. 6, pp. 437–447, Nov. 1989.

[16] L. Garibyan and N. Avashia, "Polymerase Chain Reaction," *J. Invest. Dermatol.*, vol. 133, no. 3, pp. 1–4, Mar. 2013.

[17] A. Hadidi, Ed., *Viroids*. Collingwood: CSIRO Publ. [u.a.], 2003.

[18] P. Craw and W. Balachandran, "Isothermal nucleic acid amplification technologies for point-of-care diagnostics: a critical review," *Lab. Chip*, vol. 12, no. 14, p. 2469, 2012.

[19] T. Notomi, "Loop-mediated isothermal amplification of DNA," *Nucleic Acids Res.*, vol. 28, no. 12, p. 63e–63, Jun. 2000.

[20] Y. Mori and T. Notomi, "Loop-mediated isothermal amplification (LAMP): a rapid, accurate, and cost-effective diagnostic method for infectious diseases," *J. Infect. Chemother.*, vol. 15, no. 2, pp. 62–69, 2009.

[21] P. J. Asiello and A. J. Baeumner, "Miniaturized isothermal nucleic acid amplification, a review," *Lab. Chip*, vol. 11, no. 8, p. 1420, 2011.

[22] C. H. Ahn *et al.*, "Disposable Smart Lab on a Chip for Point-of-Care Clinical Diagnostics," *Proc. IEEE*, vol. 92, no. 1, pp. 154–173, Jan. 2004.

[23] A. Pais, A. Banerjee, D. Klotzkin, and I. Papautsky, "High-sensitivity, disposable lab-on-a-chip with thin-film organic electronics for fluorescence detection," *Lab. Chip*, vol. 8, no. 5, p. 794, 2008.

[24] V. Srinivasan, V. K. Pamula, and R. B. Fair, "An integrated digital microfluidic lab-on-a-chip for clinical diagnostics on human physiological fluids," *Lab. Chip*, vol. 4, no. 4, p. 310, 2004.

[25] D. Mark, S. Haeberle, G. Roth, F. Von Stetten, and R. Zengerle, "Microfluidic Lab-on-a-Chip Platforms: Requirements, Characteristics and Applications," in *Microfluidics Based Microsystems*, S. Kakaç, B. Kosoy, D. Li, and A. Pramuanjaroenkij, Eds. Dordrecht: Springer Netherlands, 2010, pp. 305–376.

[26] G. Velve Casquillas *et al.*, "Fast microfluidic temperature control for high resolution live cell imaging," *Lab Chip*, vol. 11, no. 3, pp. 484–489, 2011.

[27] G. Velve-Casquillas, J. Costa, F. Carlier-Grynkorn, A. Mayeux, and P. T. Tran, "A Fast Microfluidic Temperature Control Device for Studying Microtubule Dynamics in Fission Yeast," in *Methods in Cell Biology*, vol. 97, Elsevier, 2010, pp. 185–201.

[28] G. Maltezos *et al.*, "Exploring the limits of ultrafast polymerase chain reaction using liquid for thermal heat exchange: A proof of principle," *Appl. Phys. Lett.*, vol. 97, no. 26, p. 264101, Dec. 2010.

[29] S. Schumacher *et al.*, "Highly-integrated lab-on-chip system for point-of-care multiparameter analysis," *Lab Chip*, vol. 12, no. 3, pp. 464–473, 2012.

[30] H. Mao, T. Yang, and P. S. Cremer, "A Microfluidic Device with a Linear Temperature Gradient for Parallel and Combinatorial Measurements," *J. Am. Chem. Soc.*, vol. 124, no. 16, pp. 4432–4435, Apr. 2002.

[31] G. Velve Casquillas *et al.*, "Fast microfluidic temperature control for high resolution live cell imaging," *Lab Chip*, vol. 11, no. 3, pp. 484–489, 2011.

[32] G. Velve-Casquillas, J. Costa, F. Carlier-Grynkorn, A. Mayeux, and P. T. Tran, "A Fast Microfluidic Temperature Control Device for Studying Microtubule Dynamics in Fission Yeast," in *Methods in Cell Biology*, vol. 97, Elsevier, 2010, pp. 185–201.

[33] T. Lederer, W. Hilber, and B. Jakoby, "Fast thermo-pneumatic actuation of a thin PDMS membrane using a micro Peltier-element for microfluidic applications," *E Elektrotechnik Informationstechnik*, vol. 126, no. 1–2, pp. 70–74, Feb. 2009.

[34] A. Bar-Cohen and P. Wang, "On-Chip Thermal Management and Hot-Spot Remediation," in *Nano-Bio- Electronic, Photonic and MEMS Packaging*, C. P. Wong, K.-S. Moon, and Y. (Grace) Li, Eds. Boston, MA: Springer US, 2010, pp. 349–429.

[35] A. Scorzoni, M. Tavernelli, P. Placidi, and S. Zampolli, "Thermal Modeling and Characterization of a Thin-Film Heater on Glass Substrate for Lab-on-Chip Applications," *IEEE Trans. Instrum. Meas.*, vol. 64, no. 5, pp. 1098–1098, May 2015.

[36] D. Moschou *et al.*, "All-plastic, low-power, disposable, continuous-flow PCR chip with integrated microheaters for rapid DNA amplification," *Sens. Actuators B Chem.*, vol. 199, pp. 470–478, Aug. 2014.

[37] Z. Jiao, X. Huang, N.-T. Nguyen, and P. Abgrall, "Thermocapillary actuation of droplet in a planar microchannel," *Microfluid. Nanofluidics*, vol. 5, no. 2, pp. 205–214, Aug. 2008.

[38] G. Maltezos, M. Johnston, and A. Scherer, "Thermal management in microfluidics using micro-Peltier junctions," *Appl. Phys. Lett.*, vol. 87, no. 15, p. 154105, Oct. 2005.

[39] Andre Marcel, Charles Joseph, Alfred Van Bokestal, and Ghislain Belhomme, "Self-regulating heating element," US 4104509 A, 23-Sep-1975.

[40] Bijan Khazai and George M. Nichols, "Self-regulating polymer composite heater," US 5902518 A, 11-May-1999.

[41] J. A. Oakes and C. L. Sandberg, "Some Aspects of a Self-Limiting Resistive Electric Heating Element," *IEEE Trans. Ind. Appl.*, vol. IA-9, no. 4, pp. 462–466, Jul. 1973.

[42] I. Wyzkiewicz *et al.*, "Self-regulating heater for microfluidic reactors," *Sens. Actuators B Chem.*, vol. 114, no. 2, pp. 893–896, Apr. 2006.

[43] J. R. Buser *et al.*, "Precision chemical heating for diagnostic devices," *Lab Chip*, vol. 15, no. 23, pp. 4423–4432, 2015.

[44] B. Weigl, G. Domingo, P. LaBarre, and J. Gerlach, "Towards non- and minimally instrumented, microfluidics-based diagnostic devices," *Lab. Chip*, vol. 8, no. 12, p. 1999, 2008.

[45] V. Miralles, A. Huerre, F. Malloggi, and M.-C. Jullien, "A Review of Heating and Temperature Control in Microfluidic Systems: Techniques and Applications," *Diagnostics*, vol. 3, no. 1, pp. 33–67, Jan. 2013.

[46] P. Craw and W. Balachandran, "Isothermal nucleic acid amplification technologies for point-of-care diagnostics: a critical review," *Lab. Chip*, vol. 12, no. 14, p. 2469, 2012.

[47] C.-C. Chang, C.-C. Chen, S.-C. Wei, H.-H. Lu, Y.-H. Liang, and C.-W. Lin, "Diagnostic Devices for Isothermal Nucleic Acid Amplification," *Sensors*, vol. 12, no. 12, pp. 8319–8337, Jun. 2012.

[48] W. Su, X. Gao, L. Jiang, and J. Qin, "Microfluidic platform towards point-of-care diagnostics in infectious diseases," *J. Chromatogr. A*, vol. 1377, pp. 13–26, Jan. 2015.

[49] S. Nie *et al.*, "Evaluation of Alere i Influenza A&B for Rapid Detection of Influenza Viruses A and B," *J. Clin. Microbiol.*, vol. 52, no. 9, pp. 3339–3344, Sep. 2014.

[50] J. Dunn, J. Obuekwe, T. Baun, J. Rogers, T. Patel, and L. Snow, "Prompt detection of influenza A and B viruses using the BD Veritor™ System Flu A+B, Quidel® Sofia® Influenza A+B FIA, and Alere BinaxNOW® Influenza A&B compared to real-time reverse transcription-polymerase chain reaction (RT-PCR)," *Diagn. Microbiol. Infect. Dis.*, vol. 79, no. 1, pp. 10–13, May 2014.

[51] S. Lutz *et al.*, "Microfluidic lab-on-a-foil for nucleic acid analysis based on isothermal recombinase polymerase amplification (RPA)," *Lab. Chip*, vol. 10, no. 7, p. 887, 2010.

[52] A. M. Foudeh, T. Fatanat Didar, T. Veres, and M. Tabrizian, "Microfluidic designs and techniques using lab-on-a-chip devices for pathogen detection for point-of-care diagnostics," *Lab. Chip*, vol. 12, no. 18, p. 3249, 2012.

[53] Y. Sun, T. L. Quyen, T. Q. Hung, W. H. Chin, A. Wolff, and D. D. Bang, "A lab-on-a-chip system with integrated sample preparation and loop-mediated isothermal amplification for rapid and quantitative detection of Salmonella spp. in food samples," *Lab Chip*, vol. 15, no. 8, pp. 1898–1904, 2015.

[54] P. LaBarre *et al.*, "A Simple, Inexpensive Device for Nucleic Acid Amplification without Electricity—Toward Instrument-Free Molecular Diagnostics in Low-Resource Settings," *PLoS ONE*, vol. 6, no. 5, p. e19738, May 2011.

[55] Z. K. Njiru, "Loop-Mediated Isothermal Amplification Technology: Towards Point of Care Diagnostics," *PLoS Negl. Trop. Dis.*, vol. 6, no. 6, p. e1572, Jun. 2012.

[56] P. LaBarre, J. Gerlach, J. Wilmoth, A. Beddoe, J. Singleton, and B. Weigl, "Non-instrumented nucleic acid amplification (NINA): Instrument-free molecular malaria diagnostics for low-resource settings," 2010, pp. 1097–1099.

[57] Haim H. Bau, Changchun Li, Michael G. Mauk, Robert W. Hart, and Xianbo Qiu, "Moisture-Activated Self-Heating Analysis Device," US20120315638A1.

[58] R. Gurrala *et al.*, "Novel pH sensing semiconductor for point-of-care detection of HIV-1 viremia," *Sci. Rep.*, vol. 6, no. 1, Dec. 2016.

[59] P. S. Nunes, P. D. Ohlsson, O. Ordeig, and J. P. Kutter, "Cyclic olefin polymers: emerging materials for lab-on-a-chip applications," *Microfluid. Nanofluidics*, vol. 9, no. 2–3, pp. 145–161, Aug. 2010.

[60] U. M. Attia, S. Marson, and J. R. Alcock, "Micro-injection moulding of polymer microfluidic devices," *Microfluid. Nanofluidics*, vol. 7, no. 1, pp. 1–28, Jul. 2009.

[61] H. Becker, "Polymer microfluidic devices," *Talanta*, vol. 56, no. 2, pp. 267–287, Feb. 2002.

[62] G. A. Mannella, V. La Carrubba, and V. Brucato, "Peltier cells as temperature control elements: Experimental characterization and modeling," *Appl. Therm. Eng.*, vol. 63, no. 1, pp. 234–245, Feb. 2014.

[63] Y. Wang, H. Song, and K. Pant, "A reduced-order model for whole-chip thermal analysis of microfluidic lab-on-a-chip systems," *Microfluid. Nanofluidics*, vol. 16, no. 1–2, pp. 369–380, Jan. 2014.

[64] S. Kumar, M. A. Cartas-Ayala, and T. Thorsen, "Thermal modeling and design analysis of a continuous flow microfluidic chip," *Int. J. Therm. Sci.*, vol. 67, pp. 72–86, May 2013.

[65] B. Weigl, G. Domingo, P. LaBarre, and J. Gerlach, "Towards non- and minimally instrumented, microfluidics-based diagnostic devices," *Lab. Chip*, vol. 8, no. 12, p. 1999, 2008.

[66] C. Liu, M. G. Mauk, R. Hart, X. Qiu, and H. H. Bau, "A self-heating cartridge for molecular diagnostics," *Lab. Chip*, vol. 11, no. 16, p. 2686, 2011.

[67] G. A. Mannella, V. La Carrubba, and V. Brucato, "Peltier cells as temperature control elements: Experimental characterization and modeling," *Appl. Therm. Eng.*, vol. 63, no. 1, pp. 234–245, Feb. 2014.

[68] Y. Wang, H. Song, and K. Pant, "A reduced-order model for whole-chip thermal analysis of microfluidic lab-on-a-chip systems," *Microfluid. Nanofluidics*, vol. 16, no. 1–2, pp. 369–380, Jan. 2014.

[69] S. Kumar, M. A. Cartas-Ayala, and T. Thorsen, "Thermal modeling and design analysis of a continuous flow microfluidic chip," *Int. J. Therm. Sci.*, vol. 67, pp. 72–86, May 2013.

[70] S. G. Kandlikar, Ed., *Heat transfer and fluid flow in minichannels and microchannels*, 1st ed. Amsterdam, Netherlands ; Boston: Elsevier, 2006.

[71] A. von Meier, *Electric power systems: a conceptual introduction*. Hoboken, N.J: IEEE Press : Wiley-Interscience, 2006.

[72] D. J. Griffiths, *Introduction to electrodynamics*, vol. 3. Upper Saddle River, NJ: Prentice hall, 1999.

[73] H. Friess, S. Haussener, A. Steinfeld, and J. Petrasch, "Tetrahedral mesh generation based on space indicator functions: TETRAHEDRAL MESH GENERATION BASED ON SPACE INDICATOR FUNCTIONS," *Int. J. Numer. Methods Eng.*, vol. 93, no. 10, pp. 1040–1056, Mar. 2013.

[74] K. Nagamine, T. Hase, and T. Notomi, "Accelerated reaction by loop-mediated isothermal amplification using loop primers," *Mol. Cell. Probes*, vol. 16, no. 3, pp. 223–229, Jun. 2002.

[75] L. Yi, W. Xiaodong, and Y. Fan, "Microfluidic chip made of COP (cyclo-olefin polymer) and comparion to PMMA (polymethylmethacrylate) microfluidic chip," *J. Mater. Process. Technol.*, vol. 208, no. 1–3, pp. 63–69, Nov. 2008.

[76] P. S. Nunes, P. D. Ohlsson, O. Ordeig, and J. P. Kutter, "Cyclic olefin polymers: emerging materials for lab-on-a-chip applications," *Microfluid. Nanofluidics*, vol. 9, no. 2–3, pp. 145–161, Aug. 2010.

[77] J. R. Buser *et al.*, "Precision chemical heating for diagnostic devices," *Lab Chip*, vol. 15, no. 23, pp. 4423–4432, 2015.

[78] B. Zalba, J. M. Marín, L. F. Cabeza, and H. Mehling, "Review on thermal energy storage with phase change: materials, heat transfer analysis and applications," *Appl. Therm. Eng.*, vol. 23, no. 3, pp. 251–283, Feb. 2003.

[79] Paul Donald LaBarre, Jay Lewis Gerlach, Bernhard Hans Weigl, Gonzalo Jose, and Domingo-Villegas, "Chemical Temperature Control," US 20090004732 A1, 01-Jun-2007.

[80] Marc Lamensdorf, "Flameless heater and method of making same," US5611329A.

[81] S. H. Ho, M. M. Rahman, and A. K. Sunol, "Analysis of thermal response of a food self-heating system," *Appl. Therm. Eng.*, vol. 30, no. 14–15, pp. 2109–2115, Oct. 2010.

[82] A. Scorzoni, M. Tavernelli, P. Placidi, and S. Zampolli, "Thermal Modeling and Characterization of a Thin-Film Heater on Glass Substrate for Lab-on-Chip Applications," *IEEE Trans. Instrum. Meas.*, vol. 64, no. 5, pp. 1098–1098, May 2015.

[83] D. Moschou *et al.*, "All-plastic, low-power, disposable, continuous-flow PCR chip with integrated microheaters for rapid DNA amplification," *Sens. Actuators B Chem.*, vol. 199, pp. 470–478, Aug. 2014.

[84] Z. Jiao, X. Huang, N.-T. Nguyen, and P. Abgrall, "Thermocapillary actuation of droplet in a planar microchannel," *Microfluid. Nanofluidics*, vol. 5, no. 2, pp. 205–214, Aug. 2008.

[85] P. Neuzil, J. Pipper, and T. M. Hsieh, "Disposable real-time microPCR device: lab-on-a-chip at a low cost," *Mol. Biosyst.*, vol. 2, no. 6–7, p. 292, 2006.

[86] V. Miralles, A. Huerre, F. Malloggi, and M.-C. Jullien, "A Review of Heating and Temperature Control in Microfluidic Systems: Techniques and Applications," *Diagnostics*, vol. 3, no. 1, pp. 33–67, Jan. 2013.

[87] Minco Products Inc., "Flexible Heaters Design Guide HDG01121806(A)." Minco Products Inc., Fridley, MN, USA, 2007.

[88] Y. H. Ting, "Self-Regulating PTC Heating Systems: A New Approach for Electric Heating Appliances," *IEEE Trans. Ind. Appl.*, vol. IA-8, no. 3, pp. 338–344, May 1972.

[89] W. Huo and Y. Qu, "Effects of Bi1/2Na1/2TiO3 on the Curie temperature and the PTC effects of BaTiO3-based positive temperature coefficient ceramics," *Sens. Actuators Phys.*, vol. 128, no. 2, pp. 265–269, Apr. 2006.

[90] F. Bohlender and N. Buchlaub, *PTC heating resistor*. Google Patents, 1989.

[91] R. Shioi, K. Umeya, K. Yonezuka, and H. Senzaki, *Heating element made of PTC ceramic material*. Google Patents, 1981.

[92] J. Qi, Z. Gui, Y. Wang, Q. Zhu, Y. Wu, and L. Li, "The PTCR effect in BaTiO3 ceramics modified by donor dopant," *Ceram. Int.*, vol. 28, no. 2, pp. 141–143, Jan. 2002.

[93] Y. Song, Y. Pan, Q. Zheng, and X.-S. Yi, "The electric self-heating behavior of graphite-filled high-density polyethylene composites," *J. Polym. Sci. Part B Polym. Phys.*, vol. 38, no. 13, pp. 1756–1763, Jul. 2000.

[94] E.-S. Park *et al.*, "Preparation of positive-temperature coefficient heaters using platinum-catalyzed silicone rubber," *J. Appl. Polym. Sci.*, vol. 92, no. 3, pp. 1611–1617, May 2004.

[95] I. Wyzkiewicz *et al.*, "Self-regulating heater for microfluidic reactors," *Sens. Actuators B Chem.*, vol. 114, no. 2, pp. 893–896, Apr. 2006.

[96] G. V. Lewis, C. R. A. Catlow, and R. E. W. Casselton, "PTCR Effect in BaTiO3," *J. Am. Ceram. Soc.*, vol. 68, no. 10, pp. 555–558, Oct. 1985.

[97] B. Huybrechts, K. Ishizaki, and M. Takata, "The positive temperature coefficient of resistivity in barium titanate," *J. Mater. Sci.*, vol. 30, no. 10, pp. 2463–2474, 1995.

[98] P. Rood, "A Visual Method of Showing The High Temperature Coefficient of Resistance of Metals as Compared with Alloys," *J. Opt. Soc. Am.*, vol. 16, no. 5, p. 357, May 1928.

[99] J. S. Steinhart and S. R. Hart, "Calibration curves for thermistors," *Deep Sea Res. Oceanogr. Abstr.*, vol. 15, no. 4, pp. 497–503, Aug. 1968.

[100] DBK David+Baader GmbH, "HP Series of PTC Heaters." European Thermodynamics Ltd., 2009.

[101] W. M. Yim and F. D. Rosi, "Compound tellurides and their alloys for peltier cooling—A review," *Solid-State Electron.*, vol. 15, no. 10, pp. 1121–1140, Oct. 1972.

[102] E. E. Antonova and D. C. Looman, "Finite elements for thermoelectric device analysis in ANSYS," 2005, pp. 215–218.

[103] European Thermodynamics Limited, "APHC-03107-S Peltier cooler module." European Thermodynamics Limited, 2010.

[104] O. Yamashita, S. Tomiyoshi, and K. Makita, "Bismuth telluride compounds with high thermoelectric figures of merit," *J. Appl. Phys.*, vol. 93, no. 1, pp. 368–374, Jan. 2003.

[105] F. Cardarelli, *Materials handbook: a concise desktop reference*, 2nd ed. London: Springer, 2008.

[106] J. Jevtuševskaja *et al.*, "Combination with antimicrobial peptide lyses improves loop-mediated isothermal amplification based method for

Chlamydia trachomatis detection directly in urine sample," *BMC Infect. Dis.*, vol. 16, no. 1, Dec. 2016.

[107] Francois Carmona, Jacques Maire, Helene Septier, Roland Canet, and Pierre Delhaes, "Material having a resistivity with a positive temperature coefficient," US4966729A, 30-Oct-1990.

KOKKUVÕTE

Kiiplabor (Lab-on-Chip: LoC) tüüpi seadised on iseseisevad miniatuursed diagnostika-vahendid, mis üldjuhul ei kasuta täiendavaid väliseid mõõteriistu. Sellest tingituna on õigustatud ka nende puhul termini mitte-seadmestatud (mitte-instrumenteeritud) testivahendite kasutamine. Näitena võib tuua nukleiinhapete detekteerimise molekulaarsed diagnostikaseadmed (Non Instrumented Nucleic Acid Amplification Tests: NINAAT). Enamuses selliseid miniatuurseid kiiplaboreid vajavad funktsioneerimiseks täpset temperatuuri kontrollimist ja selle juhtimist. Mikro-kuumutamise integreerimine molekulaar-diagnostika seadmesse on aga keeruline tingituna kulude, ruumi ja võimsuslikest piirangutest. See aga omakorda piirab tulemuste kommertsialiseerumist ning seetõttu ka kiir-testi vahendite laialdast kasutamist, mis aitaks näiteks detsentraliseerida kliinilist diagnostikat, vähendada patsientide ooteaegu ja kahandada tervishoiukulusid tervikuna.

Käesolevas doktoritöös uuritakse NINAAT tüüpi molekulaarsete diagnostikaseadmete termilisi nähtusi ja esitatakse temperatuuri kontrolli ning juhtimise tarbeks erinevaid lahendusi. Tulemused on realiseeritud ja rakendatud LoC NINAAT-i seadistes, mida tuntakse nimetuse InTime NINAAT lahenduste all.

Töö esimeses osas kirjeldatakse erinevaid temperatuuri reguleerimise võimalusi ning kirjeldatakse nelja konkreetset mikrosoojendusvõimalust: keemiline kuumutamine, isereguleeruv elektriküte, termostaadiga reguleeritav elektriküte ja termoelektriline soojendamine. Kõigi nelja meetodi hindamiseks on teostatud nii reaalsed füüsikalised katsed kui viidi läbi ka numbrilised eksperimendid (simulatsioonid lõplikel elementidel põhinevate termiliste mudelite abil). Uurimistulemuste analüüsi põhjal leiti, et optimaalseima praktilise realisatsiooni saab luua kasutades kas isereguleeruvat kuumutamist või termostaadiga reguleeritavat kuumutamist. Seega mõlemad meetodid on sobivad kasutamiseks loodavates LoC NINAAT süsteemis olles võimelised reguleerima temperatuuri kindlaksmääratud sihtvahemikus täpsusega +-0.50C (stabiilne viga (SSE)).

Töö teises osas kirjeldatakse uuritud mikrokütte lahenduste edasiarendusi ja esitatakse konkreetsed tehnoloogilised lahendused integreerimaks neid molekulaardiagnostika seadmetega. Hindamiseks kasutatakse isotermilisi NAAT-i protokolle. Süvendatud termilise analüüsi jaoks kasutati LAMP (Loop-mediated isothermal amplification)-protokolli. Mõlemad NINAAT-i platvormil välja töötatud mikroküttekehade parameetrid olid vastavuses testi nõuetega ja saavutasid LAMP-protokolli jaoks vajaliku temperatuuri. Lõpp-lahendusena valiti isereguleeruval küttel põhinev lahendus tingituna selle realiseerimise lihtsusest ja väiksemast hinnast võrreldes alternatiivsete lahendustega.

Praktilised uuringud viisid sellise lahenduseni, kus mikrosoojenemise lahus põhineb polümeervaigul PTCR, mida kasutati isereguleeriva soojendina (küttekehana) NINAAT mikrokiibi funktsionaalse prototüübi valmistamisel. Näidati, et kuumutuslahus suudab säilitada reaktsioonitemperatuure nõutavates 60-630 C vahemikus ja nimetatud temperatuurivahemik saavutatakse 10 minuti jooksul. Kasutades termilist simulatsiooni leiti, et ligikaudu 85% reaktsioonikogusest ei muutu ajaperioodi lõpuni. Uuringute tulemusel selgud, et funktsionaalne NINAAT-kiibi prototüüp koos mikrosoojendamislahusega, kasutades LAMP-protokolli on võimeline edukalt avastama ka siht-DNA-d.

Doktortöö viimases osas uuritakse mikrosoojenemise integreerimise lahendusi, mis integreeritakse InTime NINAAT-i prototüübi seadmega koos kõigi vedelike ja kasutajaliidese funktsioonidega. InTime NINAAT-seadis on seega iseseisev mitte-instrumenteeritud NAAT-platvorm, mis töötab nii, nagu seda vajab lõpptarbija.

Appendix A

Tamas Pardy, Toomas Rang, Indrek Tulp

"Modelling and experimental characterisation of self-regulating resistive heating elements for disposable medical diagnostics devices," 2015, pp. 263–271. (ETIS 3.1)

Modelling and experimental characterisation of self-regulating resistive heating elements for disposable medical diagnostics devices

T. Pardy[1], T. Rang[1] & I. Tulp[2]
[1]*Thomas Johann Seebeck Department of Electronics,*
Tallinn University of Technology, Estonia
[2]*SelfD Technologie GmbH, Germany*

Abstract

Resistive heating elements based on positive temperature coefficient (PTC) ceramics have the inherent advantage of self-regulating their temperature output via a rapid increase in resistance with increasing temperatures, and therefore require no additional control circuitry. This is particularly advantageous for medical devices, especially disposable molecular diagnostics, where minimal space requirements and power dissipation are crucial design factors, as well as low cost per device. However, rapid prototyping and design validation in silico through finite element analysis are hindered by the scarcity of material data on commercially available heating elements. The simplest characterization of the function of these heating elements is through the temperature coefficient of resistance, which is easily measured yet still provides an acceptable approximation. We propose a finite element model that relies only on the temperature coefficient to simulate the function of PTC heating elements. Model validation was done using a commercially available PTC heating element, the temperature coefficient of which was measured and inputted into the model to simulate a PMMA test structure designed to house the heater and accept Lab-on-a-Chip devices with typical dimensions (25mm x 75 mm).
Keywords: positive temperature coefficient, lab-on-a-chip, resistive heating, microfluidics, computer aided design, finite element modelling.

1 Introduction

In molecular diagnostics, temperature control is required for a wide variety of assays, particularly immunoassays and nucleic acid amplification assays. These assays require complex liquid handling, usually done via microfluidics. For a portable, disposable device, it is necessary to have a heating solution with low power dissipation, minimal space requirements and low cost per device. These criteria are easily satisfied by electrical heaters, however, including control circuitry increases development costs and complexity, while having a negative effect on the robustness of the device. For a point-of-care test intended for use at home, minimal complexity is essential to rule out possible errors. To avoid the need for control circuitry, two options are available: one is that of PTC (positive temperature coefficient) ceramic pellets, the other is using PTC resistance wires. However, the topic of integrated, portable (preferably disposable) electrical microheaters for microfluidics has not been researched extensively according to the available literature.

The group of Wyzkiewicz *et al.* [1] proposed a self-regulating heating solution for microfluidics that utilises PTC resistance wires. One of their demonstration setups used printed circuit boards (PCB) as substrate, consisting of interdigitated tracks of carbon-copper-silver, which could be a reasonably cheap microheating solution for disposable molecular diagnostics. The demonstrated setup had an output temperature range of 30–70°C, suitable for a wide variety of assays. However, looking at microheating solutions from an industrial perspective, developing a custom-tailored heating solution may be less cost-efficient than choosing a commercially available one and adapting the device geometry and parameters accordingly. In any case, several prototyping stages and device optimization are necessary, and the higher the number of steps, the more costly development is. To reduce these costs, in silico prototype validation may be employed, using finite element models to simulate and predict device behaviour for a particular design. This approach, coupled with computer aided design may significantly save on time and human labour during development.

The goal of the work described in this paper was to propose an option for the finite element modelling of microheating in disposable molecular diagnostics devices using self-regulating heaters. The proposed model was validated via a commercially available PTC heating element in an experimental setup imitating a microfluidics-based molecular diagnostics device. The finite element model relied on properties easily measured without extensive knowledge about the materials and internal structure of the heating element that would require disassembly.

2 Theoretical background

2.1 Self-regulating heating elements

In the self-regulating heating elements discussed in this paper, the positive temperature coefficient of resistance (PTCR) effect is used for the precise regulation of heat output. This effect means a rapid increase in resistance with

temperature, which essentially regulates the current passing through the heating element. Although most of the manufacturers of currently commercially available heaters do not disclose material data, the most typically used material is doped (3- or 5-valent dopants) polycrystalline barium titanate (BaTiO$_3$) ceramic, mentioned in detail by Shioi *et al.* [2].

The onset of the PTCR effect is at the Curie temperature (T$_c$) of the material, the transition temperature from ferroelectric to paraelectric phase. This temperature can be adjusted by selecting the proper dopant, such as strontium or lead as detailed by Hybrechts *et al.* [3], in turn determining the onset of the PTCR effect, and thus, the set point (or temperature range) of the heating element.

In order to characterise PTC heaters and the PTCR effect in practice, only the temperature coefficient of resistance α [1/K] and the initial resistance R_0 [Ω] are needed, but the latter is measured during recording the data points necessary for calculating the temperature coefficient, where α may be perceived as the slope of the linear curve with which the resistance of the PTC material is approximated.

2.2 Finite element models

2.2.1 Simplified model
The basis for modelling resistive heating is provided by Joule's first law, which states that electric currents passing through a conductor generate heat, which is proportional to the resistance of the conductor R [Ω] and the current I [A] passing through it:

$$Q \propto I^2 \cdot R \tag{1}$$

Q [W] is the energy (heat) released, and if direct current is applied, can be expressed via the formula of power: $P = V \cdot I = I^2 \cdot R$. This alone is enough to build a simplified model of electrical heating, if the assumption is made that the whole heating element uniformly releases the same amount of heat over its whole volume. This is valid if the size of the heater is small enough, and the heating element itself is made for a uniform power distribution. Additionally, the assumption is made that liquid in the microchannel is either slow enough to be considered stationary, or is kept stationary for the duration of heating. Therefore the model consists of two equations: heat generation is expressed by the formula of power ($P = I^2R$), and then heat is propagated through the geometry of the model by the heat transfer equation, eqn. (4). Space-dependence in the model is defined by a Cartesian coordinate system with 3 axes x [m], y [m], z [m], whereas time-dependence is described by time (t) in seconds. Scaling is permitted. Heat generation is expressed via the aforementioned formula of power, which is interpreted for the whole volume of the heater (von Meier [4]):

$$Q = \frac{P_{tot}}{V} \tag{2}$$

where P_{tot} [W] is the total power of the heater, V [m^3] the volume of the heating element. In case the temperature dependence of resistance is taken into account,

the well-known formula for calculating temperature dependent resistance (or resistivity) defines resistance changes (Rood [5]):

$$R(T) = R_0 \cdot [1 + \alpha \cdot (T - T_0)] \tag{3}$$

where $R_0 [\Omega]$ is the resistance at ambient (reference) temperature $T_0 [K]$. $T [K]$ is the current temperature of the heating element, calculated from the heat transfer equation. $\alpha \left[\frac{1}{K}\right]$ is the temperature coefficient of resistance. The heat transfer equation is used in the following form (Kandlikar [6]):

$$\rho C_p \frac{\partial T}{\partial t} - \nabla \cdot (-k\nabla T) = Q \tag{4}$$

where $\rho [kg/m^3]$ is the fluid density, $C_p [J/kg\,K]$ the specific heat capacity at constant pressure, $T [K]$ the absolute temperature in the system, $k [W/(mK)]$ the thermal conductivity, and Q $[W/m^3]$ is the heat source (sink), which in this case is calculated as the power of the heating element as a whole. Materials of the simulated geometry are simulated through the aforementioned quantities (ρ, C_p, k), solved for each spatial point in the geometry, whereas the heating element is characterized by its temperature coefficient of resistance (α).

2.2.2 Extended model

In case the space-dependence of heat generation cannot be neglected, either due to the comparable size of components, or due to the complex structure of the heating element itself, the model introduced earlier must be extended. First, Joule heating (introduced in eqn. (1)) must be rewritten in a differential form for the volume of the heater (von Meier [4]):

$$\frac{dP}{dV} = J \cdot E = J \cdot \frac{J}{\sigma} = J^2 \cdot \rho \tag{5}$$

where $P [W]$ is once more the power, V $[m^3]$ the volume of the element, J $[A/m^2]$ the current density, E [V/m] the electric field. $\sigma [S/m]$ is the conductivity, $\rho [\Omega \cdot m]$ is the resistivity of the material of the heater. Heat propagation relies on the same heat transfer equation (eqn. (4)), but heat generation is expressed as follows (Griffiths [7]):

$$\nabla J = Q_j,$$
$$J = \left(\sigma + \varepsilon_0 \varepsilon_r \frac{\partial}{\partial t}\right) E + J_e, \tag{6}$$
$$E = -\nabla V.$$

where J $[A/m^2]$ is the current density, $Q_j [A/m^3]$ are current sources (sinks), E the electric field, $J_e [A/m^2]$ an external current density (if there is one), $V [V]$ the potential drop in every direction, σ [S/m] the conductivity, ε_0 the relative permittivity of vacuum, ε_r the relative permittivity of the material at the point of

the geometry for which the equations are solved. Materials in the simulated geometry are therefore characterized electrically through their conductivity and relative permittivity. This set of equations relies on the continuity equation, or charge conservation principle:

$$\nabla J = -\frac{\partial p}{\partial t} \qquad (7)$$

The continuity equation states that charge density at a point only changes if current flows into or out of the point. Due to the fact, that heating elements with a positive temperature coefficient of resistance have a non-linear resistivity with respect to temperature, the resistivity must be calculated during simulation at each time instant from eqn. (3), substituting resistivity for resistance (conductivity: $\sigma = 1/\rho$). Resistivity at ambient temperature (ρ_0 [$\Omega \cdot m$]) is possible to calculate from the resistance at ambient temperature, extracting surface area and thickness of the heating element from the model geometry.

3   Experimental setup for model validation

For the experimental validation, a commercially available self-regulating heating element was used. The DBK HP04-1/04-24 heater plate consists of a PTC ceramic heating element, and an aluminium profile with a flat surface on one side. The operating range of this heater was 1-30 V_{DC}, and its highest measured temperature output was 65.1°C.

The experimental setup consisted of a PMMA (polymethyl methacrylate) test structure designed to house the heating element and the temperature probe adapter, a DC multimeter (Agilent 34410A) and a DC power supply (Agilent E3631A). The temperature probe adapter was designed to imitate the typical size regime of microfluidic chips (25 mm x 75 mm), and contained a 2W thermistor with 10 $k\Omega$ initial resistance. The adapter was inserted into the slot in the PMMA frame, positioned as close to the flat face of the aluminium profile of the heating element as possible. The assembled test structure is shown in Figure 1(A).
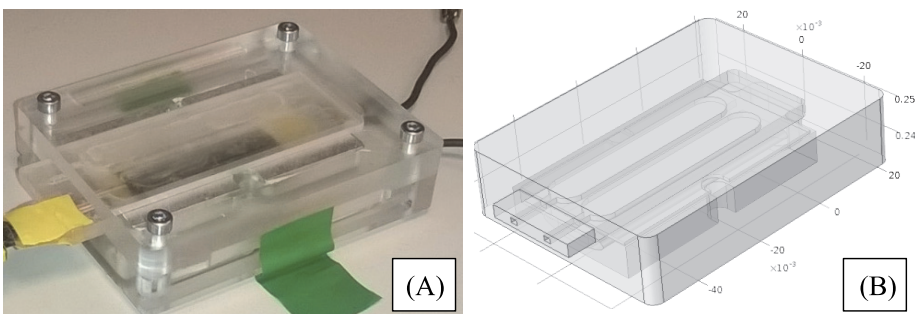

Figure 1:   Test structure (A) and model geometry (B).

4   Results and discussion

4.1 Electrical characterization of heating element

Measurements were conducted using the previously described experimental setup, recording the current flowing through the heating element, and calculating resistance using Ohm's law. The temperature coefficient of resistance calculated with eqn. (3) was 0.23 ± 0.09 [1/K].

The resistance of the heating element at ambient temperature (considered 20 °C in this case) was measured and calculated to be 10 Ω (± 0.4 Ω).

4.2 Evaluation of the simplified model

Most isothermal nucleic acid amplification methods require heating for an extended period of time with adequate temperature stability, typically at target temperatures less than 100°C. For the following evaluation, to prevent accidental heat deflection of the plastic test structure, the maximum temperature was limited at 70°C. Room temperature was defined as the range of 19–22°C, corresponding to the average ambient temperature range in the room where measurements were performed.

The simplified model was solved using the Heat Transfer Module of COMSOL® Multiphysics Version 4.4 for the model geometry shown in Figure 1(B). Materials were either used from the built-in libraries of the software package, or extracted from corresponding literature, such as the work of Shioi *et al.* [2]. To make a comparison, the model was solved for the same input voltages as were given for the experimental setup, ranging from 5 V–25 V.
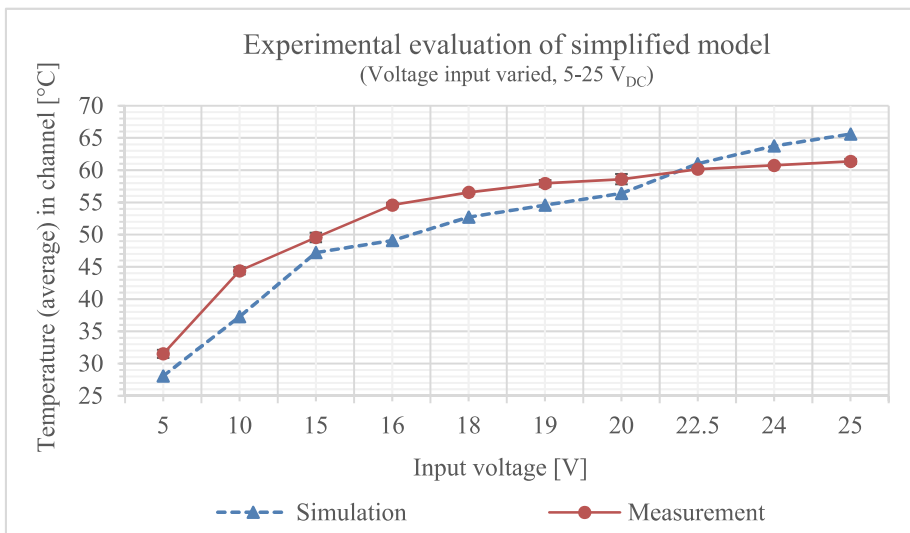

Figure 2:   Evaluation of model – 1.

Measurements were taken for 45 minutes, and the same time period was simulated. Solution time of this model was 17 minutes 24 seconds (± 8 seconds) on a PC with a Core i5-4570 CPU and 16 GB RAM for a single set of input parameters.

In the experimental setup, the temperature probe was positioned in the middle of the channel, whereas in the simulation, temperature was averaged for the volume of the channel and over the time period of the measurements. The comparison of simulated and measured data points is shown in Figure 2. The average estimation error of the model was $3.59 \pm 1.66°C$ degrees over the given range of input voltages.

4.3 Evaluation of the extended model

For this evaluation, the LAMP (loop-mediated isothermal amplification) reaction, an isothermal nucleic acid amplification method was taken into account. This is a highly sensitive and specific amplification method particularly suitable for use in molecular diagnostics, developed by Eiken Chemical Co. (Nagamine *et al.* [8]), which requires a 60–65°C temperature range to be maintained for 15–60 minutes for a successful amplification of DNA samples. The extended model was designed to provide a better approximation of reality, given that the internal structure of the heating element is known in detail. This extension takes into account the current distribution, and therefore yields a more precise definition of heat sources inside the heating element. Having the aforementioned isothermal application in mind, the target temperature range 60–65°C was taken into account for the evaluation, which was possible to reach experimentally at 24 V_{DC} input, so this voltage was used for comparison.

The extended model was solved using the Joule Heating interface of COMSOL® Multiphysics Version 4.4 using the same geometry and material composition as for the simplified model. The experimental setup generated the required heat output at 24 V input, therefore this voltage was used as a basis for comparison between modelling and measurement results. Solution time of this model was 11 minutes 50 seconds (± 16 seconds) on a PC with a Core i5-4570 CPU and 16 GB RAM for a single set of input parameters.

Temperature output was measured in a similar manner as during the evaluation of the simplified model. The extended model estimates temperature output around the set point (reached after 1800 s in both cases) with an error of $0.31 \pm 0.17°C$. Comparison of results is shown in Figure 3.

The heat generation of the experimental setup was more rapid than that of the model, which were probably attributable to the differences in model geometry. The heating elements could not be disassembled without causing irreversible damage, and the patent of Bohlender and Buchlaub [9] describing the internal structure did not include dimensions, so the geometry of the simulated model was approximate. The extended model is better used with heating elements, the internal structure of which is known in detail.
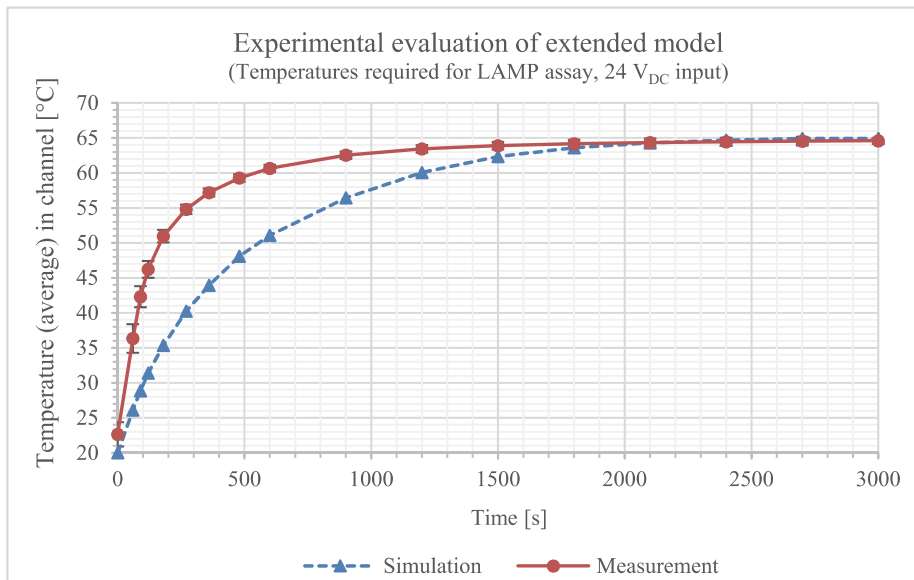
Figure 3:   Evaluation of model – 2.

5   Conclusions

A finite element model was proposed for the modelling of self-regulating resistive heating elements for applications in microheating solutions for disposable molecular diagnostics that relies only on the temperature coefficient of resistance (resistivity) for characterising the heating element. A simplified and an extended version of the model were presented and evaluated for an experimental setup that imitated a disposable diagnostics platform with a replaceable microfluidic cartridge (chip) and a commercially available self-regulating heating element. The simplified model approximated the temperature output of the experimental setup with an error of 3.59 ± 1.66°C degrees over a range of various input voltages and a time range of 45 minutes, whereas the extended model approximated temperature output at 24 V input with an error of 0.31 ± 0.17°C after the set point was reached.

The results discussed in this paper are preliminary and show an early stage of development. Nevertheless, proof was given that the proposed models are capable of estimating the heat output of microheating solutions in diagnostic devices, and as the in-house development of heating solutions proceeds, the precision of these estimations are bound to improve significantly.

Acknowledgements

References

[1] Wyzkiewicz, I., Grabowska, I., Chudy, M., Brzozka, Z., Jakubowska, M., Wisniewski, T. & Dybko, A., Self-regulating heater for microfluidic reactors, *Sens. Actuators B Chem.*, vol. 114, no. 2, pp. 893–896, Apr. 2006.

[2] Shioi, R., Umeya, K., Yonezuka, K. & Senzaki, H., Heating element made of PTC ceramic material, *Tdk Electronics Company Limited*, 1981.

[3] Huybrechts, B., Ishizaki, K., & Takata, M., The positive temperature coefficient of resistivity in barium titanate, *J. Mater. Sci.*, vol. 30, no. 10, pp. 2463–2474, 1995.

[4] Meier, A. von., Electric power systems a conceptual introduction, *Hoboken, N.J.: IEEE Press, Wiley-Interscience*, 2006.

[5] Rood, P., A visual method of showing the high temperature coefficient of resistance of metals as compared with alloys, *J. Opt. Soc. Am.*, vol. 16, no. 5, p. 357, Sep. 1928.

[6] Kandlikar, S. G., Heat transfer and fluid flow in minichannels and microchannels, *Elsevier*, 2006.

[7] Griffiths, D. J., Introduction to electrodynamics, *Prentice Hall*, 1999.

[8] Nagamine, K., Hase, T. & Notomi, T., Accelerated reaction by loop-mediated isothermal amplification using loop primers, Mol. Cell. Probes, vol. 16, no. 3, pp. 223–229, Jun. 2002.

[9] Bohlender, F. & Buchlaub, N., PTC heating resistor, *David & Baader DBK Spezialfabrik elektrischer Apparate und Heizwiderstände GmbH*, 1989.

Appendix B

Tamas Pardy, Toomas Rang, Indrek Tulp

FINITE ELEMENT MODELLING FOR THE OPTIMIZATION OF MICROHEATING IN DISPOSABLE MOLECULAR DIAGNOSTICS

T. PARDY[1], T. RANG[1] & I. TULP[2]
[1]Thomas Johann Seebeck Department of Electronics, Tallinn University of Technology, Estonia.
[2]SelfDiagnostics Deutschland GmbH, Germany.

ABSTRACT

The number of disposable molecular diagnostics tests in the IVD market has been growing rapidly and is bound to continue to grow in the near future. The internal complexity of these rapid tests increases with the complexity of the diagnostic assay implemented by them. Some assays require precise temperature control (±1°C –5°C) for an extended time (i.e. 15–60 minutes) for the reactions involved to run properly. Microheating components in them must meet strict criteria with respect to power consumption, physical size and cost. The proposed finite element model is intended to provide tools for *in silico* validation of device designs (geometries, structural materials), as well as to help in the interpretation of heat transfer processes inside the thermal system present in a molecular diagnostics device. The proposed model was developed for and validated with polyimide etched foil heating elements actively controlled via a mini-thermostat. The thermostat was designed for battery-based operation and implemented with open-source hardware (Arduino-compatible). Plastic test structures were created that emulated disposable Lab-on-a-Chip devices with microfluidic channels to hold liquid volumes on the scale of 0.1 mL. The experimental setup was demonstrated to maintain target temperatures over at least 30 minutes with at least ±1°C around the set point operated from batteries. Physical parameters of the resistive heating element used were fed into the finite element model and simulation results compared to the performance of the aforementioned experimental setup.

Keywords: computer aided design, finite element modelling, lab-on-a-chip, microfluidics, microcontrollers, resistive heating.

1 INTRODUCTION

In molecular diagnostics, temperature control is required for a wide variety of assays, particularly immunoassays and nucleic acid amplification assays. These assays require complex liquid handling, usually done via microfluidics. For a portable, disposable device, it is necessary to have a heating solution with low power dissipation, minimal space requirements and low cost per device. Electrical heaters easily satisfy these criteria. To integrate electrical heating into a portable, handheld device, device geometry must be optimized to minimize heat loss and maximize power efficiency. *In silico* validation of CAD models using finite element models is an attractive option for optimization, enabling iterative design while saving time and prototyping costs.

Existing works in the literature primarily deal with the finite element modelling of heat transfer and microheating in microfluidic Lab-on-a-Chip systems, primarily with a focus on micromachined thin film resistive heaters and microfluidic chips, as well as with a focus on PCR (polymerase chain reaction), a nucleic amplification method that requires thermal cycling, a challenging task in a portable chip format. Moschou [1] used finite element models to simulate the functionality of their PCR chip, which relied on a thin film heater for temperature control. Wang [2] proposed a Reduced Order Model for simulating microfluidic PCR chips. Models of thermoelectric heating (i.e. Peltier) elements are also discussed in the

literature but are outside the scope of our work as their unit cost is typically higher than that of resistive heaters, making them less attractive for disposable applications.

However, works where model disposable Point-of-Care devices that rely on isothermal nucleic acid amplification methods were not possible to find. Models presented in the literature typically focus on certain aspects of a device, such as a microreactor or a microfluidic chip, rather than its entirety, disregarding additional device components, such as the housing that plays a significant part in heat transfer phenomena in the size regime of such devices. For iterative design and *in silico* validation, a complete device model is necessary, and currently available hardware and software make such models possible.

Earlier we demonstrated finite element models for passively regulated (self-regulating) and non-regulated resistive heating for temperature control in disposable Point-of-Care rapid tests using commercially available resistive heating elements [3]. In this paper, we propose a finite element model for active temperature control of disposable molecular diagnostics devices, as well as demonstrate a mini-thermostat application based on open-source (Arduino-compatible) hardware for various isothermal nucleic acid amplification assays. The proposed finite element model was tested for an experimental setup that emulated microfluidics-based molecular diagnostics devices, using a commercially available heating element. The experimental setup was demonstrated to maintain target temperatures over 30 minutes with at least ± 1°C precision around the set point. Battery-based operation was also evaluated.

2 THEORETICAL BACKGROUND

2.1 Temperature control algorithm

Active control in the proposed system relies on the proportional control algorithm, expressed in the following way [4]:

$$V_{in}\left(t\right) = K_p \cdot e\left(t\right) \tag{1}$$

where $V_{in}\left[V\right]$ is the potential drop on the heating element, $K_p\left[1/K\right]$ the proportional controller gain, and $e\left(t\right) = T_{set} - T_{current}$ the process error at time instant $t\left[s\right]$. $T_{set}\left[K\right]$ is the temperature set point of the control algorithm, $T_{current}\left[K\right]$ the measured temperature at time instant *t*. Proportional control is sufficient to achieve the targeted ± 1°C precision while being simpler to implement in a finite element model than a full PID controller.

2.2 Finite element modelling

The basis for modelling resistive heating is provided by Joule's first law, which states that electric currents passing through a conductor generate heat, which is proportional to the resistance of the conductor $R[\Omega]$and the current $I\left[A\right]$ passing through it:

$$Q \propto I^2 \cdot R \tag{2}$$

$Q\left[W\right]$ is the energy (heat) released, and if direct current is applied, can be expressed via the formula of power: $P = V \cdot I = I^2 \cdot R$. The initial assumption is made that liquid in the microchannel is either slow enough to be considered stationary, or is kept stationary for the duration of heating.

Therefore, the model consists of two equations: heat generation is expressed by the formula of power eqn (3), and then heat is propagated through the geometry of the model by

the heat transfer equation, eqn (6). Space-dependence in the model is defined by a Cartesian coordinate system with 3 axes $x\,[\text{m}], y\,[\text{m}], z\,[\text{m}]$, whereas time-dependence is described by time (t) in seconds. Scaling is permitted. Heat generation is expressed via the aforementioned formula of power, written in a differential form for the volume of the heater [5]:

$$\frac{dP}{dV} = J \cdot E = J \cdot \frac{J}{\sigma} = J^2 \cdot \rho \tag{3}$$

where $P[\text{W}]$ is the power, V [m^3] the volume of the heating element, J [A/m^2] the current density, E [V/m] the electric field. σ [S/m] is the conductivity and ρ [$\Omega\cdot\text{m}$] is the resistivity of the material of the heater. Current densities and the electric field used for calculating heat generation are in turn calculated from the following set of equations [6]:

$$\nabla J = Q_j,$$

$$J = \left(\sigma + \varepsilon_0\varepsilon_r\frac{\partial}{\partial t}\right)E + J_e, \tag{4}$$

$$E = -\nabla V.$$

where J [A/m^2] is the current density, Q_j [A/m^3] are current sources (sinks), E the electric field, J_e [A/m^2] an external current density (if there is one), $V\,[\text{V}]$ the potential drop in every direction, σ [S/m] the conductivity, ε_0 the relative permittivity of vacuum and ε_r the relative permittivity of the material at the point of the geometry for which the equations are solved. The controller algorithm (Section 2.1) is coupled with the electric field equation eqn (4) as a boundary condition $V = V_{in}$ at the input terminal. Materials in the simulated geometry are characterized electrically through their conductivity and relative permittivity. The above set of equations eqn (4) relies on the continuity equation, or charge conservation principle [6]:

$$\nabla J = -\frac{\partial p}{\partial t} \tag{5}$$

The continuity equation states that charge density at a point changes only if current flows into or out of the point.

The heat transfer equation is used in the following form [7]:

$$\rho C_p \frac{\partial T}{\partial t} - \nabla \cdot \left(-k\nabla \text{T}\right) = \text{Q} \tag{6}$$

where $\rho\,[\text{kg}/\text{m}^3]$ is the fluid density, $C_p\,[\text{J}/\text{kg K}]$ the specific heat capacity at constant pressure, $T\,[\text{K}]$ the absolute temperature in the system, k[W/(mK)] the thermal conductivity and Q [W/m^3] is the heat source (sink), which in this case is calculated as the power of the heating element as a whole. With respect to heat transfer, materials of the simulated geometry are simulated through the aforementioned quantities (ρ, C_p, k), solved for each spatial point in the geometry.

In case the temperature dependence of resistivity is taken into account, the well-known formula for calculating temperature dependent resistivity defines changes [8]:

$$\rho(T) = \rho_0 \cdot \left[1 + \alpha \cdot (T - T_0)\right] \tag{7}$$

where $\rho_0[\Omega \cdot m]$ is the resistivity at ambient (reference) temperature $T_0\,[K]$. $T\,[K]$ is the current temperature of the heating element, calculated from the heat transfer equation, and $\alpha\left[\dfrac{1}{K}\right]$ is the temperature coefficient of resistivity. Resistivity is derived from resistance in an experimental setup using the following formula [5]:

$$R = \rho\,\frac{l}{A} \tag{8}$$

Where $l\,(\mathrm{m})$ is the length (thickness) of the resistive element, and $A(\mathrm{m}^2)$ its cross-sectional area. This formula stands for resistors with uniform cross-sectional area, which is true for all of the devices used in the experimental setups discussed in this paper.

3 EXPERIMENTAL SETUP FOR MODEL VALIDATION

3.1 Mini-thermostat

The mini-thermostat prototype (Fig. 1a) was created on open-source hardware to support isothermal nucleic acid amplification reactions in disposable Point-of-Care/Lab-on-a-Chip devices, preferably operated from a portable power source. Two main goals in mind were simplicity (ease of use) and scalability (downscaling to fit under chips of 5–6 cm^2 area and less powerful microcontroller chips).

The platform was first implemented on an Arduino Uno microcontroller (ATmega328P) board with an added custom circuit to handle temperature input from a 2-wire 10 kΩ NTC (negative temperature coefficient) thermistor and control current output via a MOSFET (metal-oxide semiconductor field-effect transistor). The controller was equipped with a piezo buzzer for auditory feedback to the user about its operation. Additionally, a graphical user interface was developed (Fig. 1b) based on the Microsoft .NET framework for easily updating control parameters and monitoring operation through the serial interface of the Arduino platform using a USB connection on the computer.

3.2 Setups #1 and #2

In both experimental setups, a commercially available flexible etched foil heating element was used. These resistive heating elements are typically composed of a thin metal film etched
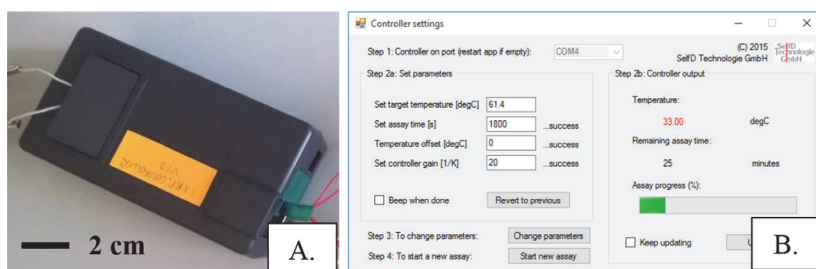

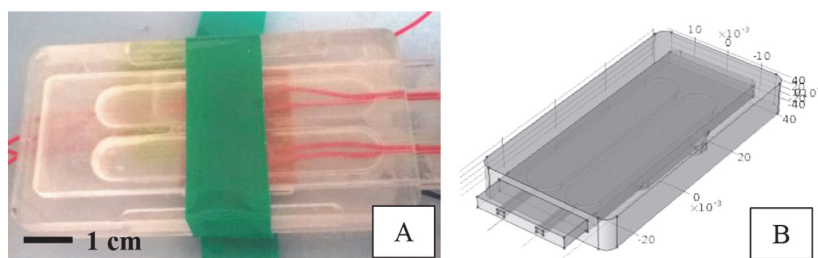Figure 1: Mini-thermostat (a) and user interface (b).

Figure 2: Test structure (a) and model geometry (b).

to form a heating element, which is sandwiched between layers of electrical insulation. The sample used in the experimental setup was an etched foil heater from Minco Products, Inc. (P/N HR5303R70.2LI2A), in which the etched resistive film was encased in polyimide and silicon rubber sheets.

According to manufacturer specifications [9], the resistance of this heating element was 70.2Ω. Temperature output of the heating element was controlled by the mini-thermostat described in Section 3.1. The thermostat regulated current input from a DC power supply (Agilent E3631A). A milled poly-methylmethacrylate (PMMA) test structure was used to emulate a Point-of-Care device with a disposable microfluidic chip (25 mm × 75 mm) that contained microreactor cavities. Both channels contained NTC 10k thermistors, one wired to the mini-thermostat, and the other to a Multimeter (Agilent 34410A) for independent temperature recording (Fig. 2a). The power supply was set up, a temperatures logged using a MATLAB script.

3.3 Setup #3

This experimental setup was similar in every regard to Setups #1 and #2 described in Section 3.2, except the power supply, which was a set of 2 pcs. of 9 V batteries (GP 1604A).

4 RESULTS AND DISCUSSION

4.1 Electrical characterization of heating element

Manufacturer specifications state the resistance of the heating element as 70.2Ω, however, in a previous work we measured initial resistance to be 76.38 ± 0.37Ω [3].

4.2 Model evaluation

4.2.1 Setup #1
Nucleic acid amplification reactions are currently the gold standard in molecular diagnostics assays for the detection of certain living organisms, suchs pathogens. Isothermal amplification reactions require a single temperature or temperature range to be maintained for the specified assay time (15–60 minutes).

Model and controller performance were evaluated on temperature targets defined for various isothermal nucleic acid amplification assays in the literature (see Table 1, Craw [10]). The maximum temperature required by these assays, 65°C, was well below the deflection

Table 1: Target temperatures for isothermal nucleic acid amplification assays.

Method	Full name	Temperature target (°C)
NASBA	Nucleic Acid Sequence Based Amplification	41
HDA	Helicase dependent amplification	64
LAMP	Loop mediated isothermal amplification	60–65
NEAR	Nicking Enzyme Amplification Reaction	55–59
RCA	Rolling Circle Amplification	30–65
RPA	Recombinase Polymerase Amplification	37–42
SPIA	Single primer isothermal amplification	45–50
RAM	Ramification amplification method	35

temperature of the plastic we used in the experimental setups. Room temperature for the model was defined as 19°C–22°C, and the thermistor baseline for temperature recording as 26°C (see Section 3.2 for more details).

The model was validated using the Joule Heating interface of COMSOL® Multiphysics Version 5.2 using the model geometry shown in Fig. 1b. Material properties were derived from the built-in libraries of the software package. The mini-thermostat received a 15 V input with 1 A current limit from the power supply, and the controller gain K_p was set to 15 [1/K]. Set temperatures were according to Table 1 and Fig. 3, taking lower and upper ends of temperature ranges as well as single target temperatures where appropriate. To evaluate model performance, the same parameters were fed into the model and a comparison made.

The model was validated using a PC with a Core i5-4570 CPU and 16 GB RAM. Solution time varied with set temperatures, showing a nearly linear increase in solution time with tem-
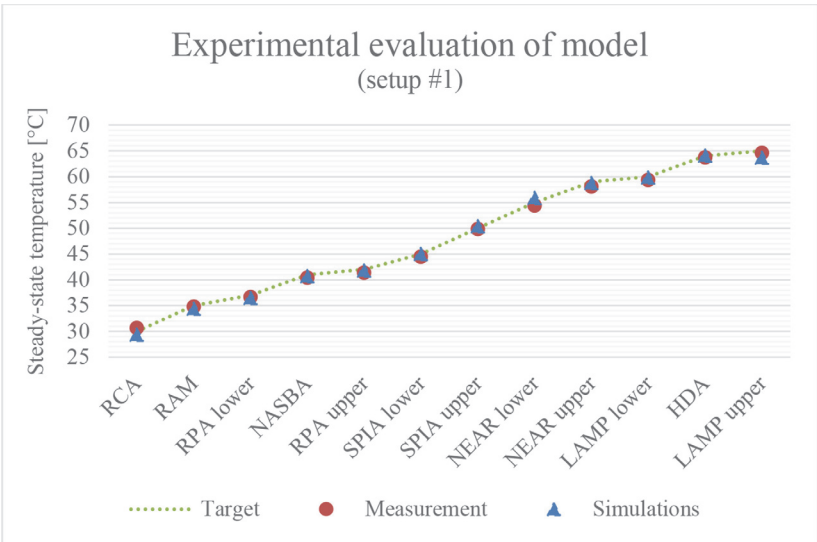

Figure 3: Experimental evaluation of setup #1.

perature increase. For a set temperature of 30°C, the model was validated in 14 minutes 42 seconds (±1 minute 43 seconds), whereas for 65°C, solution time was 55 minutes 25 seconds (±31 minutes 8 seconds). This difference was caused by an increase in complexity: at lower set temperatures, steady-state was reached in a shorter time, after which the length of time steps could be longer and, therefore, the model took a shorter time to solve, as there was no significant change. The variance of solution times is also due to a varying load on the computer from other tasks running in parallel.

Temperatures inside the experimental setup were recorded as described in Section 3.2, with an independent thermistor in a cavity adjacent to the sensor connected to the thermostat. Appropriate temperature offsets were applied to compensate for errors resulting from the different physical positions of the two sensors. Each recording was conducted for 30 minutes, during which steady-state was possible to achieve (± 1°C around the set temperature). On average, steady-state temperatures recorded in the microreactor cavity of the experimental setup were within 0.53°C ± 0.22°C from the designated set temperatures derived from Table 1. The finite element model estimated recorded temperature outputs with an error of 0.64°C ± 0.39°C. Comparison of results is shown in Fig. 3.

4.2.2 Setup #2

For this evaluation, the LAMP (loop-mediated isothermal amplification) reaction, an isothermal nucleic acid amplification method was taken into account. This is a highly sensitive and specific amplification method particularly suitable for use in molecular diagnostics, developed by Eiken Chemical Co. [10, 11], which requires a 60°C–65°C temperature range to be maintained for 15–60 minutes for a successful amplification of DNA samples.

The model was validated using the Joule Heating interface of COMSOL® Multiphysics Version 5.2 using the same model geometry and material properties as setup #1. The mini-thermostat received an 18 V input with 1 A current limit from the power supply, and the controller gain K_p was set to 20 [1/K]. Set temperature was 63.8°C. To evaluate model performance, experimental parameters were fed into the model and a comparison made.

The model was solved using a PC with a Core i5-4570 CPU and 16 GB RAM with an average solution time of 1 hour 43 minutes (± 10 minutes 45 seconds).

Temperature recordings in this experimental setup indicated a more pronounced controller error (1.54°C ± 0.09°C) in steady-state than was observed in setup #1 (Section 4.2.1). This was due to the larger controller gain and higher input voltage, and was repeatedly observed during measurements. In a side-by-side comparison of model and experimental results, the mean absolute error was 2.02°C (±2.7°C) along the whole length of the recorded time period, whereas in steady-state, this error decreased to 0.52°C (±0.19°C). Comparison of results is shown in Fig. 4.

4.2.3 Setup #3

Battery-based operation was evaluated with conditions matching those of setup #1 (Section 0), for temperature targets required by certain isothermal nucleic acid amplification reactions. A smaller set of temperature targets were chosen from Table 1 for this evaluation. Two pcs. of (fresh) 9 V batteries were used as power source and, therefore, input voltage was set to 18 V in the model.

Hardware and software used for validating the model was the same as for setup #1, which led to similar solution times (see Section 0).
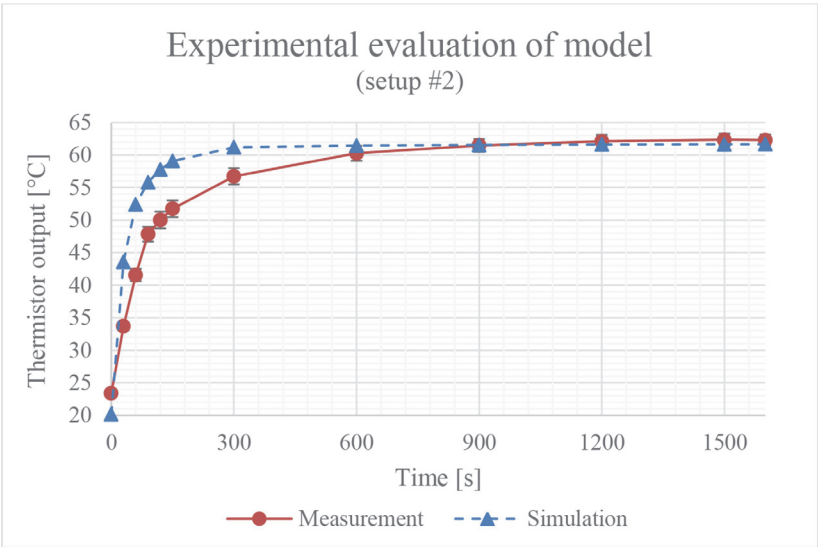
Figure 4: Experimental evaluation of Setup #2.

Temperatures in the experimental setup were recorded as in setup #1. Experimental results indicated that the controller was able to maintain target temperatures within the microreactor cavity with an average error of 0.05°C ± 0.09°C after steady-state was reached. The decrease in error compared to setup #1 (Section 4.2.1) was due to the smaller number of data points. The finite element model estimated recorded temperature outputs with an error of 0.69°C ± 0.34°C. Although initially the output was 18 V, battery voltage output decreased over the course of several experiments, which was not accounted for in the model. A comparison of the results is shown in Fig. 5.
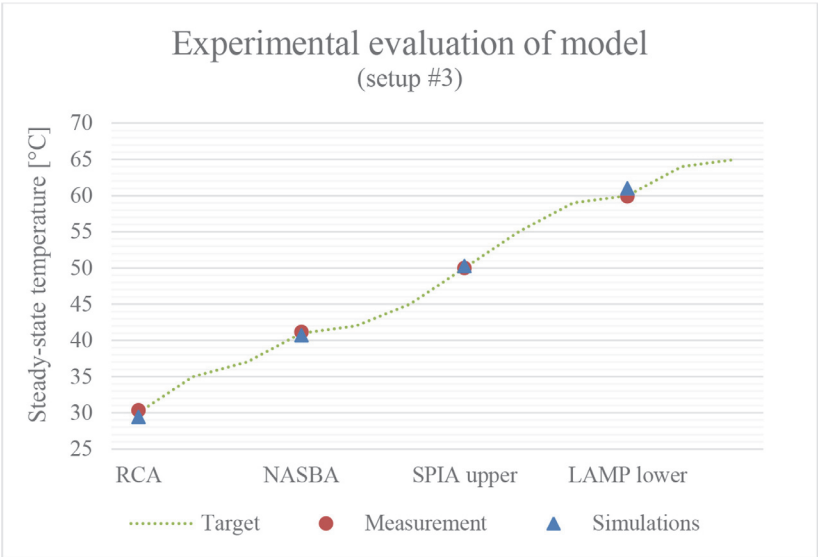

Figure 5: Experimental evaluation of setup #3.

5 CONCLUSIONS

A finite element model was proposed for the modelling of actively controlled resistive heating elements for applications in microheating solutions for disposable molecular diagnostics devices to aid in iterative optimization and *in silico* validation of device designs. The model was presented and evaluated for experimental setups imitating a disposable molecular diagnostics platform with temperature control and a replaceable cartridge (chip) with a microfluidic reactor cavity, matching the typical dimensions of such devices. For temperature control purposes, the heat output of a commercially available etched foil resistive heating element was controlled using a mini-thermostat developed for open-source Arduino-compatible hardware.

Target temperatures were chosen to match several molecular diagnostics assays (isothermal nucleic acid amplification assays). The proposed finite element model was capable of approximating temperature outputs recorded in the experimental setups with an error of 0.64°C ± 0.39°C over a range of different target temperatures between 30°C and 65°C when operated from a DC power supply. In a side-by-side comparison, approximation error was 0.52°C ± 0.19°C. During battery operation, the model was capable of estimating experimentally recorded temperatures with an average error of 0.69°C ± 0.34°C.

Furthermore, the proposed mini-thermostat device was capable of controlling temperature outputs with 0.53°C precision around 12 distinct set temperatures from 30°C to 65°C during 30 minutes of operation, when operated both from a DC power supply and batteries.

To summarize, the proposed model, despite being in early stages of development, was capable of approximating time-dependent heat transfer in a disposable molecular diagnostics device with more than 1°C precision. Additionally, a mini-thermostat based on open-source hardware was proposed and demonstrated to be able to support isothermal nucleic acid amplification assays in disposable Lab-on-a-Chip devices.

REFERENCES

[1] Moschou, D., Vourdas, N., Kokkoris, G., Papadakis, G., Parthenios, J., Chatzandroulis, S. & Tserepi, A., All-plastic, low-power, disposable, continuous-flow PCR chip with integrated microheaters for rapid DNA amplification. *Sensors and Actuators B: Chemical*, **199**, pp. 470–478, 2014.
http://dx.doi.org/10.1016/j.snb.2014.04.007

[2] Wang, Y., Song, H. & Pant, K., A reduced-order model for whole-chip thermal analysis of microfluidic lab-on-a-chip systems. *Microfluidics and Nanofluidics*, **16**(1–2), pp. 369–380, 2014.
http://dx.doi.org/10.1007/s10404-013-1210-0

[3] Pardy, T., Tulp, I. & Rang, T., Finite element modelling of the resistive heating of disposable molecular diagnostics devices. *Computational Methods and Experimental Measurements XVII*, **59**, pp. 381–391, 2015.
http://dx.doi.org/10.2495/cmem150341

[4] Srivastava, M., Srivastava, M.C. & Bhatnagar, S., *Control Systems*, Tata McGraw-Hill: New Delhi, Singapore, 2009.

[5] Meier, A.V., *Electric Power Systems: A Conceptual Introduction*, IEEE Press, Wiley-Interscience, Hoboken, N.J, 2006.

[6] Griffiths, D.J., Introduction to electrodynamics. *Prentice Hall*, **93**, p. 95, 1999.

[7] Kandlikar, S.G., Garimella, S., Li, D., Colin, S. & King, M.R., *Heat Transfer and Fluid Flow in Minichannels and Microchannels*, Elsevier, 2006.

[8] Rood, P., A visual method of showing the high temperature coefficient of resistance of metals as compared with alloys. *Journal of the Optical Society of America*, **16**(5), pp. 357–359, 1928.
http://dx.doi.org/10.1364/JOSA.16.000357

[9] Minco Products, Inc., Flexible heaters design guide HDG01121806(A), *Minco Products Inc.*, 2007.

[10] Craw, P. & Balachandran, W., Isothermal nucleic acid amplification technologies for point-of-care diagnostics: a critical review. *Lab on a Chip*, **12**(14), pp. 2469–2486, 2012.
http://dx.doi.org/10.1364/JOSA.16.000357

[11] Nagamine, K., Hase, T. & Notomi, T., Accelerated reaction by loop-mediated isothermal amplification using loop primers. *Molecular and Cellular Probes*, 16(3), pp. 223–229, 2002.
http://dx.doi.org/10.1006/mcpr.2002.0415

Appendix C

Tamas Pardy, Toomas Rang, Indrek Tulp

"Modelling and experimental characterisation of thermoelectric heating for molecular diagnostics devices," 2016, pp. 27–30. (ETIS 3.1)

Modelling and experimental characterisation of thermoelectric heating for molecular diagnostics devices

T. Pardy, T. Rang

Thomas Johann Seebeck Department of Electronics
Tallinn University of Technology
Tallinn, Estonia

I. Tulp

Selfdiagnostics Deutschland GmbH
Leipzig, Germany

Abstract—Certain novel molecular diagnostics Point-of-Care applications require precise temperature control (±1-5 °C) over an extended time (15-60 minutes) for proper function. Microheating components in portable tests must meet strict criteria with respect to size and power consumption, both of which may be met with thermoelectric heating. Our proposed finite element model is intended to provide tools for the evaluation of thermoelectric heating for molecular diagnostics as well as aid in iterative device design and in silico validation of device designs. The proposed model was developed for and validated with a commercially available thermoelectric cooler. A 3D printed test structure was created to house a glass microfluidic chip (<0.1 ml channel volume) and the heating element, imitating a tiny portable Point-of-Care test. Experimental setups were evaluated in the operating input voltage range of the heating element. Physical parameters of the setup were fed into the finite element model and a comparison made between simulated and physical temperature recordings.

Keywords—finite element modelling, Point-of-Care, thermoelectric heating, lab-on-a-chip, microfluidics, computer aided design

I. INTRODUCTION

In novel molecular diagnostics assays, precise temperature control is widely required. These assays require complex liquid handling typically performed by microfluidics. Handheld, portable diagnostics devices require a heating solution that is efficient both in power and space consumption. Thermoelectric (Peltier) elements satisfy these criteria. Additionally, contrary to regular resistive heaters, Peltier elements can heat and cool as well, with excellent temperature stability. To integrate these devices into a portable rapid test, device geometry must be optimized to minimize heat loss and maximize power efficiency. Iterative CAD (computer-aided design) and optimization by evaluating device geometries with finite element modelling is an attractive solution to save time and prototyping costs.

Peltier elements have been extensively explored in the literature as candidates for temperature control in Lab-on-a-Chip devices, both as external components attached to the chips, as well as built-in micromachined (micro-Peltier) elements. The primary focus has been on temperature control for PCR (polymerase chain reaction) in a chip format [1]. PCR has been the long-time gold standard in nucleic acid amplification assays for the detection of living organisms. However, it requires thermal cycling with 3 distinct temperature points with a specific timing that poses unique challenges in a portable, handheld, battery-operated device due to the aforementioned restrictions on size and power. Mannella et al. [2] demonstrated a 2D finite element model of a Peltier cooling cell for the temperature control of a sample vial, claiming that the model accurately predicted experimental results. Some works focus on functionally modelling thermoelectric elements themselves [3].

Existing literature works on full models of Point-of-Care devices relying on isothermal nucleic acid amplification methods were not possible to find. Works in the literature on Peltier elements typically focus on specific aspects of a device, such as a microreactor cavity or the element itself rather than the entirety of the device, disregarding additional components such as the device housing that nevertheless plays a significant part in heat transfer phenomena in the size regime of handheld, portable tests. For iterative geometry optimization and evaluation via finite element modelling, a full device model is necessary, including all device components, and currently available hardware and software can support the use of such models. Additionally, Peltier elements in the literature are typically used for cooling, or alternatively for thermal cycling in PCR applications. Isothermal amplification methods that require a single temperature (or range) to be maintained over a given time are simpler to implement in portable devices.

In earlier works we demonstrated models for temperature control of Point-of-Care rapid tests using commercially available resistive heating elements [4], [5]. In this paper we propose a finite element model for temperature control of molecular diagnostics devices using a commercially available thermoelectric (Peltier) device, focusing on the temperature range required by various isothermal nucleic acid amplification reactions. The proposed finite element model was evaluated for an experimental setup that imitated microfluidics-based molecular diagnostics devices, made up of a small glass microfluidic chip with a microchannel (<0.1 ml volume) to house reactions and a 3D printed plastic device housing. The model was also evaluated on a setup of said glass chip directly attached to the thermoelectric device.

A. Thermoelectric heating

In the experimental setups described in this paper, thermoelectric cooling elements were used. The Seebeck effect describes the phenomenon by which different temperatures applied at two sides of a junction of dissimilar materials causes a potential difference, characterized by the Seebeck electromotive force [6]:

$$emf = \Delta\alpha(T_h - T_c) \qquad (1)$$

Where $\Delta\alpha = \alpha_B - \alpha_A$ is the difference between the absolute Seebeck coefficients α [V/K] of the materials, $T_h[K]$ and $T_c[K]$ the temperature of the hot and cold sides of the junction, respectively. This electromotive force contributes to local current density as well:

$$J_e = -\sigma S\nabla T \qquad (2)$$

Where $J_e[A/m^2]$ marks the current density, σ [S/m] the electrical conductivity, $S[V/K]$ the Seebeck coefficient in a vector form and $T[K]$ the temperature. The Peltier effect describes the phenomenon by which a current flowing through said junction will cause a temperature difference between the two sides of the junction, characterized by the Peltier coefficient P [V]. The second Thomson relation relates the Seebeck and Peltier coefficients:

$$P = ST \qquad (3)$$

The commercially available thermoelectric (Peltier) cooling elements used in our setups rely on series of junctions made up of n-doped and p-doped semiconductors.

B. Finite element model

The proposed model for thermoelectric heating relies on our previously proposed model for resistive (Joule) heating [4], adding terms for the thermoelectric effect. The Joule heating model is based on Joule's first law, which states that electric currents passing through a conductor generate heat, which is proportional to the resistance of the conductor R [Ω] and the current I [A] passing through it:

$$Q \propto I^2 \cdot R \qquad (4)$$

Q [W] is the energy (heat) released, and if direct current is applied, can be expressed via the formula of power: $P = V \cdot I = I^2 \cdot R$. The initial assumption is made that liquid in the microchannel is either slow enough to be considered stationary, or is kept stationary for the duration of heating.

Therefore, the model consists of two equations: heat generation is expressed by the formula of power (4), and then heat is propagated through the geometry of the model by the heat transfer equation (8). Space-dependence in the model is defined by a Cartesian coordinate system with 3 axes x [m], y [m], z [m], whereas time-dependence is described by time (t) in seconds. Scaling is permitted. Heat generation is expressed via the aforementioned formula of power, written in a differential form for the volume of the heater [7]:

$$\frac{dP}{dV} = J \cdot E = J \cdot \frac{J}{\sigma} = J^2 \cdot \rho \qquad (5)$$

Where P [W] is the power, V [m^3] the volume of the heating element, J [A/m^2] the current density, E [V/m] the electric field. σ [S/m] is the conductivity, ρ [Ω ·m] is the resistivity of the material of the heater. Current densities and the electric field used for calculating heat generation are in turn calculated from the following set of equations [8]:

$$\nabla J = Q_j,$$
$$J = \left(\sigma + \varepsilon_0\varepsilon_r\frac{\partial}{\partial t}\right)E + J_e, \qquad (6)$$
$$E = -\nabla V.$$

Where J [A/m^2] is the current density, Q_j [A/m^3] are current sources (sinks), E the electric field, J_e [A/m^2] an external current density (if there is one), V [V] the potential drop in every direction, σ [S/m] the conductivity, ε_0 the relative permittivity of vacuum, ε_r the relative permittivity of the material at the point of the geometry for which the equations are solved. In the current density equation in (6), an additional term is added for the contribution of the thermoelectric effect as an external current density J_e resulting from the Seebeck effect (2) as described in section II.A. Materials in the simulated geometry are characterized electrically through their conductivity and relative permittivity, whereas thermoelectric properties are characterized by the Seebeck coefficient. Set of equations (6) relies on the continuity equation, or charge conservation principle [8]:

$$\nabla J = -\frac{\partial p}{\partial t} \qquad (7)$$

The continuity equation states that charge density at a point only changes if current flows into or out of the point.

The heat transfer equation is used in the following form [9]:

$$\rho C_p \frac{\partial T}{\partial t} + \nabla q = Q \qquad (8)$$

where $\rho[kg/m^3]$ is the fluid density, C_p [$J/kg\,K$] the specific heat capacity at constant pressure, T [K] the absolute temperature in the system, k [$W/(mK)$] the thermal conductivity, and Q [W/m^3] are heat sources (sinks), which in this case are calculated as the power of the heating element as a whole. Contributions from the thermoelectric effect are added through the term for conductive heat flux, $q = -k\nabla T + PJ$, where P is the Peltier coefficient (3) as described in section II.A. With respect to heat transfer, materials of the simulated geometry are simulated through the aforementioned quantities (ρ, C_p, k), solved for each spatial point in the geometry.

III. EXPERIMENTAL SETUP FOR MODEL VALIDATION

A. Setup #1

In this setup, a commercially available thermoelectric module (European Thermodynamics Ltd. APHC-03107-S) was used. As described in section II.A, the module was composed of a series of junctions made up of n-doped and p-doped semiconductors, which were sandwiched between two metal plates (hot and cold sides). According to manufacturer data [10], this particular module could create a maximum temperature gradient of 65 °C between its two sides, at a maximum voltage input of 3.6 V and maximum current input of 7.4 A.

The thermoelectric module was attached to a milled glass microfluidic chip with its hot side (Fig. 1/A.). The chip had a microchannel that was designed to hold liquid on the order of 0.1 ml to house reactions required for diagnostic assays.

The thermoelectric device was connected to a DC power supply (Agilent E3631A) for current input, and a 10kΩ NTC thermistor was attached to the channel floor for temperature recording. The power supply was set up, and temperatures logged using a MATLAB® script.
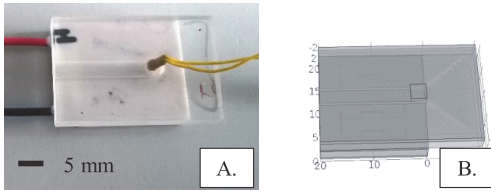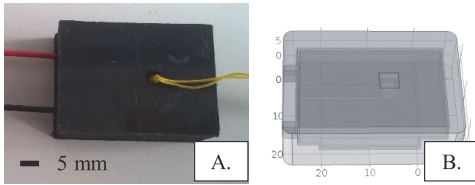

Fig. 1. Experimental setup (A.) and model geometry (B.)

B. Setup #2

This setup was created to emulate a handheld Point-of-Care device with a disposable microfluidic cartridge/chip, and compared to setup #1 (III.A), included a plastic (ABS) 3D printed frame to house device components. In every other respect the setup was the same as setup #1.

IV. RESULTS AND DISCUSSION

A. Evaluation of setup #1

Nucleic acid amplification reactions are the current gold standard for the detection of living organisms in molecular diagnostics. Isothermal amplification reactions only require a single temperature (range) to be maintained for the specified assay time (15-60 minutes). Most such assays require temperatures in a 30 - 65 °C temperature range [11], which was well below the deflection temperature of plastics used in our experiments. To evaluate model performance, input voltages

were chosen from the operating range of the thermoelectric module with an equal distribution. Room temperature for evaluation was defined as 19-22 °C. Model geometry and boundary conditions for the thermoelectric device were set up based on the example provided in COMSOL Multiphysics® 5.2 [12], fine-tuned for the commercial thermoelectric module used in the setup. Although not stated explicitly by the manufacturer, the thermoelectric module was assumed to be made up of Bi_2Te_3 junctions, the most typical material composition for such devices [2].

The model was solved using the Joule Heating interface of COMSOL Multiphysics® Version 5.2 with couplings for the Thermoelectric Effect as described in section II.B. The model was solved for the geometry shown in Fig. 1/B. Material properties were derived from built-in libraries of the software package. In the experimental setup, the thermoelectric element received voltage inputs in a 1-3 V range with 0.25 V steps to characterize the voltage vs. steady-state temperature relation of the module as a heater. To evaluate model performance, the same parameters were fed into the model and a comparison made.

The model was solved using a PC with a Core i5-4570 CPU and 16 GB RAM. Solution time was, on average 4 minutes 57 seconds (± 19 seconds) for a single set of input parameters. Temperatures inside the microchannel of the experimental setup were recorded as described in section III.A.

Each recording was conducted for 30 minutes, during which steady-state was achieved (defined as ± 1°C deviation over 5 minutes). An evaluation of model performance, comparing model outputs to experimental records is shown in Fig. 2. The finite element model estimated recorded temperature outputs with an average error of 0.54 ± 0.42 °C in this setup.
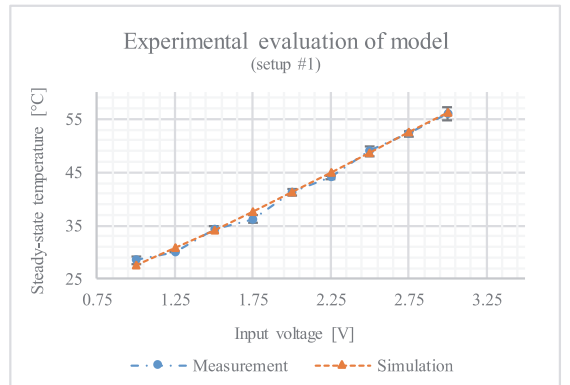

Fig. 2. Experimental evaluation of model for setup #1

B. Evaluation of setup #2

As described in section III.B, this setup was similar in every regard to setup #1, except the 3D printed housing for the chip and thermoelectric module. Measurements were conducted with the same input parameters as for setup #1, and the model for

setup #2 was fed with these parameters. The model was run using the same software and hardware as for setup #1.

Average solution time was 8 minutes 1 second (± 38 seconds) for a single set of parameters.

An evaluation of model performance, comparing model outputs to experimental records is shown in Fig. 3. The finite element model estimated recorded temperature outputs with an average error of 0.97 ± 0.97 °C in this setup. An increase in estimation error is observable compared to setup #1. Our analysis suggests this was due to the lack of a good heat sink. In setup #1, the cold side of the thermoelectric module was placed on the surface of a table that absorbed heat better than the ABS plastic in setup #2. The cold side warmed up more significantly in setup #2, causing a smaller gradient to form. In case the heater is to be applied in Point-of-Care diagnostics tests, a proper heat sink must be used.
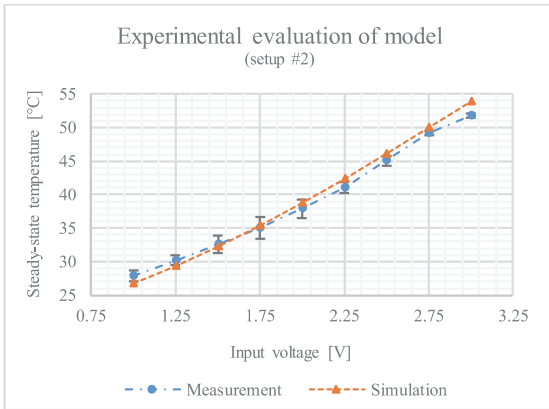

Fig. 3.   Experimental evaluation of model for setup #2

V. CONCLUSIONS

A finite element model was proposed for the modelling of thermoelectric heating applied to Point-of-Care molecular diagnostics devices. The model was developed to aid in iterative optimization and *in silico* validation of device designs. The model was presented and evaluated for an experimental setup of a glass microfluidic chip and a commercially available thermoelectric element, as well as another setup housing these two components in a 3D printed ABS plastic frame imitating a handheld diagnostics device with a disposable microfluidic cartridge. The glass chip contained a microchannel for < 0.1 ml liquid to house reactions required for the diagnostics assay.

Experimental setups were evaluated with various input potentials applied to the thermoelectric module, equally distributed over the operating range of the module. The finite element model was evaluated for the same input parameters and was able to estimate recorded temperature outputs with an accuracy of 0.54 ± 0.42 °C for the setup of the glass chip and the

thermoelectric module, and a precision of 0.97 ± 0.97 °C for the setup including the 3D printed ABS plastic frame. In the first setup, for the prescribed input voltage range, steady-state temperature outputs were in the range of 28 - 56 °C, whereas in the second setup with the 3D printed frame, the range was $24 - 51.8$ °C. Therefore, the evaluated setup would be capable of temperature control for several isothermal nucleic acid amplification assays.

Summarily, the proposed model, despite being early in development, was capable of approximating time-dependent heat transfer in a molecular diagnostics device with better than 1 °C precision on average. Furthermore, the proposed experimental setup with thermoelectric heating was proven to be capable of supporting the temperature control requirements of several isothermal nucleic acid amplification assays.

REFERENCES

[1] V. Miralles, A. Huerre, F. Malloggi, and M.-C. Jullien, "A Review of Heating and Temperature Control in Microfluidic Systems: Techniques and Applications," *Diagnostics*, vol. 3, no. 1, pp. 33–67, Jan. 2013.

[2] G. A. Mannella, V. La Carrubba, and V. Brucato, "Peltier cells as temperature control elements: Experimental characterization and modeling," *Appl. Therm. Eng.*, vol. 63, no. 1, pp. 234–245, Feb. 2014.

[3] E. E. Antonova and D. C. Looman, "Finite elements for thermoelectric device analysis in ANSYS," 2005, pp. 215–218.

[4] T. Pardy, T. Rang, and I. Tulp, "Finite element modelling of the resistive heating of disposable molecular diagnostics devices," in *WIT Transactions on Modelling and Simulation*, Opatija, Croatia, 2015, pp. 381–391.

[5] T. Pardy, T. Rang, and I. Tulp, "Modelling and experimental characterisation of self-regulating resistive heating elements for disposable medical diagnostics devices," in *WIT Transactions on Engineering Sciences*, Valencia, Spain, 2015, pp. 263–271.

[6] F. Cardarelli, *Materials Handbook*. London: Springer London, 2000.

[7] A. von Meier, *Electric power systems: a conceptual introduction*. Hoboken, NJ: Wiley-Interscience [u.a.], 2006.

[8] D. J. Griffiths, *Introduction to electrodynamics*. Prentice Hall, 1999.

[9] S. G. Kandlikar, *Heat transfer and fluid flow in minichannels and microchannels*. Amsterdam, Netherlands; San Diego, CA; Oxford, UK: Elsevier, 2006.

[10] European Thermodynamics Limited, "APHC-03107-S Peltier cooler module." 2010.

[11] P. Craw and W. Balachandran, "Isothermal nucleic acid amplification technologies for point-of-care diagnostics: a critical review," *Lab. Chip*, vol. 12, no. 14, p. 2469, 2012.

[12] *Thermoelectric Cooler*. COMSOL Multiphysics® v. 5.2. COMSOL AB, Stockholm, Sweden. 2015, 2015.

Appendix D

Tamas Pardy, Toomas Rang, Indrek Tulp

"Development of Temperature Control Solutions for Non-Instrumented Nucleic Acid Amplification Tests (NINAAT)," Micromachines, vol. 8, no. 7, p. 180, Jun. 2017. (ETIS 1.1)

Article

Development of Temperature Control Solutions for Non-Instrumented Nucleic Acid Amplification Tests (NINAAT)

Tamás Pardy [1,2,*], Toomas Rang [1] and Indrek Tulp [2]

[1] Thomas Johann Seebeck Department of Electronics, Tallinn University of Technology, Ehitajate Tee 5, 12616 Tallinn, Estonia; toomas.rang@ttu.ee
[2] Selfdiagnostics Deutschland GmbH, 04103 Leipzig, Germany; indrek.tulp@selfdiagnostics.com
* Correspondence: tamas.pardy@ttu.ee; Tel.: +372-582-30626

Abstract: Non-instrumented nucleic acid amplification tests (NINAAT) are a novel paradigm in portable molecular diagnostics. They offer the high detection accuracy characteristic of nucleic acid amplification tests (NAAT) in a self-contained device, without the need for any external instrumentation. These Point-of-Care tests typically employ a Lab-on-a-Chip for liquid handling functionality, and perform isothermal nucleic acid amplification protocols that require low power but high accuracy temperature control in a single well-defined temperature range. We propose temperature control solutions based on commercially available heating elements capable of meeting these challenges, as well as demonstrate the process by which such elements can be fitted to a NINAAT system. Self-regulated and thermostat-controlled resistive heating elements were evaluated through experimental characterization as well as thermal analysis using the finite element method (FEM). We demonstrate that the proposed solutions can support various NAAT protocols, as well as demonstrate an optimal solution for the loop-mediated isothermal amplification (LAMP) protocol. Furthermore, we present an Arduino-compatible open-source thermostat developed for NINAAT applications.

Keywords: lab-on-a-chip; LoC; finite element modelling; resistive heating; Point-of-Care; PoC; temperature control; computer aided design; microfluidics; isothermal nucleic acid amplification tests; NINAAT; NAAT

1. Introduction

Lab-on-a-Chip (LoC) non-instrumented nucleic acid amplification tests (NINAAT) are novel molecular diagnostics devices promising to bring high-accuracy, portable Point-of-Care rapid tests. Isothermal nucleic acid amplification protocols require a single well-defined temperature range for a specific incubation time, and are particularly well-suited for NINAAT applications [1,2]. However, the platform introduces constraints on physical size, power dissipation, and material costs, which pose a unique challenge for temperature control solutions. At present, off-the-shelf solutions for temperature control in LoC NINAAT devices are not readily available, which limits commercialization efforts.

Most reported LoC systems are instrumented and rely on external means for temperature control [3–5], which decreases their portability. A fully portable system requires an integrated solution. Most commonly, electrical heating elements are integrated, primarily Peltier cells [6,7]. Another popular solution is to use a thin film heating element [8–10], such as a resistive heater or a micro-Peltier cell. In the case of microfabricated LoC systems, the thin film heater can be integrated on the same substrate as the fluidic channels, resulting in a more compact and power-efficient layout.

Integrated self-regulating resistive heating is a viable candidate for NINAAT applications [11], as it does not require the addition of a thermostat; however, its power efficiency is still an issue that limits portability. An interesting alternative is offered by chemical heating, which is a heating element based on a highly exothermic chemical reaction of two or more components [12,13], typically an oxidative process regulated by the addition of a phase-change material (PCM). Advantages are their low cost and simplicity; disadvantages are their large size and the difficult regulation of their temperature output.

Many LoC systems with integrated temperature control methods are designed for polymerase chain reaction (PCR) [9,14,15] rather than isothermal nucleic acid amplification test (NAAT) protocols [2,15]. PCR requires thermal cycling, that is, rapid incubation temperature changes, which is even more challenging to implement in a chip format than a single, well-defined incubation temperature.

Resistive electrical heaters are well-known and well-defined, and therefore pose the lowest development risk for an integrated microheating solution. Injection molded plastics as the substrate of choice for LoC are becoming popular [16], primarily due to the low cost and the high aspect ratio achievable in mass-production. However, mold design and manufacturing is expensive, and therefore errors in geometry design are costly to correct. Finite element thermal analysis can greatly reduce development time by providing a tool to analyze and thermally optimize device geometry. Most research efforts have targeted the thermal analysis of integrated heating elements developed in-house, primarily within the same clean room process as the fluidic chip itself [17–19]. However, injection molded plastics require a separately manufactured heating element—preferably a commercially available heating element—which requires optimization of the thermal system.

In previous works, we investigated finite element modelling as a tool for the thermal analysis of various commercially available heating elements [20–22]. In this work, we demonstrate the process by which commercially available resistive heating elements can be evaluated for use as temperature control solutions for NINAAT systems. We also demonstrate an optimal temperature control solution for isothermal NAATs in a LoC format. We evaluate a self-regulated and thermostat-controlled resistive heating solution through experimental characterization as well as thermal analysis. Furthermore, we present an Arduino-compatible open-source thermostat developed for NINAAT applications.

2. Materials and Methods

2.1. Thermal Analysis via Finite Element Modelling

For thermal analysis, we use a Joule heating model with terms added for the specific heating element used. The initial assumption is made that the liquid in the simulated microreactor cavity is stationary for the duration of heating. The model consists of two sets of equations. The heat generation (for a known and experimentally characterized heating element) is expressed by the formula of power $\frac{dP}{dV} = J \cdot E$ [23], where P [W] is the power, V [m^3] the volume of the heating element, J [A/m^2] the current density, and E [V/m] the electric field. The generated heat is propagated through the geometry of the model by the heat transfer equation [24]. Fields J and E are derived from the following set of equations [25]:

$$\nabla J = Q_j$$
$$J = \left(\sigma + \varepsilon_0 \varepsilon_r \frac{\partial}{\partial t}\right) E + J_e \tag{1}$$
$$E = -\nabla V$$

where Q_j [A/m^3] are current sources (sinks), J_e [A/m^2] the external current density (if there is one), V [V] the potential drop in all directions, σ [S/m] the conductivity, ε_0 the relative permittivity of vacuum, and ε_r the relative permittivity of the material at the point of the geometry where the equations are evaluated. The materials in the simulated geometry are characterized electrically through their conductivity and relative permittivity, whereas heat transfer properties are characterized by their density (ρ [kg/m^3]), heat conductivity (k [$W/(m \cdot K)$]), and specific heat capacity (C_p [$J/kg \cdot K$]) for each spatial point of the geometry. The heat losses to the ambient (i.e., via convection) are defined as

boundary conditions on the appropriate boundaries. The assumption is made that the modelled device is in a closed, controlled environment, with restricted ambient temperature variations, and ventilation kept at a minimum for the observed duration. Self-regulating resistive heating elements contribute to the conductivity term in Equation (1) as the reciprocal of the temperature-dependent resistivity of the heater substrate. This can be represented in one of three ways:

(1)   If the heating element is electrically and structurally well-defined, the resistivity profile is directly fed into the model.
(2)   For a rough approximation of heating elements that are not well-defined, the linear approximation of resistivity [26] is used: $R(T) = R_0 \cdot [1 + \alpha \cdot (T - T_0)]$.
(3)   For PTC thermistors with known coefficients, the Steinhart–Hart equation is used [27].

Thermostat-regulated heating elements contribute to the electric potential in Equation (1) by adding a variable potential on the input terminals of the heating element. For the demonstrated proportional control algorithm, the input was expressed as follows [28]:

$$V_{in}(t) = K_p \cdot e(t) \tag{2}$$

where V_{in} [V] is the potential drop on the heating element, K_p [1/K] the proportional controller gain, and $e(t) = T_{set} - T_{current}$ the process error at time instant t [s]. T_{set} [K] is the temperature set point of the control algorithm, and $T_{current}$ [K] is the measured temperature at time instant t.

The finite element model was implemented in COMSOL® Multiphysics (version 5.2) using the Heat Transfer and Electric Currents interfaces coupled through the Joule Heating interface. All models were three-dimensional and the model geometry was imported from Autodesk Inventor. The boundary conditions and the initial values were derived from the physical prototypes used for experimental characterization. For the steady-state thermal analysis (Section 3.1), COMSOL's Stationary solver was used, whereas for the spatiotemporal analysis (Section 3.2), the Time-Dependent solver was used. All the domains of the physical prototype device were taken into account in the simulation, but the geometry was defeatured to decrease mesh complexity. The wires, screws, and labels were removed. Where applicable, axes of symmetry were used to cut the geometry. The convective, conductive, and radiative heat losses were calculated on the external boundaries. The temperature sensors in the physical prototype were modelled by Domain Point Probes. The proportional control algorithm was implemented as a user-defined equation, and coupled to the input voltage boundary condition. For both models, COMSOL generated a tetrahedral mesh. The average mesh element quality—based on the widely used radius ratio method [29]—for the self-regulated model was 0.674 (element size: 0.21 mm^3), whereas for the thermostat-regulated model it was 0.673 (element size: 0.18 mm^3).

2.2. Open-Source Thermostat

An open-source mini-thermostat was developed for temperature regulation of isothermal NAAT protocols in LoC devices. The primary implementation was on an Arduino Uno demo board, with an additional circuit board developed for taking temperature sensor readouts and applying proportional control on the current input of a resistive heating element via a metal-oxide semiconductor field-effect transistor (MOSFET) switch. Proportional control was chosen over proportional-integral-derivative (PID) control for its minimal computational space requirements, and to ensure easy downscaling further on in the development process for integrated controller solutions, while maintaining enough space for the integrated timer and user feedback functionalities. The thermostat was packaged in an enclosure and equipped with a piezo buzzer for auditory feedback. A graphical user interface was implemented in the Microsoft .NET framework to control the thermostat from a PC through a serial connection. The primary use case for this prototype is to connect a two-wire thermistor probe for sensing and a two-wire resistive heating element for temperature control in a LoC NAAT system. The user can configure the desired assay time and target temperature, and the

thermostat will beep to indicate when the reaction is done. The thermostat can be powered from a wall socket using a standard direct current (DC) transformer, or alkaline batteries with at least 5 V output (depending on the specifications of the heating element). Please refer to the Appendix A for more information and schematics.

2.3. Plastic NINAAT Thermal Models and Measurement Setup

For the experimental thermal characterization, two setups were created based on polymethyl methacrylate (PMMA) plastic prototypes manufactured by milling. The centerpiece was a model for a disposable microfluidic NAAT chip (25 mm × 75 mm area), with two reactor cavities designed to hold up to 0.7 mL of reaction volume each. Two enclosures were created for the two heating elements with slots for the chip (Figure 1b, d).
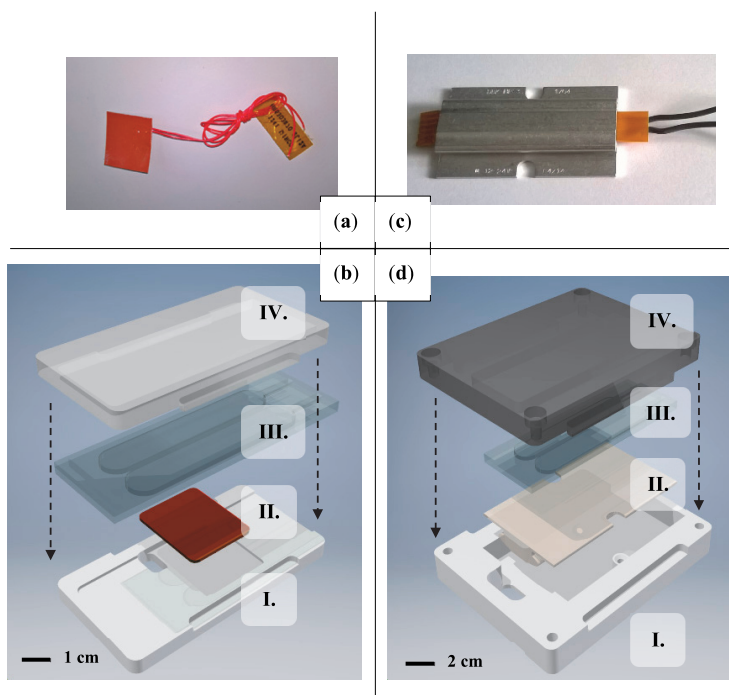
Figure 1. Minco HR5303 heating element for thermostat-regulated temperature control evaluations (**a**) DBK HP04 heating element for self-regulated temperature control evaluations; (**c**) the prototype for evaluating self-regulated heating; (**d**) consists of a milled plastic enclosure (I. and IV.), the plastic nucleic acid amplification test (NAAT) chip model (III.), and the heating element (II.). The prototype for evaluating thermostat-regulated heating (**b**) had the same basic layout and a different heating element.

The NAAT mock-chip had two two-wire 10-kΩ negative temperature coefficient (NTC) thermistor probes sealed into each reaction chamber. One thermistor was connected to an Agilent 34410A digital multimeter for temperature recording. The other probe was only used in thermostat-regulated heating experiments as the temperature input for the thermostat. The heating elements were powered from an Agilent E3631A triple-channel DC power supply (Agilent Technologies Inc., Santa Clara, CA, USA). Two-digit precision was used for recording temperatures as well as the output current values of the power supply. The power supply was operated as a voltage source (output set with two-digit precision) and a 1 A current limit was applied.

2.4. Heating Elements and Thermal Interface

The self-regulating heating element discussed in this paper (Figure 1a) was a ceramic PTCR (positive temperature coefficient of resistance) heater produced by DBK (model DBK HP04-1/04-24, DBK David + Baader GmbH, Rülzheim, Germany). It consisted of a ceramic heating element and an aluminum profile with a flat surface, originally designed for enclosure heating. Its operating voltage range by design was 1–30 V_{DC} [30]. The PTCR effect entails a rapid increase in substrate resistivity with elevated temperatures, which limits input current on the heating element and thus its heat output. Although structural or material data was not disclosed by DBK, most ceramic PTCR heaters are constructed from doped polycrystalline barium titanate ($BaTiO_3$) ceramics [31]. The onset of the PTCR effect occurs at the Curie temperature (T_c) of the material that marks a transition from the ferroelectric to the paraelectric phase. Dopants such as strontium or lead [32] can shift T_c and thereby define temperature set points as needed by the application. Besides material properties, the input voltage affects the onset of the PTCR effect as well, enabling accurate temperature control in a well-insulated device, as will be demonstrated in this paper.

For thermostat-regulated heating, an etched foil heating element (Figure 1c) from Minco Products Inc. was used (P/N HR5303R70.2L12A, Minco Products Inc., Fridley, MN, USA). These heaters typically rely on an etched resistive film (e.g., chrome–nickel) as the heater substrate, encased in polyimide and silicone rubber sheets. According to manufacturer data, the element used had a base resistance of 70.2 Ω [33].

Initially, the heating elements were characterized electrically and thermally. The resistance values were measured at room temperature using a digital multimeter (Agilent 34410A, Agilent Technologies Inc., Santa Clara, CA, USA). The temperature dependence of the self-regulated heating element was modelled by linear approximation (see Section 2.1). The heating element was encased in a polyurethane mold for thermal insulation, then connected to the power supply (Agilent E3631A), and the input current recorded at 1–24 V input voltage with 1 V steps while recording surface temperatures. At each step, the heater was allowed to reach a steady state and then to cool down to room temperature. The reference temperature was defined as 24 °C (room temperature), and monitored with a digital thermometer. The temperature coefficient of resistivity was calculated at 0.16 (±0.09) [1/K], whereas the base resistance at room temperature was measured at 10 (±0.4) Ω.

The resistance of the etched foil heating element was considered constant in the temperature range studied, and was measured at 76.38 ± 0.37 Ω [20], rather than the 70.2 Ω [33] disclosed by the manufacturer.

The thermal structure was similar in both experimental setups. The heating element was directly interfaced with the plastic NAAT chip, and the temperature sensors were encased in the microreactor cavities of the chip. No thermal interface material was used, as the system was designed for removable single-use NAAT chips.

3. Results and Discussion

3.1. Steady-State Performance for Multiple NAAT Protocols

As the first step in the optimization process of temperature control for NINAAT systems, an experimental thermal characterization was performed for both experimental setups. The thermostat-regulated setup was run with 15 V input voltage at a 1 A current limit and various temperature set points. The proportional gain of the thermostat was set to 20 [1/K] for rapid heating. The self-regulated setup was run with various voltage inputs in the 5–24 V range with a 1 A current limit. In both cases, target temperatures for the evaluation were selected from a set of targets for various NAAT protocols as listed in Table 1, and steady-state temperatures were recorded for evaluation. The ambient temperature was maintained at 22–24 °C and monitored with a digital thermometer. The experimental conditions were set according to the targeted application (Point-of-Care (POC) testing), thus the device prototype was tested in free air, in a closed laboratory environment with minimal ventilation. A climate chamber was not used for testing, as any prospective end-user device

is intended for use in offices and at home, where some ventilation is present. The results are shown in Figure 2. For the self-regulated heating evaluation, the steady-state error (SSE) was 0.59 °C (±0.39 °C) for the selected temperature targets, whereas for the thermostat-regulated evaluation it was 0.53 °C (±0.19 °C). Considering the average of all experiments, the controller regulated temperatures had a ±1 °C accuracy around the set point, which is a suitable accuracy for most isothermal NAAT protocols.
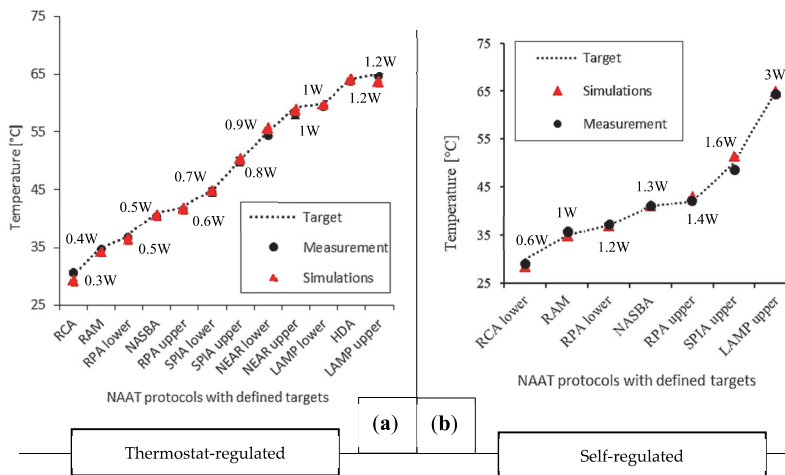
Figure 2. Steady-state thermal characterization and performance evaluation of commercial heating elements in test setups modelling non-instrumented nucleic acid amplification test (NINAAT) systems for multiple NAAT temperature targets ranging from 30 to 65 °C (**a**,**b**). A finite element thermal model was set up and trained for the heating element used. The model was demonstrated to accurately estimate steady-state temperature outputs, and is useable as a tool for spatial thermal analysis to evaluate temperature control performance.

The second step was to set up and train our finite element model for thermal analysis, given the two heating elements under study and the experimental setups. Both setups were modelled in COMSOL® Multiphysics and the boundary conditions were defined according to experimental parameters. The heating elements were fully defined, including their internal structure. The material properties were either literature or COMSOL library values, except for the resistivity profiles of the heating elements. The total element number (tetrahedral domain elements) for the generated mesh was 195114 for the self-regulated setup and 338064 for the thermostat-regulated setup. Both setups had nine simulated domains, but in the self-regulated setup only half of the model was simulated due to the axial symmetry. The model was solved on a PC with a Core i5-4570 CPU and 16 GB RAM. The typical execution time for a single set of parameters ranged from 2 min to 55 min depending on complexity. Complexity was heavily affected by the rate of change in the simulated system, especially since the thermostat-regulated system included a feedback loop for the controller. For the self-regulated heating setup, the model estimated experimental results with a mean absolute error (MAE) of 0.96 °C over the defined set of input parameters. For the thermostat-regulated setup, MAE was 0.64 °C. A summary of the steady-state measurements and the simulation results are shown in Figure 2.

For the selected temperature targets, the control precision was similar in both systems; however, the thermostat-regulated system offered a higher degree of freedom in choosing the target temperature. The self-regulated setup was limited to a lower number of targets. Therefore, the thermostat-regulated system was proven a better candidate for this temperature control scenario.

Table 1. Target temperatures for isothermal nucleic acid amplification tests (NAAT) protocols [15].

Method	Full Name	Target	Steady-State Error (SSE) (Self-Regulated)	SSE (Thermostat)
NASBA	Nucleic Acid Sequence Based Amplification	41 °C	0.1 °C	0.6 °C
HDA	Helicase Dependent Amplification	64 °C	Not tested	0.3 °C
LAMP	Loop Mediated Isothermal Amplification	60–65 °C	0.6 °C	0.3 °C
NEAR	Nicking Enzyme Amplification Reaction	55–59 °C	Not tested	0.7 °C
RCA	Rolling Circle Amplification	30–65 °C	0.9 °C	0.6 °C
RPA	Recombinase Polymerase Amplification	37–42 °C	0.2 °C	0.2 °C
SPIA	Single Primer Isothermal Amplification	45–50 °C	1.2 °C	0.2 °C
RAM	Ramification Amplification Method	35 °C	0.75 °C	0.2 °C

3.2. Spatiotemporal Performance Analysis for Specific NAAT Protocol

Loop-mediated isothermal amplification (LAMP) is a highly sensitive and specific DNA amplification method developed by Eiken Chemical Co. [15], which requires incubation for 15–60 min at 60–65 °C temperature. We chose LAMP for this evaluation due to its high-temperature requirement that makes it very challenging to support in a portable, and especially disposable, system. We targeted at least 15 min in the prescribed temperature range with our temperature control solutions. First, we attempted to demonstrate with experimental thermal characterization that both prototypes could reach the target. Then, using the thermal models that we previously adjusted to the heating elements, we performed a thermal analysis to compare the performance of the two temperature control solutions. The setups were configured for the specified target range based on the input parameters defined in the previous section (Figure 2).

The time constants were determined experimentally. The self-regulated setup reached the control target after 7.5 min during the experimental characterization, whereas the thermostat-regulated setup reached it in 9 min. The self-regulated setup reached steady-state in 35 min, and the thermostat-regulated setup reached it in 10 min. No overshoot was detected. Both temperature control solutions could maintain the target range for a minimum of 15 min. Figure 3 shows a comparison of results between the two setups.
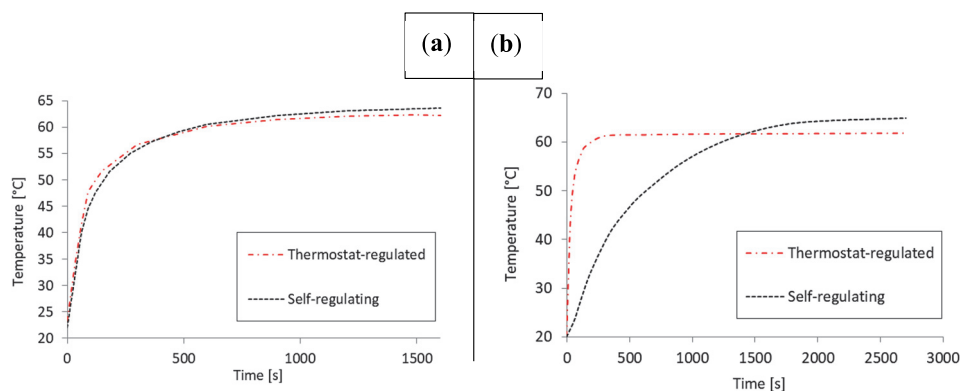
Figure 3. Temporal analysis specifically for the LAMP NAAT protocol that required 60–65 °C reaction temperature. Experimental characterization (**a**) indicated time constants below the required 15 min as well as successful regulation within the set temperature range for both solutions. The thermal transient simulation indicated a more pronounced difference: the setting time was significantly lower for the thermostat-regulated setup than the self-regulating setup (**b**).

The finite element models were solved as described previously for both setups using the same input parameters as during the experiments. The solution time was 20 min for the self-regulated setup, and up to 1.5 h for the thermostat-regulated setup due to the increased complexity resulting from higher rates of change. The self-regulated heating model estimated experimental results with an MAE of 9.15 °C, whereas the thermostat-regulated model had an MAE of 4.55 °C. However, in steady-state, the error decreased to 0.36 °C and 0.5 °C respectively. The measured time constants were estimated with an MAE of 8.7 min for the self-regulated setup and 5.5 min for the thermostat-regulated setup.

The higher error for the self-regulated heating model resulted in part from the linear resistivity model chosen for its simplicity. The linear model fails to capture the non-linearity of temperature-dependent resistivity inherent in ceramic semiconductors. Furthermore, it is not possible to accurately represent thermal interfaces and thermal capacities in a model due to the limited amount of data available on structural details, as well as the necessity to simplify the geometry representations in order to fit them into the available computational space.

The model was applied in a spatiotemporal thermal analysis to determine the volumetric heating efficiency η_h in the two test structures. The evaluation was performed based on the following expression:

$$\eta_h = \frac{1}{coord} \cdot \sum_{coord} (T > 59.99[°C] \cap T < 65.01[°C]) \tag{3}$$

where coord denotes the spatial coordinates (x, y, z), and $\eta_h \in [0;1]$. First, this expression was evaluated in steady-state to determine the maximum heating efficiency for both setups for a direct comparison. In the self-regulated setup, 95% of the reaction volume was in range (0.66 mL out of 0.7 mL). In the thermostat-regulated setup, 8% of the reaction volume was in range (0.06 mL). However, adding a heat spreader—a 1 mm thick aluminum sheet—to the heater–chip interface increases the reaction volume in range to 95% (0.66 mL). The results are shown in Figure 4.
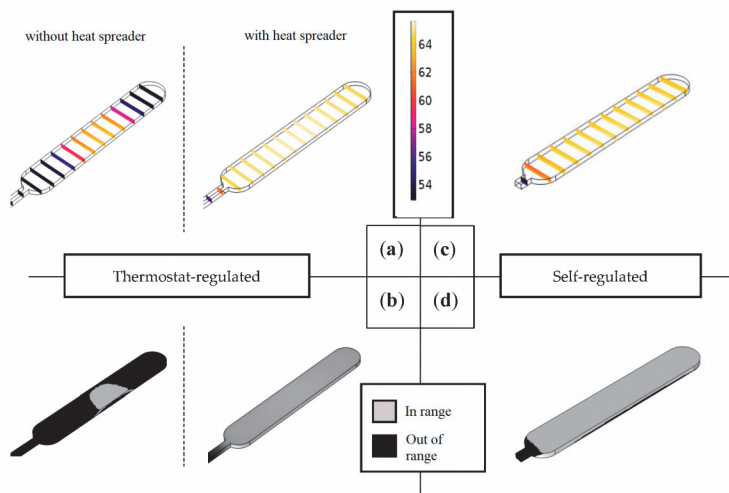
Figure 4. Application of finite element thermal analysis: steady-state temperatures are shown inside the reaction chamber for both the thermostat-regulated (**a**) and self-regulated experimental setups (**c**) visualizing heating efficiency. Visualizing the reaction volume in the target range (**b**,**d**) reveals deficiencies in heat transfer and insulation. The installation of a heat spreader improves the performance of the thermostat-regulated setup to the level of the self-regulated setup.

The experimental evaluation indicated that the self-regulated setup reached the control target 1.5 min earlier than the thermostat-regulated setup, whereas steady-state was reached 25 min earlier in the thermostat-regulated system. The controller gain was set high to ensure rapid heating, but the algorithm cut down the output near the set point to prevent overheating, which resulted in a longer heat up. The power input required by the self-regulated setup was 9 V higher than for the thermostat-regulated setup, making the latter more favorable for portable applications. However, the presented plastic prototypes were created to fit the dimensions of the heating elements rather than optimal power efficiency. The demonstrated setups could be powered using 2–3 pieces of 9 V alkaline batteries, which would form a major part of any portable device using this system. However, reducing the size of the heated area and the heating element in turn reduces the size of the power supply, and therefore the size of the whole device. In any NINAAT design scenario, the reaction chamber size must be minimized and heat transfer efficiency on the chip–heater interface maximized.

To summarise, at the present stage of development, the self-regulated setup offers better temperature control performance for the LAMP protocol (the incubation target temperature is reached faster). Additionally, despite the fact that it needs a more sizeable power supply than the alternative, it does not need the thermostat, which reduces cost and complexity. Including a battery compartment, this NINAAT temperature control solution would have dimensions of 8 cm × 6 cm × 4 cm. The thermostat alone has dimensions of 11 cm × 6 cm × 4 cm. Therefore, for an integrated test device, the overall footprint is smaller for the self-regulated system. This makes it more favorable for portable applications.

4. Conclusions

We demonstrated a process by which commercial off-the-shelf heating elements can be evaluated for and built into Lab-on-a-Chip devices that require precise temperature control. The primary application area for this technique is non-instrumented isothermal nucleic acid amplification in a chip format, where the heating element is a major technical challenge and a potential hurdle that slows down the commercialization of these devices. Two commercially available heating elements were evaluated and compared as potential temperature control solutions, and an optimal candidate was proposed. The demonstrated solution was capable of creating and maintaining the temperature range required for the loop-mediated isothermal amplification protocol inside a microreactor cavity within a time range expected from a rapid test. The proposed finite element model for thermal analysis can help optimize device geometry and insulation, as well as evaluate volumetric heating efficiency.

Author Contributions: T.P. and I.T. conceived and designed the experiments; T.P. performed the experiments; T.P., I.T. and T.R. analyzed the data; T.P. built the finite element models for thermal analysis; T.R. and I.T. contributed materials and analysis tools; T.P. wrote the paper; I.T. and T.R. provided support and supervision.

Conflicts of Interest: The authors declare no conflict of interest.

Appendix A

Hardware schematics and code for a basic implementation of the mini-thermostat are available at https://www.hackster.io/salhar1/mini-thermostat-e732ed, under the GPL3+ license.

References

1. Yager, P.; Edwards, T.; Fu, E.; Helton, K.; Nelson, K.; Tam, M.R.; Weigl, B.H. Microfluidic diagnostic technologies for global public health. *Nature* **2006**, *442*, 412–418. [CrossRef] [PubMed]

2. Chang, C.-C.; Chen, C.-C.; Wei, S.-C.; Lu, H.-H.; Liang, Y.-H.; Lin, C.-W. Diagnostic Devices for Isothermal Nucleic Acid Amplification. *Sensors* **2012**, *12*, 8319–8337. [CrossRef] [PubMed]

3. Rodriguez, N.M.; Wong, W.S.; Liu, L.; Dewar, R.; Klapperich, C.M. A fully integrated paperfluidic molecular diagnostic chip for the extraction, amplification, and detection of nucleic acids from clinical samples. *Lab Chip* **2016**, *16*, 753–763. [CrossRef] [PubMed]

4. Kim, T.-H.; Park, J.; Kim, C.-J.; Cho, Y.-K. Fully Integrated Lab-on-a-Disc for Nucleic Acid Analysis of Food-Borne Pathogens. *Anal. Chem.* **2014**, *86*, 3841–3848. [CrossRef] [PubMed]

5. Mao, H.; Yang, T.; Cremer, P.S. A Microfluidic Device with a Linear Temperature Gradient for Parallel and Combinatorial Measurements. *J. Am. Chem. Soc.* **2002**, *124*, 4432–4435. [CrossRef] [PubMed]

6. Velve-Casquillas, G.; Fu, C.; Le Berre, M.; Cramer, J.; Meance, S.; Plecis, A.; Baigl, D.; Greffet, J.J.; Chen, Y.; Piel, M.; et al. Fast microfluidic temperature control for high resolution live cell imaging. *Lab Chip* **2011**, *11*, 484–489. [CrossRef] [PubMed]

7. Velve-Casquillas, G.; Costa, J.; Carlier-Grynkorn, F.; Mayeux, A.; Tran, P.T. A Fast Microfluidic Temperature Control Device for Studying Microtubule Dynamics in Fission Yeast. *Methods Cell Biol.* **2010**, *97*, 185–201. [PubMed]

8. Scorzoni, A.; Tavernelli, M.; Placidi, P.; Zampolli, S. Thermal Modeling and Characterization of a Thin-Film Heater on Glass Substrate for Lab-on-Chip Applications. *IEEE Trans. Instrum. Meas.* **2015**, *64*, 1098. [CrossRef]

9. Moschou, D.; Vourdas, N.; Kokkoris, G.; Papadakis, G.; Parthenios, J.; Chatzandroulis, S.; Tserepi, A. All-plastic, low-power, disposable, continuous-flow PCR chip with integrated microheaters for rapid DNA amplification. *Sens. Actuators B Chem.* **2014**, *199*, 470–478. [CrossRef]

10. Jiao, Z.; Huang, X.; Nguyen, N.-T.; Abgrall, P. Thermocapillary actuation of droplet in a planar microchannel. *Microfluid. Nanofluid.* **2008**, *5*, 205–214. [CrossRef]

11. Wyzkiewicz, I.; Grabowska, I.; Chudy, M.; Brzozka, Z.; Jakubowska, M.; Wisniewski, T.; Dybko, A. Self-regulating heater for microfluidic reactors. *Sens. Actuators B Chem.* **2006**, *114*, 893–896. [CrossRef]

12. Buser, J.R.; Diesburg, S.; Singleton, J.; Guelig, D.; Bishop, J.D.; Zentner, C.; Burton, R.; LaBarre, P.; Yager, P.; Weigl, B.H. Precision chemical heating for diagnostic devices. *Lab Chip* **2015**, *15*, 4423–4432. [CrossRef] [PubMed]

13. Weigl, B.; Domingo, G.; LaBarre, P.; Gerlach, J. Towards non- and minimally instrumented, microfluidics-based diagnostic devices. *Lab. Chip* **2008**, *8*, 1999–2014. [CrossRef] [PubMed]

14. Miralles, V.; Huerre, A.; Malloggi, F.; Jullien, M.-C. A Review of Heating and Temperature Control in Microfluidic Systems: Techniques and Applications. *Diagnostics* **2013**, *3*, 33–67. [CrossRef] [PubMed]

15. Craw, P.; Balachandran, W. Isothermal nucleic acid amplification technologies for point-of-care diagnostics: A critical review. *Lab Chip* **2012**, *12*, 2469–2686. [CrossRef] [PubMed]

16. Nunes, P.S.; Ohlsson, P.D.; Ordeig, O.; Kutter, J.P. Cyclic olefin polymers: Emerging materials for lab-on-a-chip applications. *Microfluid. Nanofluid.* **2010**, *9*, 145–161. [CrossRef]

17. Mannella, G.A.; la Carrubba, V.; Brucato, V. Peltier cells as temperature control elements: Experimental characterization and modeling. *Appl. Therm. Eng.* **2014**, *63*, 234–245. [CrossRef]

18. Wang, Y.; Song, H.; Pant, K. A reduced-order model for whole-chip thermal analysis of microfluidic lab-on-a-chip systems. *Microfluid. Nanofluid.* **2014**, *16*, 369–380. [CrossRef] [PubMed]

19. Kumar, S.; Cartas-Ayala, M.A.; Thorsen, T. Thermal modeling and design analysis of a continuous flow microfluidic chip. *Int. J. Therm. Sci.* **2013**, *67*, 72–86. [CrossRef]

20. Pardy, T.; Rang, T.; Tulp, I. Finite element modelling of the resistive heating of disposable molecular diagnostics devices. In *Computational Methods and Experimental Measurements XVII*; WIT Transactions on Modelling and Simulation: Opatija, Croatia, 2015; pp. 381–391.

21. Pardy, T.; Rang, T.; Tulp, I. Modelling and experimental characterisation of thermoelectric heating for molecular diagnostics devices. In Proceedings of the 2016 15th Biennial Baltic Electronics Conference Electronics Conference (BEC), Tallinn, Estonia, 3–5 October 2016; pp. 27–30.

22.   Pardy, T.; Tulp, I.; Rang, T. Finite Element Modelling for the Optimization of Microheating in Disposable Molecular Diagnostics. In Proceedings of the 14th International Conference on Simulation and Experiments in Heat Transfer and its Applications, Ancona, Italy, 7–9 September 2016; Volume 106.

23.   Von Meier, A. *Electric Power Systems: A Conceptual Introduction*; Wiley-Interscience [U.A.]: Hoboken, NJ, USA, 2006.

24.   Kandlikar, S.; Garimella, S.; Li, D.; Colin, S.; King, M.R. *Heat Transfer and Fluid Flow in Minichannels and Microchannels*, 1st ed.; Kandlikar, S.G., Ed.; Elsevier: Amsterdam, The Nederland, 2006.

25.   Griffiths, D.J. *Introduction to Electrodynamics*; Prentice Hall: Upper Saddle River, NJ, USA, 1999.

26.   Rood, P. A Visual Method of Showing The High Temperature Coefficient of Resistance of Metals as Compared with Alloys. *J. Opt. Soc. Am.* **1928**, *16*, 357–359. [CrossRef]

27.   Steinhart, J.S.; Hart, S.R. Calibration curves for thermistors. *Deep Sea Res. Oceanogr. Abstr.* **1968**, *15*, 497–503. [CrossRef]

28.   Srivastava, M.; Srivastava, M.C.; Bhatnagar, S. *Control Systems*; Tata McGraw-Hill: New Delhi, India, 2009.

29.   Friess, H.; Haussener, S.; Steinfeld, A.; Petrasch, J. Tetrahedral mesh generation based on space indicator functions. *Int. J. Numer. Methods Eng.* **2013**, *93*, 1040–1056. [CrossRef]

30.   DBK David+Baader GmbH. HP Series of PTC Heaters. European Thermodynamics Ltd., 2009. Available online: http://www.farnell.com/datasheets/11488.pdf (accessed on 10 January 2017).

31.   Shioi, R.; Umeya, K.; Yonezuka, K.; Senzaki, H. Heating Element Made of PTC Ceramic Material. U.S. Patent 05,882,922, 13 January 1981.

32.   Huybrechts, B.; Ishizaki, K.; Takata, M. The positive temperature coefficient of resistivity in barium titanate. *J. Mater. Sci.* **1995**, *30*, 2463–2474. [CrossRef]

33.   Minco Products Inc. *Flexible Heaters Design Guide HDG01121806(A)*; Minco Products Inc.: Fridley, MN, USA, 2007.

Appendix E

Tamas Pardy, Indrek Tulp, Clemens Kremer

"Microfluidic test device", PA 2017 70310 (patent application)

The patent application is available as a confidential appendix.

CURRICULUM VITAE

Personal data

Name: Tamas Pardy

Date of birth: 19.05.1988

Place of birth: Hungary

Citizenship: Hungarian

Contact data

Address: Mäepealse 16-7, Tallinn, Estonia

Phone: +37258230626

E-mail: tamas.pardy@ttu.ee

Education

Educational institution	Year	Degree
Tallinn University of Technology	2014-2017 (expected)	PhD, Electronics and Telecommunication
Peter Pazmany Catholic University, Budapest, Hungary	2012-2014	Info-Bionics Engineer (MSc)
Peter Pazmany Catholic University, Budapest, Hungary	2008-2012	BSc in Molecular Bionics
Eotvos Jozsef Gimnazium, Tata, Hungary	2003-2008	Certificate of Secondary Education

Language competence

Hungarian: Native

English: Proficient

German: Intermediate

Estonian: Elementary

Professional employment

2014 – present day: Medical Device Engineer at Selfdiagnostics Deutschland GmbH, Leipzig, Germany

2013 – 2014: System and Application Engineer at HRX Central European Kft., Dabas, Hungary

ELULOOKIRJELDUS

Isikuandmed

Nimi: Tamas Pardy

Sünniaeg: 19.05.1988

Sünnikoht: Ungari

Kodakondsus: Ungarlane

Kontaktandmed

Aadress: Mäepealse 16-7, Tallinn, Estonia

Telefon: +37258230626

E-mail: tamas.pardy@ttu.ee

Hariduskäik

Haridusasutus	Aasta	Haridus
Tallinna Tehnikaülikool	2014-2017 (expected)	PhD, elektroonika ja telekommunikatsioon
Peter Pazmany Catholic University, Budapest, Ungari	2012-2014	Magister, Info-Bioonika
Peter Pazmany Catholic University, Budapest, Ungari	2008-2012	Bakalaureus, Molecular Bionics
Eotvos Jozsef Gimnazium, Tata, Ungari	2003-2008	Keskkool

Keelteoskus

Ungari keel: emakeel

Inglise keel: kõrgtase

Saksa keel: kesktase

Eesti keel: kõrgem algtase

Teenistuskäik

2014 – …: Medical Device Engineer at Selfdiagnostics Deutschland GmbH, Leipzig, Germany

2013 – 2014: System and Application Engineer at HRX Central European Kft., Dabas, Hungary